Approximation and representation of functions on the sphere. Applications to inverse problems in geodesy and medical imaging.

Ana-Maria Nicu

UNIVERSITY OF NICE - SOPHIA ANTIPOLIS

DOCTORAL SCHOOL STIC

SCIENCES AND TECHNOLOGIES OF INFORMATION AND COMMUNICATION SCIENCES

T H E S I S

to obtain the degree of

Docteur of Science

of University of Nice Sophia - Antipolis

Field of study: Control, signal and image processing

presented and defended by

Ana-Maria NICU

Approximation and representation of functions on the sphere

Applications to inverse problems in geodesy and medical imaging.

Adviser: Juliette LEBLOND

defended on 15 February 2012

Jury :

Aline Bonami	-	Professor emeritus, Universiy of Orleans	-	Examiner
Fahmi Ben Hassen	-	Assistant professor, ENIT, LAMSIN, Tunis, Tunisia	-	Examiner
Henda El Fekih	-	Professor, ENIT, LAMSIN, Tunis, Tunisia	-	Jury member
Abderrazek Karoui	-	Professor, Faculty of Sciences, Bizerte, Tunisia	-	Jury member
Juliette Leblond	-	Director of Research, INRIA, Sophia-Antipolis	-	Adviser
Martine Olivi	-	Support research, INRIA, Sophia-Antipolis	-	Jury member

UNIVERSITÉ DE NICE - SOPHIA ANTIPOLIS

ÉCOLE DOCTORALE STIC

SCIENCES ET TECHNOLOGIES DE L'INFORMATION ET DE LA COMMUNICATION

T H È S E

pour l'obtention du grade de

Docteur en Sciences

de l'Université de Nice - Sophia Antipolis

Mention: Automatique, traitement du signal et des images

présentée et soutenue par

Ana-Maria NICU

Approximation et representation des fonctions sur la sphère.

Applications aux problèmes inverse de la géodésie et de l'imagerie médicale.

Thèse dirigée par Juliette LEBLOND

soutenue le 15 Février 2012

Jury :

Aline Bonami	-	Professeure émérite, Université d'Orléans	-	Rapporteure
Fahmi Ben Hassen	-	Maître assistant, ENIT, LAMSIN, Tunis, Tunisie	-	Rapporteur
Henda El Fekih	-	Professeure, ENIT, LAMSIN, Tunis, Tunisie	-	Examinatrice
Abderrazek Karoui	-	Professeur, Faculté des Science, Bizerte, Tunisie	-	Examinateur
Juliette Leblond	-	Directrice de recherche, INRIA, Sophia Antipolis	-	Directrice de thèse
Martine Olivi	-	Chargée de recherche, INRIA, Sophia Antipolis	-	Examinatrice

Contents

Chapter 1

Introduction

In this chapter we begin by presenting the direct or forward problem of certain engineering, physical applications. Then we introduce the corresponding inverse problems and we classify them by Hadamard criteria [29]. We give also the mathematical model of these two problems and we conclude by the tridimensional elliptic partial differential equations which defines our two main practical problems of interest: the geophysical and magneto/electro-encephalography (M/EEG) inverse problems.

1.1 General framework and state of the art

Inverse problems are very important in science, engineering and bioengineering. They have applications to many practical examples. Among this applications, we quote the geodesy and M/EEG inverse problems.

Before introducing inverse problems, we consider the associated direct or forward problem.

Given a domain $\Omega \subset \mathbb{R}^3$ and a (continuous or discrete) density supported inside the domain Ω, *the direct problem* consists in computing the generated potential at the surface of the considered domain. Then, *the inverse problem* consists in recovering the interior density from measurements of the potential taken (in some points) at the boundary of the domain. For appropriated models, the issue is to find the density which means to find the parameters (some of them or all) which describe it (like source positions, moments, etc.). As measurements, we can have values of the potential, its first derivative or its Hessian which can be observed on different surfaces (orbits). Nowadays, many problems in science like geophysics and medicine

are inverse problems [30, 54]. Graphically, the inverse problem can be illustrated by the next image:

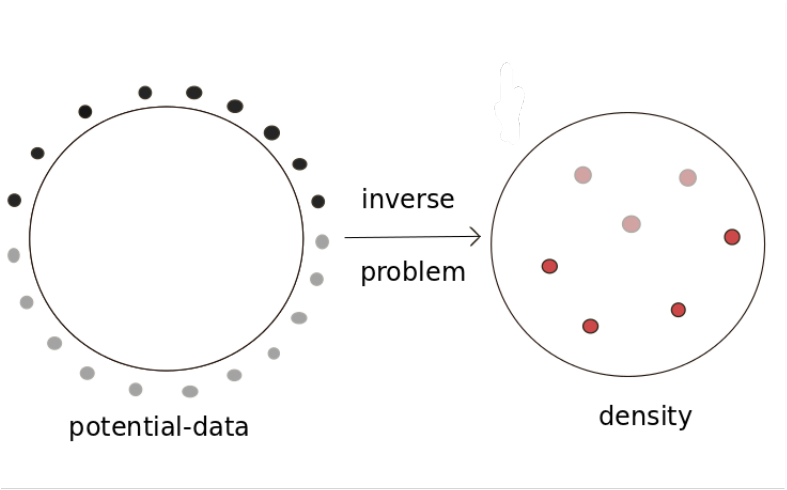

Figure 1.1: *From partial measurements outside the domain to sources (masses, density) in the domain*

In both cases, M/EEG [31] and geophysics [54] problems, the considered geometrical domain Ω is assumed to be a ball. The measurements can be taken over the sphere $\partial\Omega$ (boundary of the ball) or in the realistic case just over a part of the sphere (the superior hemisphere of the head or the satellite orbits). In this later case, we express the data in the Slepian basis (with good local properties)[46]. After we have the development of the data in the adapted basis, the next step is the extrapolation over all the sphere-data transmission problem (TP)-and the recovery of the density (DR) with an intermediate discretisation step called source recovery (SR) inside the ball using the rational approximation method (see Chapter 4 and 5). The source identification issue is translated as families of 2D best rational approximation problems in disks [8], whose solutions allow to localize and estimate the original 3D sources and their moments.
Briefly, the work of this thesis is concentrated on the representation of the disposed data over the sphere (Chapter 3) and as a following step, the recovery of the density in the ball using the rational approximation method (Chapter 5). The two problems are modeled by the next partial differential equation:

$$-\Delta Pot = \rho \text{ with } \rho = \underbrace{\rho_r}_{smooth} + \underbrace{\rho_s}_{singular\ \ part} \tag{1.1}$$

where Pot can be the electrical, magnetic or gravitational potential and it can be written as the convolution between the Green function (see Chapter 2, Section 2.2.1) and the density ρ. The link between these two quantities will be expressed by an operator called *"forward operator"* denoted by T:

$$Pot = G * \rho = T\rho \tag{1.2}$$

1.2 Geophysics

The purpose of this section is to present the physical frame of geophysical inverse problem. The knowledge of the Earth's gravity field is essential for many domains. The gravity field being connected with the internal density of the Earth, it permits to geophysicists to study the structure, the dynamic but also different physical properties of the Earth at different scales: from its surface layers to its center. One particular equipotential surface, the geoid, which coincides with the average of the ocean surfaces, was proposed as the "mathematical figure of the Earth" (C.F. Gauss). It is still frequently considered by many to be the fundamental surface of physical geodesy. Referring to the curvature of the interior level surfaces, these change discontinuously with the density. Because the geodetic measurements (theolite measurements, satellite techniques, etc.) are referred to the system of the level surface, the geoid plays an important role and thus, we see that one of the physical aim is the determination of the level surfaces of the Earth's gravity field.

The gravity field, at various temporal and space scales, is also used for orbitography and navigation, locate and characterize different reserves or deposits, to evaluate the groundwater resource and study polluted sites. The time variations of the gravity field reflect the mass displacements inside the Earth system, from the Earth's core to the top of the atmosphere. Such mass transfer occurs in a wide range of spatial and temporal scales, and they are dominated by the water redistribution related to the global water cycle in the Earth's superficial envelopes (atmosphere, oceans, polar ice caps, continental hydrology). They also reflect solid Earth deformations such as earthquakes. Measuring and modeling the time variations of the gravity field, and hence of the mass displacements, allow to better understand the dynamical processes and changes in the global Earth system.

The gravimetry inverse problem

After Isaac Newton, the gravitational potential of the Earth is given by the following formula:

$$V(X) = G \iiint_{\Omega} \frac{\rho(Y)}{|X-Y|} \mathrm{d}Y, X \in \mathbb{R}^3 \setminus \Omega \tag{1.3}$$

where G is the gravitational constant and ρ is the Earth density.

At the exterior of the Earth modeled by Ω, in empty space, the density is zero and the gravitational potential V satisfies the Laplace equation:

$$\Delta V = 0$$

Inside the Earth Ω, V is solution of the Poisson equation:

$$\Delta V = -4\pi G\rho$$

In what follows, we will suppose $4\pi G \simeq 1$. At the surface of the Earth, we can measure the gravitational potential V, but we can also observe measurements of normal derivative $\frac{\partial V}{\partial n}$. The normal derivative is the derivative along the outward-directed surface normal n to the spherical surface of the Earth. According to the satellite missions CHAMP (Challenging Minisatellite Payload), GRACE (Gravity Recovery and Climate Experiment) and GOCE (Gravity Field and Steady-State Ocean Circulation Explorer) we can also have the second order derivative of V (Hessian of V) on satellite orbits. The time-varying component offered by GRACE satellite improves our knowledge of the data at all spatial scales. Usually, the data are modeled using a linear combination of spherical harmonics. For regional measurements, local basis functions as Slepian functions, are used.

The direct problem of gravimetry is to find V given the density ρ.

The inverse problem: find the density ρ from boundary measurements of V, $\frac{\partial V}{\partial n}$ or Hessian V at ground or on satellite orbits.

Geometric model of the Earth

Historically, many physicians did scientific observations related to the structure of the Earth.

The first ones that observed the structure multi-shells of the Earth and the different densities for each of them, are *Burnet Woodward* and *Whiston* in the XVII century.

A little bit later, *Roche* proposed 2 shells: a iron kernel of density 7 and a rocks shell of density 3.

In the first decade of the XX century, *Lehmann* discovered a new structure inside the kernel. Consequently, the new model is composed by a grain (inner core), a core, a mantle and it is called the *Lehmann model*.

Bullen proposed in 1936 a concentric model of the Earth with a density which increase towards the center (the inner of the Earth).

In 1906, *Mohorovici* identified a discontinuity between the crust and the mantle.

There are also *Gutenberg* discontinuity between the lower mantle and outer core and *Lehmann* discontinuity between the external and the inner core.

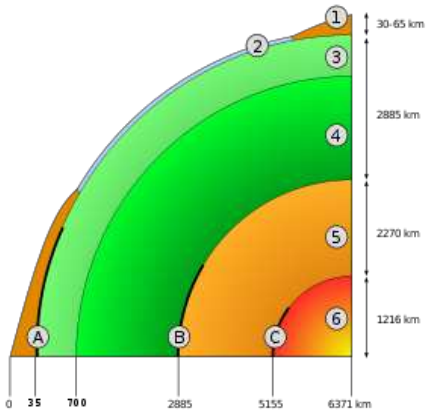

Figure 1.2: *Schematic view of the interior of Earth. 1. continental crust - 2. oceanic crust - 3. upper mantle - 4. lower mantle - 5. outer core - 6. inner core. A: Mohorovici discontinuity - B: Gutenberg Discontinuity - C: Lehmann discontinuity (Source: http://en.wikipedia.org/wiki)*

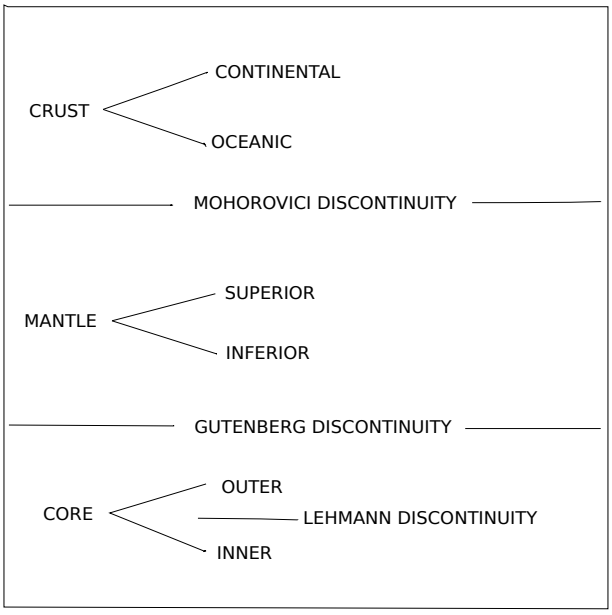

Figure 1.3: *Shells of the Earth and their discontinuities*

1.3 M/EEG

The progress of the medical imaging techniques is very important and it is of high utility because it permits to improve continuously the care available for patients. The electroencephalography (EEG) and magnetoencephalography (MEG) are two complementary methods which are used for measuring the electric and magnetic potential of the brain [45]. The electromagnetic activity of the brain gives rise to an electric and magnetic potential which can be measured on the scalp (by electrodes) or outside the head by SQUID (Superconducting Quantum Interference) device.

Magnetoencephalography (MEG) is a technique for measuring the magnetic field induced by the electrical activity of neurons in the brain, classically modeled with current dipoles [31]. The electroencephalography (EEG) records variations of electrical potential at the surface of the scalp.

Both techniques are used for the investigations in neuroscience like the study and the care of certain cerebral disorders. These two techniques are complementary and can be measured simultaneously. Nowadays, EEG is relatively inexpensive and commonly used. MEG is, comparatively, more expensive because the SQUID device can be used just in a shielded room isolated from the ambient noise (sensitivity of the device due to the fact that the recorded magnetic potential is of a magnitude of one billion times smaller than the Earth magnetic potential).

Medical engineering aims to localize sources within the brain from measurements of the electromagnetic potential they produce (the inverse source MEG problem-(IP)). When a limited number of sources are modeled as pointwise and dipolar, in general there are more measurements than unknowns. In the literature of EEG-MEG source localization problem, there exists several families of methods to solve it, when sources can be modeled as the superposition of a small number of dipoles [45]:

- *Dipole fitting methods*: minimize a non-convex function, with an outcome that is unstable with respect to the number of dipoles in the model [18].

- The *MUSIC method* applies a principal component analysis to the measurements, identifies a "noise subspace" and a "signal subspace" and determines the dipole positions by analyzing the signal subspace [41].

- With *Beamforming method* the sources can be estimated by scanning the region of interest and by comparing the covariance of the measurement to that of the noise.

- In this thesis for solving the inverse M/EEG problem, we used the *rational approximation method* in planar sections of the 3D domains and show how the sources are recovered [8]. This method belongs to a new category of source estimation algorithms that are grounded in Harmonic Analysis and Best Approximation theory. This method, as well as MUSIC and Beamforming methods, requires no prior information on the number of sources. It works instant by instant and it does not require sources to be decorrelated across time.

Geometric model of the head

The simplified spherical model of the head that can be assumed is the union of three disjoint homogeneous spherical layers $\mathbb{B}_0$, $\mathbb{B}_1$, $\mathbb{B}_2$, namely the brain, the skull and the scalp. The spheres which separate these volumes are denoted by $\mathbb{S}_0, \mathbb{S}_1, \mathbb{S}_2 = \mathbb{S}$. The main source model available for describing the neuronal activity is the dipolar model described by their number, positions and moments. For practical reasons, the data are available only on the outer layer (scalp) by electrodes. For the resolution of the inverse problem, the APICS team uses a technique which consists to decompose the 3 dimensional problem in some others 2 dimensional problems for which rational approximation techniques are applied (ARL2 theory, for more details see Chapter 5).

For EEG inverse problem we need to pass by a step called «cortical mapping» which allows to propagate the data from the scalp to the interior shell: the brain. In MEG, for the spherical model, this step is not necessary because the data measurements depend only on the primary current and not anymore on conductivities [45].

1.4 Unified framework

In practice the measured data (electric, magnetic or gravitational potential) are generally available just over a region $\Theta \subset \mathbb{S}$ or $\Theta \subset \mathbb{S}_R, R \geq 1$ (the nord hemisphere-M/EEG or satellite orbits-geodesy). Disposing of the partial data, we want to estimate this data over the whole sphere $\mathbb{S}$, that means to propagate the data potential from the region Θ of $\mathbb{S}_R$ to the sphere $\mathbb{S}$ (geodesy, MEG) or directly

from $\Theta \subset \mathbb{S}$ to whole sphere $\mathbb{S}$. This step called transmission inverse data problem (TP) will be detailled in Chapter 4.

After having the data over the sphere $\mathbb{S}$, we solve the inverse problem (DR) which consists to localize the density inside the ball $\mathbb{B}$. An "intermediate" step to this problem is the (SR) problem which suppose to approximate the density by pointwise sources and hence to localize the discrete density, as an approximate of the continuous density. Source recovery problem from exterior measurements is an ill-posed inverse problem in the sense of Hadamard: formally, it is unstable and, in the distributed source case, non-unique. Constraints, or regularization, are necessary in order to guarantee a unique and stable solution [29].
We say that a problem is not well-posed if one of the next conditions are satisfied:

- it is not solvable (existence of solution);
- it is not uniquely solvable (uniqueness);
- the solution does not depend continuously on the data (stability)

1.5 Overview

Chapter 1 presents an introduction around the geodesy and M/EEG inverse problems. In **Chapter 2** we introduce the background necessary for the study of the problems of this thesis. As it was briefly described, the resolution of the inverse problem (IP) involves the resolution of two problems: the transmission data (TP) and density recovery (DR) problem. In practice, as we know, the data are available just on some regions as the north hemisphere of the head (M/EEG) or continents, spherical caps, etc. (geodesy). For this purpose, we will build a new adaptative basis on which we express the data. The **Chapter 3** provides a new efficient method for building the convenient Slepian basis. The step which consists in passing from the partial data expressed in the new Slepian basis, to data over the whole sphere $\mathbb{S}$ and expressed in spherical harmonic basis, is called the transmisson data problem (TP). For more details, see **Chapter 4**. The second step of the (IP) resolution problem is the density recovery (DR) problem, see **Chapter 5**. In **Chapter 6** we present some numerical tests to illustrate the sources localization for geodesy and M/EEG problems when we dispose of partial data.

The main contributions of this work concern:

- the development of a quadrature method for the construction of Slepian bases functions on the sphere, together with a study of numerical aspects concerning

their use for the representation of potentials on a sphere from partial data (data transmission);

- the application of best quadratic rational approximation techniques on planar sections (circles) to the extended potential, especially for geophysical issues where the gravitational potential is generated by a special piecewise continuous density, and in medical engineering, for electroencephalography (and a current density with pointwise dipolar sources). Numerical experiments are provided and discussed (see also [33]).

Chapter 2

Notations, backgrounds, main problems

In this chapter, we will introduce the main notations and definitions that we use throughout this thesis and that are necessary for the well comprehension of the next chapters.

2.1 Notations, definitions

The function space $L^2(\mathcal{B})$ represents the set of all square-Lebesgue integrable functions from a domain $\mathcal{B} \subset \mathbb{R}^n$ into $\mathbb{R}$. The space $L^2(\mathcal{B})$ is equipped with the inner product [19]:

$$\langle f, g \rangle_{L^2(\mathcal{B})} := \int_{\mathcal{B}} f(x)g(x)\mathrm{d}x \quad f, g \in L^2(\mathcal{B}) \tag{2.1}$$

and the norm $\|f\|_{L^2(\mathcal{B})} := \sqrt{\langle f, f \rangle}_{L^2(\mathcal{B})}$. In this thesis, for simplicity, we will index the $L^2(\mathcal{B})$ norm of a function f just by the domain, i.e. $\|f\|_{\mathcal{B}}$. The same remark is valid for the scalar product (2.1), i.e. $\langle f, g \rangle_{\mathcal{B}}$. For $p \neq 2$, we denote the L^p norms of f by $\|f\|_{L^p(\mathcal{B})}$.
If $\mathcal{B} = [a, b]$ and the product is defined in terms of a weighted function $\omega : [a, b] \to \mathbb{R}$, we note it by $\langle f, g \rangle_{\omega}$.

2.2 Harmonic functions and elliptic partial derivative equations

A function F is called *harmonic function on* $\mathbb{R}^n$ if it is solution of Laplace equation [19]:

$$\Delta F = 0 \tag{2.2}$$

More precisely, a function is called *harmonic* in a region $\mathcal{B} \subset \mathbb{R}^n$ if it satisfies equation of Laplace at every point of $\mathcal{B}$.

Definition 2.2.1. *Let $\mathcal{L}$ be a linear differential operator of order m with constant coefficients acting on functions $f : \mathcal{B} \to \mathbb{E}$ of k variables. Thus*

$$(\mathcal{L}f)(x) = \sum_{|\alpha| \leq m} A_\alpha (\frac{\partial^{|\alpha|} f}{\partial x_1^{\alpha_1} \dots \partial x_k^{\alpha_k}})(x)$$

where $\mathbb{E}$ is a given finite-dimensional vector space (typically $\mathbb{E} = \mathbb{R}^p$ or $\mathbb{C}^p$, $p > 1$). Here $\alpha_i, i = 1, 2, \dots, k$ are nonnegative integers, $\alpha = (\alpha_1, \alpha_1, \dots, \alpha_k)$,$|\alpha| = \alpha_1 + \alpha_2 + \dots \alpha_k$ and A_α are the coefficients. The linear partial differential operator $\mathcal{L}$ is said to be strongly elliptic if for every $\xi \in \mathbb{S}^{k-1}$ and unit vector $\mathbf{e} \in \mathbb{E}$,

$$Re\langle \mathcal{P}_m(\xi)\mathbf{e}, \mathbf{e}\rangle_{\mathbb{E}} > \mathbf{0}$$

where $\mathcal{P}_m$ is called principal symbol and is given by:

$$\mathcal{P}(\xi) = \mathcal{P}_m(\xi) = \sum_{|\alpha|=m} \xi^\alpha A_\alpha, \xi^\alpha = \xi_1^\alpha \dots \xi_k^\alpha \in \mathbb{R}$$

for $\xi \in \mathbb{R}^k$.

In this thesis we consider the Laplace elliptic operator of order $m = 2$ in $k = 3$ variables:

$$\Delta f(x) = \frac{\partial^2 f}{\partial x_1^2} + \frac{\partial^2 f}{\partial x_2^2} + \frac{\partial^2 f}{\partial x_3^2}$$

Definition 2.2.2. *We recall the Sobolev spaces $W^{m,p}(\mathcal{B}), m \in \mathbb{Z}^+, 1 \leq p \leq \infty$ of a open domain $\mathcal{B}$:*

$$W^{m,p} = \{u \in L^p(\mathcal{B}) : D^\alpha(u) \in L^p(\mathcal{B}), for\ 0 \leq |\alpha| \leq m\} \tag{2.3}$$

A general stability property for the Neumann problems is given by the following theorem:

Theorem 2.2.1. *[14] Given a bounded domain $\mathcal{B}$ with a C^2-boundary Γ, then the Neumann problem:*

$$\begin{cases} \Delta u = f \in W^{r,2}(\mathcal{B}), r \geq -1 \\ \partial_n u = g \in W^{s,2}(\Gamma), s \in \mathbb{R} \end{cases} \tag{2.4}$$

has a solution $u \in W^{\alpha,2}(\mathcal{B})$, $\alpha = \min(r+2, s+\frac{3}{2})$ *if and only if:*

$$\int_\Gamma g \mathrm{d}\gamma = \int_\mathcal{B} f \mathrm{d}x$$

is verified, where $\mathrm{d}\gamma$ *is a measure on* Γ. *If* u *is a solution,* $u+c$ *is also a solution for* $\forall c \in \mathbb{R}$. *More, we have:*

$$\inf_{c\in\mathbb{R}} \|u+c\|_{W^{\alpha,2}(\mathcal{B})} \leq C(\|f\|_{W^{\alpha,2}(\mathcal{B})} + \|g\|_{W^{s,2}(\Gamma)}),$$

where the constant C *depends just on* $\mathcal{B}$.

2.2.1 Fundamental solutions and Green functions

The fundamental solution of Laplacian (2.2) in $\mathbb{R}^n$ is a distribution $E_n \in \mathbb{R}^n$ which is solution of Poisson equation [19]:

$$\Delta E_n = \delta \text{ on } \mathbb{R}^n, \tag{2.5}$$

with

$$\begin{cases} E_n(x) = \frac{1}{n(2-n)\omega_n}|x|^{2-n}, & n > 2,\ x \in \mathbb{R}^n; \\ E_2(x) = \frac{1}{2\pi}\log|x|, \end{cases}$$

with $\omega_n = -(n-2)\sigma_n$, where σ_n is the total surface of the sphere in $\mathbb{R}^n$. E_n verifies (2.5) and is the *fundamental solution of Laplacian*. We introduce also the *Green function* over the ball $\mathbb{B}(x_0, r_0) := \mathbb{B}_{r_0}$.

$$G(x,x_0) = G(x_0,x) = \begin{cases} E_n(x-x_0) - E_n(x_0), & n \geq 3; \\ \frac{1}{2\pi}\log\frac{|x-x_0|}{r_0}, & n = 2. \end{cases} \quad \text{with } r_0 = |x_0|.$$

Related also to the fundamental solution of Laplacian, we introduce the simple and double layer potential. If $\varphi \in C^0(\mathbb{S})$, then the expression:

$$u_1(x) = \int_\mathbb{S} E_n(\sigma - x)\varphi(\sigma)\mathrm{d}\omega(\sigma),\ \sigma \in \mathbb{S}$$

is everywhere defined on $\mathbb{R}^n$ and it is called *single layer potential* [14].

$$u_2(x) = \int_\mathbb{S} \frac{\partial}{\partial n} E_n(\sigma - x)\varphi(\sigma)\mathrm{d}\omega(\sigma) = \frac{1}{\sigma_n}\int_\mathbb{S} \Sigma \frac{(\sigma_i - x_i)n_i(\sigma)}{|\sigma - x|^n}\varphi(\sigma)\mathrm{d}\omega(\sigma)$$

It is called *double layer potential*, where $\varphi(\sigma)\mathrm{d}\omega(\sigma)$ is a measure on $\mathbb{S}$, $n(\sigma)$ is the vector normal to $\mathbb{S}$ in $\sigma \in \mathbb{S}$ and exterior to $\mathbb{B}$.

Proposition 2.2.1. *Given* $\mathbb{B}_{r_0}$ *and* $u \in \mathcal{H}(\mathbb{B}_{r_0}) \cap \mathcal{C}^0(\overline{\mathbb{B}}_{r_0})$. *For* $\forall x \in \mathbb{B}_{r_0}$, *we have the Poisson formula:*

$$u(x) = \frac{1}{r_0 \sigma_n} \int_{\mathbb{S}_{r_0}} \frac{r_0^2 - |x - x_0|^2}{|t - x|^n} u(t) \mathrm{d}w_{r_0}(t), \tag{2.6}$$

where $\mathrm{d}w_{r_0}(t)$ *is a measure on the sphere* $\mathbb{S}_{r_0}$ *and* $\mathcal{H}(\mathbb{B}_{r_0})$ *is the space of the harmonic functions on* $\mathbb{B}_{r_0}$.

2.2.2 Mean-value property

Theorem 2.2.2. *[19]* ***Mean-value property for the ball*** *Given* $\mathbb{B}_{r_0}$, u *harmonic and* $u \in L^1(\mathbb{B}_{r_0})$, *we have:*

$$u(x_0) = \frac{n}{\sigma_n r_0^n} \int_{\mathbb{B}_{r_0}} u(x) \mathrm{d}x = \frac{n}{\sigma_n r_0^{n-1}} \int_{\mathbb{B}} u(x_0 + r_0 y) \mathrm{d}y.$$

where σ_n / n *is the volume of the unit ball* $\mathbb{B}$.

Theorem 2.2.3. *[19]* ***Mean-value property for the sphere*** *Given* $\mathbb{B}_{r_0}$, u *harmonic and* $u \in \mathcal{C}^0(\overline{\mathbb{B}}_{r_0})$, *for every* x, *we have:*

$$u(x_0) = \frac{1}{\sigma_n r_0^{n-1}} \int_{\mathbb{S}_{r_0}} u(t) \mathrm{d}\omega_{r_0}(t) = \frac{1}{\sigma_n r_0^{n-2}} \int_{\mathbb{S}} u(x_0 + r_0 \sigma) \mathrm{d}\omega(\sigma).$$

2.3 Data representation

In solving theoretical and mathematical physical problems, we usually use various special functions. Such kind of problems we can find in connection with heat conduction, propagation of electromagnetic or acoustic waves, etc. Usually, the special functions are solutions of differential equations. In the following we introduce several classes of special functions as: the classical orthogonal polynomials (Jacobi, Laguerre, Hermite, Legendre), spherical harmonics, Bessel and hypergeometric functions [4, 52].

2.3.1 Orthogonal polynomials

General properties

In the literature of orthogonal polynomials, there exists many definitions of orthogonality [4, 52].

Let be $[a, b] \subset \mathbb{R}$. The simplest way to say that two polynomials $p(x)$ and $q(x)$ are *orthogonal* is to write the inner product $\langle p, q\rangle = 0$. The operator $\langle \cdot, \cdot \rangle$ is defined in terms of the integral of a weighted product $\langle p, q\rangle_\omega = \int_a^b p(x)q(x)\omega(x)\mathrm{d}x$, with $\mathrm{d}\omega(x) = \omega(x)\mathrm{d}x$, where $\omega : [a, b] \to \mathbb{R}$ is a weight function.

A sequence of polynomials $p_0, p_1, p_2, \ldots$ is called *sequence of orthogonal polynomials* if p_n is of degree n and all distinct members of the sequence are orthogonal between them.

To construct a sequence of orthogonal polynomials, one may use the Gram-Schmidt procedure. For this, we define a projection operator on the polynomials as: $\mathrm{proj}_f(g) = \dfrac{\langle f, g\rangle}{\langle f, f\rangle} f = \dfrac{\int_a^b f(x)g(x)\mathrm{d}x}{\int_a^b (f(x))^2\mathrm{d}x} f(x), [a, b] \subset \mathbb{R}$. To apply the algorithm, we define our set of original polynomials $g_1, g_2, \ldots, g_k$ by $g_p(x) = x^p, p = 1, \ldots, k$ which generate a sequence of orthogonal polynomials $f_1, f_2, \ldots, f_k$ using:

$$
\begin{aligned}
f_1 &= g_1, \\
f_2 &= g_2 - \mathrm{proj}_{f_1}(g_2), \\
f_3 &= g_3 - \mathrm{proj}_{f_1}(g_3) - \mathrm{proj}_{f_2}(g_3), \\
&\vdots \\
f_k &= g_k - \sum_{j=1}^{k-1} \mathrm{proj}_{f_j}(g_k).
\end{aligned}
$$

Here, the polynomials are supposed to be dense in $L^2[a, b]$.

A second method which can be used for the construction of orthogonal polynomials is given by the following method of moments:
Let $\mu_n = \int_{\mathbb{R}} x^n \mathrm{d}\omega$ be the moments of a measure $\mathrm{d}\omega$. Then the polynomial sequence defined by:

$$p_n(x) = \det \begin{bmatrix} \mu_0 & \mu_1 & \mu_2 & \cdots & \mu_n \\ \mu_1 & \mu_2 & \mu_3 & \cdots & \mu_{n+1} \\ \mu_2 & \mu_3 & \mu_4 & \cdots & \mu_{n+2} \\ \vdots & \vdots & \vdots & & \vdots \\ \mu_{n-1} & \mu_n & \mu_{n+1} & \cdots & \mu_{2n-1} \\ 1 & x & x^2 & \cdots & x^n \end{bmatrix}$$

is a sequence of orthogonal polynomials with respect to the measure $\mathrm{d}\omega$ on $\mathbb{R}$. For more details, see [3, 35].

This section is devoted to present the properties of the orthogonal polynomials. Orthogonal polynomials are frequently used to construct highly accurate Gaussian quadrature associated with some weight function ω on $[a, b]$.
The following properties of the orthogonal polynomials are from [4].

Definition 2.3.1. *We say that a sequence of polynomials $\{p_n(x)\}_0^\infty$, where $p_n(x)$ has exact degree n, is orthogonal with respect to the measure $\mathrm{d}\omega(x)$ on $[a, b]$ if:*

$$\int_a^b p_n(x)p_m(x)\mathrm{d}\omega(x) = h_n\delta_{mn}. \tag{2.7}$$

Theorem 2.3.1. ***Three-term recurrence relation**: A sequence of orthogonal polynomials $\{p_n(x)\}$ satisfies:*

$$p_{n+1}(x) = (A_n x + B_n)p_n(x) - C_n p_{n-1}(x) \text{ for } n \geq 0,$$

where we set $p_{-1}(x) = 0$. Here A_n, B_n and C_n are real constants, $n = 0, 1, 2, \ldots$ and $A_{n-1}A_nC_n > 0$, $n = 1, 2, \ldots$. If the highest coefficient of $p_n(x)$ is $k_n > 0$, then

$$A_n = \frac{k_{n+1}}{k_n}, C_{n+1} = \frac{A_{n+1}}{A_n}\frac{h_{n+1}}{h_n},$$

where h_n is given by (2.7).

An other useful general property of orthogonal polynomials is the following Christofell Darboux formula:

Theorem 2.3.2. ***Christofell-Darboux formula**: Suppose that the $p_n(x)$ are normalized so that:*

$$h_n = \int_a^b p_n^2(x)\mathrm{d}\omega(x) = 1.$$

Then

$$\sum_{m=0}^{n} p_m(y)p_m(x) = \frac{k_n}{k_{n+1}} \frac{p_{n+1}(x)p_n(y) - p_{n+1}(y)p_n(x)}{x-y}, \tag{2.8}$$

where k_n is the highest coefficient of $p_n(x)$.
When $h_n = 1$ and $x = y$, then:

$$\sum_{k=0}^{n} p_k^2(x) = \frac{k_n}{k_{n+1}}(p'_{n+1}(x)p_n(x) - p_{n+1}(x)p'_n(x))$$

with $p'_{n+1}(x)p_n(x) - p_{n+1}(x)p'_n(x) > 0$ for all x.

Remark 2.3.1. *If $h_n \neq 1$, then (2.8) takes the form:*

$$\sum_{m=0}^{n} \frac{p_m(y)p_m(x)}{h_m} = \frac{k_n}{k_{n+1}} \frac{p_{n+1}(x)p_n(y) - p_{n+1}(y)p_n(x)}{(x-y)h_n} \text{ for } x \neq y.$$

For $x = y$, we have:

$$\sum_{m=0}^{n} \frac{(p_m(x))^2}{h_m} = \frac{k_n}{h_n k_{n+1}}(p_{n+1}(x)p_n(x) - p_{n+1}(x)p_n(x)).$$

Remark 2.3.2. *Given a sequence of polynomials $\{p_n(x)\}$ orthogonal with respect to a measure $\omega(x)$, the coefficients $a(k,m,n)$ in*

$$p_m(x)p_n(x) = \sum_{k=0}^{m+n} a(k,m,n)p_k(x)$$

are given by:

$$a(k,m,n) = \frac{1}{h_k} \int_I p_m(x)p_n(x)p_k(x)\mathrm{d}\omega(x). \tag{2.9}$$

A very important class of orthogonal polynomials arises from a differential equation of the form, see [35]:

$$Q(x)\, f'' + L(x)\, f' + \lambda f = 0, \tag{2.10}$$

where Q is a given at most quadratic polynomial, and L is a given linear polynomial. The function f, and the constant λ, are to be found. Letting D be the differential operator, $D(f) = Qf'' + Lf'$, and changing the sign of λ, the problem is to find the eigenvectors (eigenfunctions) f and the corresponding eigenvalues λ, such that f does not have singularities and $D(f) = \lambda f$. The solutions of this differential equation

have singularities unless λ takes on specific values. There is a sequence of numbers $\lambda_0, \lambda_1, \lambda_2, \ldots$ that lead to a sequence of polynomial solutions $P_0, P_1, P_2, \ldots$. If Q is actually quadratic, it has two distinct real roots, the root of L lies strictly between the roots of Q, and the leading terms of Q and L have the same sign. Fore more details see [3]. Letting $R(x) = e^{\int \frac{L(x)}{Q(x)}\,dx}$, the polynomials are orthogonal under the weight function $W(x) = \dfrac{R(x)}{Q(x)}$. Because of the constant of integration, the quantity $R(x)$ is determined only up to an arbitrary positive multiplicative constant.
Also, under the previous section, we have $\lambda_n = -n\left(\dfrac{n-1}{2}Q'' + L'\right)$. Since Q is quadratic and L is linear, Q'' and L' are constants, so these are just real numbers.
Note that the orthogonal polynomial, $p_n(x)$ is proportional to $\dfrac{1}{\omega(x)}\,\dfrac{\mathrm{d}^n}{\mathrm{d}x^n}\left(\omega(x)[Q(x)]^n\right)$.
In fact, we have the normalized polynomial:

$$p_n(x) = \frac{\mu}{\omega(x)}\frac{\mathrm{d}^n}{\mathrm{d}x^n}\left(\omega(x)[Q(x)]^n\right) \tag{2.11}$$

with μ a normalizing constant. This is known as Rodrigues formula [4, 52]. We distinguish the follow cases:

1. $a = -1$, $b = +1$, $\omega(x) = (1+x)^\alpha(1-x)^\beta$, $\alpha > -1$, $\beta > -1$.
   Then, except for a constant factor, the orthogonal polynomial $p_n(x)$ is the *Jacobi polynomial* $P_n^{(\alpha,\beta)}(x)$.

   If $\alpha = \beta$, there are some special cases, excepting the constant factors:

   (a) for $\alpha = \beta = -\frac{1}{2}$ the *Chebychev polynomials* of first kind;

   (b) for $\alpha = \beta = +\frac{1}{2}$ the *Chebychev polynomials* of second kind;

   (c) for $\alpha = \beta = 0$ we have the *Legendre polynomials*.

2. $a = 0$, $b = +\infty$, $\omega(x) = \mathrm{e}^{-x}x^\alpha, \alpha > -1$.
   In this case, $p_n(x)$ is except for a constant, the *Laguerre polynomial* $L^\alpha(n)$;

3. $a = -\infty, b = \infty$, $\omega(x) = \mathrm{e}^{-x^2}$.
   In this case, $p_n(x)$ is, save for a constant factor, the *Hermite polynomial* $H_n(x)$.

Zeros of orthogonal polynomials

It is important to mention that orthogonal polynomials have the same general properties concerning the number of their zeros and the way to compute these zeros.

Theorem 2.3.3. *[4] Suppose that $\{p_n(x)\}$ is a sequence of orthogonal polynomials with respect to the distribution $\mathrm{d}\omega(x)$ on the interval $[a,b]$. Then $p_n(x)$ has n simple zeros in $[a,b]$.*

Proposition 2.3.1. *If $\{p_n(x)\}$ satisfies the three term recursive formula (2.3.1), then:*

$$p_n(x) = \det \begin{bmatrix} A_0x+B_0 & 1 & 0 & 0 & 0 \\ C_1 & A_1x+B_1 & 1 & 0 & 0 \\ 0 & C_2 & A_2x+B_2 & 1 & 0 \\ \vdots & \ddots & \ddots & & \vdots \\ & & & A_{n-2}x+B_{n-2} & 1 \\ 0 & & & C_{n-1} & A_{n-1}x+B_{n-1} \end{bmatrix}.$$

More, under the hypothse that $A_n = 1, \forall n$ and $C_n = |d_n|^2 = d_n\overline{d}_n$, then the zeros of $p_n(x)$ are the eigenvalues of the matrix:

$$M = \begin{bmatrix} -B_0 & d_1 & 0 & \dots & 0 & 0 & 0 & 0 \\ \overline{d}_1 & -B_1 & d_2 & \dots & & 0 & 0 & 0 \\ 0 & \overline{d}_2 & -B_2 & d_3 & & & & \vdots \\ \vdots & \ddots & \ddots & & \ddots & & & \\ & & & & & & 0 & 0 \\ 0 & & & & & \overline{d}_{n-2} & -B_{n-2} & d_{n-1} \\ 0 & & & & & 0 & \overline{d}_{n-1} & -B_{n-1} \end{bmatrix}.$$

We note that the matrix M is an Hermetian matrix, with $B_n \in \mathbb{R}$.

2.3.2 Legendre polynomials and functions, Gauss Legendre quadrature formula

For $a = -1, b = 1$ we have the special case of orthonormal polynomials, called *Legendre polynomials* [4].

They are given by the formula:

$$P_n(x) = \frac{1}{2^n n!}\frac{\mathrm{d}^n}{\mathrm{d}x^n}(x^2-1)^n. \tag{2.12}$$

The Legendre polynomials form a complete orthogonal set of $L^2[-1,1]$:

$$\int_{-1}^{1} P_{n'}(x)P_n(x)\mathrm{d}x = \frac{2}{2n+1}\delta_{n'n}. \tag{2.13}$$

By using Theorem 2.3.2, the relations (2.12) and (2.13), one gets the following recursion formula for Legendre polynomials:

Remark 2.3.3. ***Recursive formula****:*

$$P_0(x) = 1, P_1(x) = x, P_n(x) = -\frac{n-1}{n}P_{n-2}(x) + \frac{2n-1}{n}xP_{n-1}(x). \tag{2.14}$$

Since the Legendre polynomials form a complete set of $L^2[-1,1]$, any function $f(x) \in L^2[-1,1]$ can be expanded in terms of them:

$$f(x) = \sum_{n=0}^{\infty} A_n P_n(x), \tag{2.15}$$

where

$$A_n = \frac{2n+1}{2}\int_{-1}^{1} f(x)P_n(x)\mathrm{d}x.$$

We note that it is possible to compute the successive derivatives of the Legendre polynomials in an explicit manner. This is done as follows. If $P_n^{(\alpha,\beta)}(x)$ denote the Jacobi polynomials, then we have [4]:

Proposition 2.3.2.

$$\frac{\mathrm{d}}{\mathrm{d}x}P_n^{(\alpha,\beta)}(x) = \frac{n+\alpha+\beta+1}{2}P_{n-1}^{(\alpha+1,\beta+1)}(x).$$

Consequently, it is easy to see that $\forall k,\ 0 \leq k \leq n$*, we have:*

$$\frac{\mathrm{d}^k}{\mathrm{d}x^k}P_n^{(\alpha,\beta)}(x) = \frac{n+\alpha+\beta+1}{2}\cdot\frac{n+\alpha+\beta+2}{2}\cdot\ldots\cdot\frac{n+\alpha+\beta+k}{2}P_{n-k}^{(\alpha+k,\beta+k)}(x).$$

If now, we take $\alpha = \beta = 0$ *one gets the* k*-derivative of Legendre polynomials* P_n *in function of the Jacobi polynomials* $P_{n-k}^{(k,k)}$*:*

$$\frac{\mathrm{d}^k}{\mathrm{d}x^k}P_n(x) = \frac{n+1}{2}\cdot\frac{n+2}{2}\cdot\ldots\cdot\frac{n+k}{2}P_{n-k}^{(k,k)}(x). \tag{2.16}$$

Remark 2.3.4. *We denote the Legendre polynomial $P_n^{(0,0)}(x)$ by $P_n(x)$.*

We introduce Legendre function $g(\theta) = P_{nm}(\cos\theta)$ as a solution of Legendre differential equation:

$$g''(\theta)\sin\theta + g'(\theta)\cos\theta + \left[n(n+1)\sin\theta - \frac{m^2}{\sin\theta}\right]g(\theta) = 0,\ 0 \le \theta \le \pi. \tag{2.17}$$

The subscript n is the degree and the subscript m the order of P_{nm}.

It is convenient to transform Legendre differential equation (2.17) by the substitution $x = \cos\theta \in [-1, 1]$. We use overbar to denote g as a function of x. Using this and the substitutions:

$$\begin{aligned} g(\theta) &= \overline{g}(x), \\ g'(\theta) &= \frac{\mathrm{d}g}{\mathrm{d}\theta} = \frac{\mathrm{d}g}{\mathrm{d}x}\frac{\mathrm{d}x}{\mathrm{d}\theta} = -\overline{g}'(x)\sin\theta, \\ g''(\theta) &= \overline{g}''(x)\sin^2\theta - \overline{g}'(x)\cos\theta \end{aligned}$$

and then substituting $\sin^2\theta = 1 - x^2$, we get:

$$(1-x^2)\overline{g}''(x) - 2x\overline{g}'(x) + \left[n(n+1) - \frac{m^2}{1-x^2}\right]\overline{g}(x) = 0,\ x \in [-1, 1]. \tag{2.18}$$

The Legendre function $P_{nm}(x)$ is defined by :

$$P_{nm}(x) = \frac{1}{2^n n!}(1-x^2)^{\frac{m}{2}}\frac{\mathrm{d}^{n+m}}{\mathrm{d}x^{n+m}}(x^2-1)^n. \tag{2.19}$$

For fixed m the functions $P_{nm}(x)$ form an orthogonal set on the interval $-1 \le x \le 1$. They satisfy:

$$\int_{-1}^{1} P_{n'm}(x)P_{nm}(x)\mathrm{d}x = \frac{2}{2n+1}\frac{(n+m)!}{(n-m)!}\delta_{n'n}.$$

We introduce also the normalized associated Legendre functions $\overline{P}_{nm}$:

$$\overline{P}_{nm}(x) := \sqrt{\frac{(2n+1)}{2}\frac{(n-m)!}{(n+m)!}}P_{nm}(x). \tag{2.20}$$

Remark 2.3.5. *For $m = 0$ in (2.19) we obtain the Legendre polynomials.*

In the following, we introduce the addition theorem for Legendre polynomials:

Theorem 2.3.4. *Given two points (θ, ϕ_1) and (θ', ϕ_2) on the unit sphere, we have the identity [4]:*

$$\begin{aligned} & P_n(\cos\theta\cos\theta' + \sin\theta\sin\theta'\cos\phi) \\ = \;& P_n(\cos\theta)P_n(\cos\theta') + 2\sum_{m=1}^{n}\frac{(n-m)!}{(n+m)!}P_{nm}(\cos\theta)P_{nm}(\cos\theta')\cos(m\phi), \end{aligned} \tag{2.21}$$

where $\phi = \phi_1 - \phi_2$ is the spherical distance between (θ, ϕ_1) and (θ', ϕ_2).

Gaussian quadrature formula

We want to approximate an integral which can not be evaluated exactly.
Let us consider $\{P_n(x), n \in \mathbb{N}\}$ a sequence of polynomials orthogonal with respect to measure $\mathrm{d}\omega$:

$$\int_a^b P_n(x)P_m(x)\mathrm{d}\omega(x) = 0, \quad \text{for } m \neq n. \tag{2.22}$$

Let x_j, $j = 1, 2, \ldots, n$ denote the zeros of $P_n(x)$.

Theorem 2.3.5. *[4] Using the above notations, there are positive numbers $\lambda_1, \lambda_2, \ldots, \lambda_n$ such that for every polynomial $f(x)$ of degree at most $2n-1$:*

$$\int_a^b f(x)\mathrm{d}\omega(x) = \sum_{j=1}^{n}\lambda_j f(x_j). \tag{2.23}$$

Remark 2.3.6. *If $f(x)$ is not a polynomial of degree $\leq 2n-1$, then (2.23) is not exact, but we have an approximation of the integral by the finite left sum.*

Remark 2.3.7. *Gauss considered the case where $\mathrm{d}\omega(x) = \mathrm{d}x$, Lebesgue measure on $\mathbb{R}$ in Theorem 2.3.5. The orthogonal polynomials are then the Legendre polynomials for the interval $[-1, 1]$ introduced in Section 2.19.*

For an interval $[a, b]$, the integral is approximated by the finite sum:

$$\int_a^b f(x)\mathrm{d}x \simeq \sum_{j=1}^{n}\lambda_j f(x_j),$$

where the nodes x_j are the roots of the Legendre polynomials $P_n(x)$ and the weights λ_j are given by the formula:

$$\lambda_j = -\frac{a_{n+1}}{a_n}\frac{1}{P_{n+1}(x_j)P_n'(x_j)}, \tag{2.24}$$

where a_n denotes the coefficient of x^n in P_n.
The error of the Gaussian quadrature is given as follows:

$$\int_a^b f(x)\mathrm{d}x = \sum_{k=1}^{n} \lambda_k f(x_k) + \frac{1}{a_n^2}\frac{f^{(2n)}(\eta)}{(2n)!}\int_a^b P_n^2(x)\mathrm{d}x, a \leq \eta \leq b. \tag{2.25}$$

2.3.3 Fourier expansion

We identify $\mathbb{R}^2 = \{(x, y)\}$ by the complex space $\mathbb{C} = \{z = x + iy = R\mathrm{e}^{i\theta}\}$ and the unit circle by $\{\mathrm{e}^{i\theta}; \theta \in \mathbb{R}\}$.
Using the theory of Fourier series, we know that on the unit circle, every $f \in L^2(\mathbb{T})$ has an expansion of the form:

$$f(\mathrm{e}^{i\theta}) = \sum_{n\in\mathbb{Z}} f_n \mathrm{e}^{in\theta} = \sum_{n\geq 0} f_n \mathrm{e}^{in\theta} + \sum_{n<0} f_n \mathrm{e}^{in\theta} = f_+(\mathrm{e}^{i\theta}) + f_-(\mathrm{e}^{i\theta}),$$

where

$$f_+(z) = \sum_{n\geq 0} f_n z^n,$$
$$f_-(z) = \sum_{n<0} f_n z^n.$$

For $z = r\mathrm{e}^{i\theta}$ we have:

$$f_+(z) = \sum_{n\geq 0} f_n r^n \mathrm{e}^{in\theta},$$
$$f_-(z) = \sum_{n<0} f_n r^n \mathrm{e}^{in\theta} = \sum_{n>0} f_{-n} r^{-n} \mathrm{e}^{-in\theta}.$$

Given $f_+(z) = \sum_{n\geq 0} f_n z^n$ and $h_-(z) = \sum_{k>0} h_k z^{-k}$, the inner product is computed as:

$$< f_+, h_- >_{L^2(\mathbb{T})} = Re \int_0^{2\pi} f_+(\mathrm{e}^{i\theta}) h_-(\mathrm{e}^{i\theta}) \frac{\mathrm{d}\theta}{2\pi} = Re \sum_{n,k} f_n \overline{h}_k \int_0^{2\pi} \mathrm{e}^{i(n+k)\theta} \frac{\mathrm{d}\theta}{2\pi} = 0, k > 0, n \geq 0.$$

Proposition 2.3.3. *Recall briefly that a function f_+ is analytic in $\mathbb{D}$ if and only if $f_+(z) = u(x, y) + iv(x, y)$, where u and v are conjugate harmonic functions (they satisfy the Cauchy-Riemann equations):*

$$\frac{\partial u}{\partial x} = \frac{\partial v}{\partial y},$$
$$\frac{\partial v}{\partial x} = -\frac{\partial u}{\partial y},$$

2.3.4 Hardy spaces

Given f an analytic function on the disk denoted by $\mathbb{D}$, we define:

$$M_2(f,r) = \Big[\frac{1}{2\pi}\int_{-\pi}^{\pi} |f(r\exp^{i\theta})^2|\mathrm{d}\theta\Big]^{\frac{1}{2}} \text{ and } M_\infty(f,r) = \sup_\theta |f(re^{i\theta})|,$$

where r, θ are polar coordinates on $\mathbb{D}$.

$$\|f\|_p = \lim_{r\to 1} M_p(f,r),\ p = 2,\infty.$$

The Hardy spaces $H^p(\mathbb{D}), p = 2,\infty$ are defined being the set of the holomorphic functions f on $\mathbb{D}$ such that $\|f\|_p < \infty$ [44].

Definition 2.3.2. $\overline{H}_0^2(\mathbb{D})$ *Hardy space is the orthogonal complementary of* $H^2(\mathbb{D})$ *on* $L^2(\mathbb{T})$*:*

$$L^2(\mathbb{T}) = H^2(\mathbb{D}) \oplus \overline{H}_0^2(\mathbb{D}). \tag{2.26}$$

For $n \geq 3$, the analogous expansion for functions $f \in L^2(\mathbb{S})$ is got using the spherical harmonics instead of the exponentials $e^{in\theta}$, see the following Section.

2.3.5 Spherical harmonics

Laplace equation in spherical coordinates

In spherical coordinates (r,θ,ϕ), the Laplace equation (2.2) can be written in the following form, see [30]:

$$\frac{1}{r}\frac{\partial^2}{\partial r^2}(rF) + \frac{1}{r^2\sin\theta}\frac{\partial}{\partial\theta}\Big(\sin\theta\frac{\partial F}{\partial\theta}\Big) + \frac{1}{r^2\sin^2\theta}\frac{\partial^2 F}{\partial\phi^2} = 0. \tag{2.27}$$

The method of separation of variables is used to solve a wide range of linear partial differential equations with boundary and initial conditions, such as Laplace equation, heat equation, wave equation, and Helmholtz equation. Using the separation of variables, we look for F under the form:

$$F(r,\theta,\phi) = \frac{U(r)}{r}P(\theta)Q(\phi). \tag{2.28}$$

Substituting (2.28) into (2.27) we get:

$$Q(\phi) = \mathrm{e}^{\pm im\phi},\ m \text{ is a constant}$$

as solution of the equation

$$\frac{1}{Q}\frac{\mathrm{d}^2 Q}{\mathrm{d}\phi} = -m^2. \tag{2.29}$$

Moreover, P and U satisfy the two differential equations:

$$\frac{1}{\sin\theta}\frac{\mathrm{d}}{\mathrm{d}\theta}\Big(\sin\theta\frac{\mathrm{d}P}{\mathrm{d}\theta}\Big) + \Big[n(n+1) - \frac{m^2}{\sin^2\theta}\Big]P = 0 \tag{2.30}$$

$$\frac{\mathrm{d}^2 U}{\mathrm{d}r^2} - \frac{n(n+1)}{r^2}U = 0 \tag{2.31}$$

with $n(n+1)$ a real constant. The solution of (2.31) is :

$$U = A_n r^{n+1} + B_n r^{-n}.$$

The coefficients A_n and B_n will be determined from the boundary conditions of the problem. In (2.28), the solution of Laplace equation was decomposed into a product of factors for three variables r, θ and ϕ. Now, if we combine the angular factors, we construct orthonormal functions over the unit sphere. These functions are called *spherical harmonics* or *tesseral harmonics* in older books. The functions $Q_m(\phi) = \mathrm{e}^{im\phi},\ m \in \mathbb{Z}$ form a set of orthogonal functions on the interval $0 \leq \phi \leq 2\pi$. The functions $P_{nm}(\cos\theta)$ form a similar set in the index n for each m value on the interval $-1 \leq \cos\theta \leq 1$. Therefore their product $P_{nm}Q_m$ will form an orthogonal set on the surface of the unit sphere in the two indexes n, m. Using the normalization constant, given in [42], the suitable normalized spherical harmonics, denoted by $Y_{n,m}$ are given as follows:

$$Y_{nm}(\theta,\phi) = \sqrt{\frac{2n+1}{4\pi}\frac{(n-m)!}{(n+m)!}}\tilde{Y}_{nm}(\theta,\phi) \tag{2.32}$$

$$\int_{\mathbb{S}} Y_{nm}^2(\theta,\phi)\mathrm{d}\omega(\theta,\phi) = 1.$$

with

$$\tilde{Y}_{nm}(\theta,\phi) = P_{nm}(\cos\theta)\mathrm{e}^{im\phi}, \tag{2.33}$$

with P_{nm} the Legendre functions and $Q_m = \mathrm{e}^{im\phi}$. For $m = 0$ the spherical harmonic functions are identified with Legendre's polynomials, which as we have seen they have n zeros in the interval $-1 \leq t \leq 1$ ($0 \leq \theta \leq \pi$). Therefore, the spherical harmonics functions for $m = 0$, which in this case they do not depend on θ, they change their sign n times in the interval. Since they divide the sphere into zones, they are also called *zonal harmonics*.

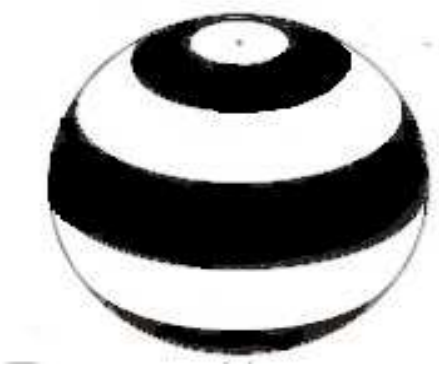

Figure 2.1: *Zonal spherical harmonics*

We notice that Y_{nm} can be also written as a product of a function $g(\theta)$ and $h(\phi)$ (method of separation of variables). The function g, respectively h verify the equation (2.18) and (2.29), respectively. We notice also that the Legendre functions P_{nm} verify the equation (2.30). Therefore, the solution of Laplace equation (2.2) can be written in terms of spherical harmonics and powers of r as:

$$F(r,\theta,\phi) = \sum_{n=0}^{\infty} \sum_{m=-n}^{n} \Big[A_{nm} r^n + B_{nm} r^{-(n+1)} \Big] Y_{nm}(\theta,\phi).$$

Dimension of the space of spherical harmonics

Let V_n be the vector space of homogeneous polynomials of degree n in k variables. Each polynomial $p \in V_n$ has the form [4, 19]:

$$p(x) = \sum_{|\alpha|=n} c_\alpha x^\alpha,$$

where $\alpha = (\alpha_1, \alpha_2, \ldots, \alpha_k), x = (x_1, x_2, \ldots, x_k), c_\alpha = c_{\alpha_1,\alpha_2,\ldots,\alpha_n}, x^\alpha = x_1^{\alpha_1} \cdot \ldots \cdot x_k^{\alpha_k}$ and $|\alpha| = \sum_{i=1}^k \alpha_i$, where α_i are nonnegative integers. The dimension of V_n is the number of k-tuples $(\alpha_1, \alpha_2, \ldots, \alpha_k)$ with $\sum_{i=1}^k \alpha_i = n$. For instance, in the case of two variables, the dimension of the space of harmonic polynomials of degree $n > 0$ is 2, but $d_{n,2} = n + 1$ (the number of solutions of $\sum_{i=1}^k \alpha_i = n$ with α_i nonnegative).

Remark 2.3.8. *The number of linearly independent harmonic polynomials of degree n in k variables is [42]:*

$$c_{n,k} = d_{n,k-1} + d_{n-1,k-1} = (2n + k - 2)\frac{(n + k - 3)!}{n!(k - 2)!}. \tag{2.34}$$

Observe that $c_{n,2} = 2$ and $c_{n,3} = 2n + 1$ for $n > 0$. In the special case where $k = 3$, (2.34) tells us that the space of spherical harmonic functions of degree n is a vector space of independent harmonic polynomials in 3 variables for a dimension $2n + 1$.

Orthogonality of spherical harmonics

On the space $L^2(\mathbb{S})$ of square integrable functions on $\mathbb{S}$, we have the inner product:

$$\langle f, g\rangle_{\mathbb{S}} = \int_{\mathbb{S}} f(\sigma)\overline{g}(\sigma)\mathrm{d}\omega(\sigma),\ \sigma \in \mathbb{S},\ f, g \in L^2(\mathbb{S}). \tag{2.35}$$

Here $\mathrm{d}\omega(\sigma) = \sin\theta \mathrm{d}\theta\mathrm{d}\phi, \sigma = (\theta, \phi) \in \mathbb{S}$ is the usual surface measure on the sphere.

Proposition 2.3.4. *Spherical harmonics of different degrees are orthogonal with respect to the inner product (2.35). Moreover, they verify:*

$$\langle Y_{nm}, Y_{n'm'}\rangle_{\mathbb{S}} = \delta_{nn'}\delta_{mm'}. \tag{2.36}$$

Proposition 2.3.5. *[19] The spherical harmonics are the eigenfunctions of the Laplacian:*

$$\Delta Y_{nm}(\sigma) = -n(n + 1)Y_{nm}(\sigma),\ \forall\sigma \in \mathbb{S}. \tag{2.37}$$

Proposition 2.3.6. *The functions Y_{nm} form an orthonormal baisis for the space of spherical harmonics functions of degree n of the space $\mathbb{R}^3$.*

We have:

$$\int_{-1}^{1}[P_{nm}(x)]^2\mathrm{d}x = \frac{2}{2n + 1}\frac{(n + m)!}{(n - m)!}$$

so that an orthonormal set of spherical harmonics of degree n for $k = 3$ is given by:

$$\sqrt{\frac{2n + 1}{4\pi}}P_n(x),\ A_{nm}\cos m\phi P_{nm}(x),\ A_{nm}\sin m\phi P_{nm}(x),\ m = 1, \ldots, 2n$$

where

$$A_{nm} = \sqrt{\frac{(n - m)!(2n + 1)}{(n + m)!2\pi}}.$$

Now take:

$$\xi = (\cos\alpha, \sin\alpha\cos\phi_1, \sin\alpha\sin\phi_1)$$

and

$$\eta = (\cos\beta, \sin\beta\cos\phi_2, \sin\beta\sin\phi_2)$$

so that $(\xi, \eta) = \cos\alpha\cos\beta + \sin\alpha\sin\beta\cos\phi$ when $\phi = \phi_1 - \phi_2$.

Proposition 2.3.7. *Addition formula for spherical harmonics:*

$$\sum_{m=-n}^{n} Y_{nm}(\theta,\phi)Y_{nm}(\theta',\phi') = \frac{2n+1}{4\pi}P_n(\cos\gamma), \tag{2.38}$$

where $\cos\gamma = \cos\theta\cos\theta' + \sin\theta\sin\theta'\cos\phi$ *is the spherical distance between* (θ,ϕ) *and* (θ',ϕ').

In the next paragraph we introduce important properties of spherical harmonics:

Proposition 2.3.8. *[42] Recursive formula:*

$$\cos\theta \cdot Y_{nm} = \Big(\frac{(n+1)^2 - m^2}{4(n+1)^2 - 1}\Big)^{1/2} Y_{n+1,m} + \Big(\frac{n^2 - m^2}{4n^2 - 1}\Big)^{1/2} Y_{n-1,m}.$$

Proposition 2.3.9. *[42] Differentiation formula:*

$$\frac{\partial Y_{nm}(\theta,\phi)}{\partial\theta} = -\sin\theta \frac{e^{im\phi}}{\sqrt{2\pi}} \cdot \frac{\mathrm{d}\overline{P}_{nm}(x)}{\mathrm{d}x}|_{x=\cos\theta}.$$

Note that any square-integrable function on the sphere can be expanded in terms of spherical harmonics as:

$$f(\theta,\phi) = \sum_{n=0}^{\infty}\sum_{m=-n}^{n} f_{nm}Y_{n,m}(\theta,\phi), \tag{2.39}$$

where f_{nm} are the spherical harmonics coefficients associated to $Y_{n,m}(\theta,\phi)$.
These spherical Fourier coefficients f_{nm} can be computed by

$$f_{nm} = \langle f, Y_{nm}\rangle_{\mathbb{S}} = \int_0^{2\pi}\int_0^{\pi} f(\theta,\phi)Y_{nm}(\theta,\phi)\sin\theta \mathrm{d}\theta\mathrm{d}\phi \tag{2.40}$$

which by discretization of the integrals is approximately equal to the sum:

$$\sum_{d=1}^{D} w_d f(\theta_d,\phi_d)Y_{nm}(\theta_d,\phi_d). \tag{2.41}$$

We note that here the spherical harmonics functions Y_{nm} are normalized, see (2.32). The integral over the sphere

$$\int_{\mathbb{S}} f(x)\mathrm{d}\omega(x) \tag{2.42}$$

is approximately equal to the sum:

$$\sum_{d=1}^{D} w_d f(\theta_d, \phi_d) Y_{nm}(\theta_d, \phi_d)$$

by considering the Gauss-Legendre quadrature formula (χ_S, W_S), see [34], where $\omega(x)$ is the Lebesgue measure on the sphere and $(\theta_d, \phi_d) \in \chi_S = \{\theta_j, j = 0, \ldots, S\} \times \{\phi_k, k = 0, \ldots, 2S+1\}$- a sampling set of the nodes with

$$\phi_k = \tfrac{k\pi}{S+1}, \phi_k \in [0, 2\pi],\ S \in \mathbb{N}.$$

The θ_j and ϕ_k are called the co-latitudinal and longitudinal nodes, respectively. For the co-latitudinal direction we use the Gauss-Legendre quadrature with θ_j nodes and w_j weights which can be obtained as the solution of an eigenvalue problem, see [20], pp. 95. The weights

$$W_S = \{w_d = w_{j,k}, j = 0, \ldots, S, k = 0, \ldots, 2S+1\}$$

for the entire quadrature formula are then given by:

$$w_{j,k} = \frac{2\pi}{2S+2} w_j \tag{2.43}$$

Comparing with Gaussian quadrature where the nodes are computed as zeros of Legendre polynomials and the weights are given by 2.43, (see Section 2.3.2), here, the nodes and the weights are given by the couple (χ_S, W_S). Using the Gauss-Legendre quadrature formula, the integral over the sphere:

$$\int_{\mathbb{S}} f(x)\mathrm{d}w(x) = \int_0^{2\pi} \int_0^{\pi} f(\theta, \phi) \sin\theta \mathrm{d}\theta \mathrm{d}\phi$$

is approximately equal to the double sum:

$$\sum_{j \in \{0,\ldots,S\}} \sum_{k \in \{0,\ldots,2S+1\}} w_{j,k} f(\theta_j, \phi_k).$$

In the previous integral, we apply a variable change for the interior one and we get:

$$\int_0^{2\pi} \int_{-1}^{1} f(\arccos x, \phi)\mathrm{d}x\mathrm{d}\phi \tag{2.44}$$

which using Gauss-Legendre quadrature formula we get that the initial integral is approximately equal to:

$$\sum_{j=0}^{S} w_j \int_0^{2\pi} f(\arccos x_j, \phi)\mathrm{d}\phi$$

The same step is applied for the second integral over $[0, 2\pi]$ and we get:

$$\sum_{j=0}^{S} w_j \sum_{k=0}^{2S+1} \alpha_k f(\arccos x_j, \phi_k)$$

Now, we denote the weights for the entire quadrature formula $w_j\alpha_k$ by $w_{j,k}$, see (2.43). With this we obtain that the integral on the sphere is approximately equal to:

$$\sum_{k=0}^{2S+1} \sum_{j=0}^{S} \frac{2\pi w_j}{2S+2} f(\arccos x_j, \phi_k).$$

2.4 Statement of the problems

2.4.1 M/EEG

Notations

In this section we introduce the main notations used for the description of M/EEG problem.
For a real value function $f(\vec{\mathbf{r}})$, respectively $f(\vec{\mathbf{r}}')$, we denote by ∇f, respectively $\nabla' f$ the gradient of f, i.e the vector field whose components are the partial derivatives of f with respect to $\vec{\mathbf{r}} \in \mathbb{R}^3$, respectively to $\vec{\mathbf{r}'}$-variable.

We denote by:

- $\vec{\mathbf{r}}$ the position of the point r in $\mathbb{R}^3$;
- $\rho_c(\vec{\mathbf{r}}, t)$ the (volumic) charge density at location $\vec{\mathbf{r}}$ and time t;
- $\vec{\mathbf{E}}(\vec{\mathbf{r}}, t)$ the electric field vector;

- $\vec{\mathbf{B}}(\vec{\mathbf{r}}, t)$ the magnetic field vector;
- $\vec{\mathbf{J}}(\vec{\mathbf{r}}, t)$ the current density vector.

Maxwell's equations

Using quasi-static assumptions, Maxwell's equations lead to a formulation of the magnetic potential $\vec{\mathbf{B}}$ as a solution of a differential partial equation.
The Maxwell's equations in vacuum are [30]:

$$\nabla \cdot \vec{\mathbf{E}} = \frac{\rho_c}{\varepsilon_0}, \qquad \vec{\nabla} \times \vec{\mathbf{E}} = -\frac{\partial \vec{\mathbf{B}}}{\partial t}, \tag{2.45}$$

where $\varepsilon_0 \simeq 8.85\ 10^{-12} Fm^{-1}$ is *the electrical permittivity of the vacuum* and ρ_c is the *total charge density*:

$$\nabla \cdot \vec{\mathbf{B}} = 0, \qquad \vec{\nabla} \times \vec{\mathbf{B}} = \mu_o \left(\vec{\mathbf{J}} + \varepsilon_0 \frac{\partial \vec{\mathbf{E}}}{\partial t} \right)$$

and $\mu_o = 4\pi 10^{-7} Hm^{-1}$ is the *magnetic permeability*. Because the frequencies of the electromagnetic signals of the brain are very low, the quasi-static approximation of Maxwell's equations allows us to neglect the derivatives with respect to time. With this assumption, the fourth Maxwell's equation becomes:

$$\vec{\nabla} \times \vec{\mathbf{B}} = \mu_o \vec{\mathbf{J}}. \tag{2.46}$$

Because $\mu_o = 0$ at the exterior of the head, the curl of the magnetic field is zero:

$$\vec{\nabla} \times \vec{\mathbf{B}} = 0. \tag{2.46'}$$

Since the curl of the electric field is zero, this field is the gradient of electric potential U:

$$\vec{\mathbf{E}} = -\vec{\nabla} U. \tag{2.47}$$

Inside the head, the current density $\vec{\mathbf{J}}$, can be decomposed into:
-a volumic density $\vec{\mathbf{J}}^v = \sigma \vec{\mathbf{E}}$ where σ is the head conductivity;
-a primary current $\vec{\mathbf{J}}^p$:

$$\vec{\mathbf{J}} = \vec{\mathbf{J}}^p + \sigma \vec{\mathbf{E}}.$$

Using (2.47), we have:

$$\vec{\mathbf{J}} = \vec{\mathbf{J}}^p - \sigma\vec{\nabla}U. \tag{2.48}$$

Using (2.46) and that the curl of the divergence is zero, we have:

$$\nabla \cdot \vec{\mathbf{J}} = 0$$

Thus, using (2.48):

$$\nabla \cdot (\sigma\vec{\nabla}U) = \nabla \cdot \vec{\mathbf{J}}^p.$$

The primary current generated by N dipolar sources C_k of moments p_k is:

$$\vec{\mathbf{J}}^p = \sum_{k=1}^{N} p_k \cdot \delta_{C_k},$$

where δ_{C_k} is the Dirac distribution. Then, we have:

$$\nabla \cdot \vec{\mathbf{J}}^p = \sum_{k=1}^{N} p_k \cdot \nabla\delta_{C_k}$$

and

$$\nabla \cdot (\sigma\vec{\nabla}U) = \sum_{k=1}^{N} p_k \cdot \nabla\delta_{C_k}. \tag{2.49}$$

Because the sources are localized inside the interior layer (brain), (2.49) becomes:

$$\left\{ \begin{array}{ll} \sigma\Delta U = \sum_{k=1}^{N} p_k.\nabla\delta_{C_k} & \text{in } \mathbb{B} \\ \sigma\frac{\partial U}{\partial n}_{|\mathbb{S}} = g & \text{on } \mathbb{S} \\ \Delta U = 0 & \text{in } \mathbb{B}^e. \end{array} \right\} \tag{2.50}$$

where, here σ is the brain conductivity.

2.4.2 Geophysics

We recall that inside the Earth, the gravitational potential verifies [54]:

$$-\Delta V(X) = \rho(X).$$

Outside the Earth, the potential verifies the Laplace equation:

$$\Delta V(X) = 0.$$

Now, if we consider a system of several point masses $m_1, m_2, \ldots, m_N$, the potential of the system is the sum of each contribution:

$$V(X) = \frac{m_1}{|X - C_1|} + \frac{m_2}{|X - C_2|} + \ldots + \frac{m_N}{|X - C_N|} = \sum_{k=1}^{N} \frac{m_k}{|X - C_k|}.$$

Here, the density ρ is approximated by a monopolar discrete distribution $\rho_N(X) = \sum_{k=1}^{N} m_k \delta_{C_k}(X)$. For (1.3) we assume that point masses are distributed continuously over the volume v of the Earth (which is modeled by the unit ball) with density $\rho \in L^2$:

$$\rho = \frac{\mathrm{d}m}{\mathrm{d}v}$$

with $\mathrm{d}m$ an element of the mass and $\mathrm{d}v$ an element of volume. In Newton's integral (1.3), $|X - Y|$ represents the distance between the mass elements $\mathrm{d}m = \rho \mathrm{d}v$ and the point Y. Let us consider (x, y, z) the coordinates of the point X and (ξ, η, ζ) the coordinates of the point Y. Then, the distance $|X - Y|$ becomes:

$$|X - Y| = \sqrt{(x - \xi)^2 + (y - \eta)^2 + (z - \zeta)^2}.$$

The gravitational force $\mathbf{F}$ is the gradient of V:

$$F_x = \frac{\partial V}{\partial x}, \; F_y = \frac{\partial V}{\partial y}, \; F_z = \frac{\partial V}{\partial z}.$$

In vector notation, the force vector $\mathbf{F}$ is the gradient of the scalar function V:

$$\mathbf{F} = [F_x, F_y, F_z] = \mathrm{grad} V.$$

The disposed measurements can be values of the potential V, of the gravitaional force $\mathbf{F}$ or of the Hessian of V.

2.4.3 Unified formulation

As we have seen, the both inverse problems are modeled by the partial differential equation:

$$-\Delta Pot = \rho$$

inside the domain (here, the ball $\mathbb{B}$), and

$$\Delta Pot = 0 \tag{2.51}$$

outside the domain ($\mathbb{B}^e$). To underline this commune feature, in the following, we give a mathematical description of the M/EEG and geophysics problems and we introduce briefly the paleomagnetism problem. In all these cases, the direct (forward) problem (FP) and the inverse problem (IP) can be formulated by:

$$(FP) : \begin{cases} T\rho = Pot \text{ in } \mathbb{B}; \\ \frac{\partial Pot}{\partial n}_{|\mathbb{S}} = g \text{ in } \mathbb{S}; \end{cases}$$

and

$$(IP) : \begin{cases} \Delta Pot = \rho \text{ in } \mathbb{B}; \\ \Delta Pot = 0 \text{ in } \mathbb{B}^e = \mathbb{R} \setminus \overline{\mathbb{B}}; \\ T\rho_N \simeq Pot \text{ in } \mathbb{S}. \end{cases}$$

The resolution of the inverse problem (IP) consists on two inverse problems: data transmission problem (TP) and density recovery (DR) by passing by (SR)-source recovery. In general, we dispose of the data just over a region and in this case we pass by the transmission of the data (TP) towards the surface of all the sphere ($\partial\mathbb{B} = \mathbb{S}$):

(TP): *Given values of Pot over a region of* $\mathbb{S}$ *or* $\mathbb{S}_R$ $(R > 1)$ *estimate Pot over whole the sphere* $\mathbb{S}$.

The second step which consist in solving the inverse problem is the sources recovery:

(SR): *Find the density* $\rho_N = \sum_{k=1}^{N} m_k \delta_{C_k}$ *given measurements of the discrete potential* Pot_N.
We recall that the problems of our interest are modeled by the next partial differential equation:

$$-\Delta Pot = \rho \text{ with } \rho = \underbrace{\rho_r}_{smooth} + \underbrace{\rho_s}_{singular\ \ part} \tag{2.52}$$

In *geodesy*, we have:

$$\rho = \rho_r \in L^2(\mathbb{B}) \text{ and } \rho_s = 0.$$

We can dispose of gravimetric measurements ∇V (the gravitational force) on the surface of the Earth or of satellite measurements of gravitational potential V [1].

Remark 2.4.1. *The measurements can be given directly as pointwise values at the sphere surface or as data obtained after the extrapolation step of the transmission problem, which is the case that we discuss in this thesis.*

In *electroencephalography (EEG)*, we have:

$$\rho_s = \sum m_k . \nabla \delta_{C_k} \text{ and } \rho_r = 0,$$

where m_k, C_k are the masses of points, respectively the coordinates of these points. The measurements of the electrical potential U or electrical flux $\partial_n U$ are taken on the scalp of the head [8].

In *magnetoencephalography (MEG)*, we have:

$$\rho_s = \sum m_k . \nabla \delta_{C_k} \text{ and } \rho_r = 0.$$

Here, m_k are the moments of the sources C_k. Radial measurements of the magnetic field $\vec{\mathbf{B}}$ are taken at a distance of the head [31]. The magnetic field $\vec{\mathbf{B}}$ is the curl of a vector field $\vec{A}$ called potential vector: $\vec{\mathbf{B}} = \vec{\nabla} \times \vec{A}$, where $\vec{A}$ verifies $\Delta \vec{A} = -\mu_0 \vec{\mathbf{J}}$, in this case we have a vectorial density, so $\rho = -\mu_0 \vec{\mathbf{J}}$.

In *paleomagnetism*:

$$\rho_s = \nabla \cdot \vec{M} \text{ and } \rho_r = 0 \text{ where } \vec{M} \in L^1 \text{ is a distribution.}$$

The magnetic field of the Earth, $\vec{\mathbf{B}}$, is resumed through the time and it is used to determine the age of rocks, reconstructions of the deformational histories of parts of the crust, etc.

Chapter 3

Slepian bases on the sphere

In this chapter we present a new basis which is used for the partial representation of the data on the sphere. This basis was introduced by Slepian and it was used after, in many domains of applied mathematics. Here we will present two computation methods already existed in the literature and we introduce one method based on the Gauss-Legendre quadrature method.

3.1 Construction of Slepian functions on the sphere

3.1.1 Preliminaries

For the two inverse problems that we considered, the data (the gravitational, electrical or magnetic potential) can be measured over the whole sphere or just on a part of it, as the north hemisphere or a spherical cap, continents, etc. When such a limited area is studied, the spherical harmonic basis is prone to error, since it is no longer orthogonal over the partial area. Therefore, the construction of a local spherical harmonic basis that is orthogonal over the studied area of the sphere is required for the study of the inverse problem. This issue of finding such a basis was first studied in [2, 36] for an interval of the real line and for balls of $\mathbb{R}^n$. The authors discovered bases of functions (called Slepian functions) with energies concentrated in the considered regions. This procedure is very useful in several domains of applied mathematics and physics, notably geophysics [2], cosmology [27] and image processing [15, 48].

Bandlimited functions

We recall that any real-valued square-integrable function on the unit sphere can be expanded as:

$$g(\theta,\phi)=\sum_{n=0}^{\infty}\sum_{m=-n}^{n}g_{nm}Y_{nm}(\theta,\phi) \tag{3.1}$$

Here, we are interested on the space of square-integrable functions with no power above a bandwidth L, i.e g belongs to the space of bandlimited functions denoted by B_L with:

$$B_L=\{g\in L^2(\mathbb{S})|g=\sum_{n=0}^{L}\sum_{m=-n}^{n}g_{nm}Y_{nm}\}$$

Data concentration within a region of the sphere

Definition 3.1.1. *The bandlimited functions $g\in B_L$ that are optimally concentrated within a region Θ of the sphere are called spherical Slepian functions or simply Slepian functions, in this thesis.*

Slepian functions are those bandlimited functions $g\in B_L$ for which the concentration within Θ is maximum, i.e. to maximize the ratio:

$$\mu=\frac{\int_\Theta g^2(\theta,\phi)\mathrm{d}w}{\int_{\mathbb{S}} g^2(\theta,\phi)\mathrm{d}\omega}. \tag{3.2}$$

These functions are the analogues of one dimensional Slepian's time-frequency concentration problem, see [36], on the surface of the unit sphere. They form an orthonormal basis on the sphere and they are orthogonal over the studied region. Such a basis is a useful tool in data analysis and representation in a variety of applications. The spherical Slepian functions can be found by solving an algebraic eigenvalue problem or an integral equation [46], see Section Method 1. In [40], the Slepian functions are seen as a basis for the space of eigenfunctions of an integral operator, see Definition (3.1.2).

In the case of real line, the computation of one-dimensional Slepian functions was done using the fact that the differential operator of Sturm Liouville defined on $C^2([-1,1])$:

$$\mathcal{L}=\frac{\mathrm{d}}{\mathrm{d}x}(1-x^2)\frac{\mathrm{d}}{\mathrm{d}x}-c^2x^2,|x|\leq 1 \tag{3.3}$$

obtained by solving the Helmotz equation by the separation of variables method with the use of prolate spheroidal coordinates, commutes with the integral operator

$$\int_{-1}^{1} \frac{\sin c(x-y)}{\pi(x-y)} \psi(y) \mathrm{d}y = \mu\psi(x), |x| \leq 1 \tag{3.4}$$

where $c > 0$ is a given real number. The functions ψ are called proloidal spherical wave functions (PSWF).

Method 1

This method was studied by Simons in [46, 47].

In order to maximize the ratio (3.2), we replace g by its bandlimited expansion and we get:

$$\mu = \frac{\sum_{n=0}^{L} \sum_{m=-n}^{n} g_{nm} \sum_{n'=0}^{L} \sum_{m'=-n'}^{n'} D_{nm,n'm'} g_{n'm'}}{\sum_{n=0}^{L} \sum_{m=-n}^{n} g_{nm}^2},$$

where the orthonormality relation of the spherical harmonics is used for the denominateur. Define the quantity:

$$D_{nm,n'm'} = \int_{\Theta} Y_{nm}(\theta,\phi) Y_{n'm'}(\theta,\phi) \mathrm{d}\omega. \tag{3.5}$$

Now, the maximization problem becomes:

$$\mu = \frac{\mathbf{g^T D g}}{\mathbf{g^T g}} \tag{3.6}$$

where $\mathbf{D}$ is a $(L+1)^2 \times (L+1)^2$ matrix with elements $D_{nm,n'm'}$ and $\mathbf{g} = (g_{00}, \ldots, g_{nm}, \ldots, g_{LL})^T$ the vector of spherical harmonic coefficients associated to the function g. The matrix $\mathbf{D}$ depends on the size of the region Θ and the bandwidth L.

Every eigenvector $\mathbf{g}_\alpha$, $\alpha = 1, \ldots, (L+1)^2$ gives rise to an associated eigenfunction $g_\alpha \in B_L$. Thanks to the bandwidth L, the eigenfunctions g that are well concentrated within the region Θ will have eigenvalues which are near unity, whereas those that are poorly concentrated will have eigenvalues near zero. Using the index notation, (3.6) is given as follows:

$$\sum_{n=0}^{L} \sum_{m=-n}^{n} D_{nm,n'm'} g_{n'm'} = \mu g_{nm}. \tag{3.7}$$

If we multiply (3.6) by Y_{nm} and sum over n and m we deduce that the eigenfunction g satisfies the integral eigenvalue equation of the second kind in Θ:

$$\mathcal{D}(g)(\theta,\phi) = \int_\Theta D((\theta,\phi),(\theta',\phi'))g(\theta',\phi')\mathrm{d}w = \mu g(\theta,\phi),\ (\theta,\phi)\in\Theta, \tag{3.8}$$

where $\mathcal{D}$ is the integral operator and D is its associated kernel. The kernel D is symmetric and depends on the spherical distance γ between (θ,ϕ) and (θ',ϕ') given by $\cos\gamma = \cos\theta'\cos\theta + \sin\theta'\sin\theta\cos(\phi'-\phi)$:

$$D((\theta,\phi),(\theta',\phi')) = \sum_{n=0}^{L}\frac{2n+1}{4\pi}P_n(\cos\theta'\cos\theta + \sin\theta'\sin\theta\cos(\phi'-\phi))). \tag{3.9}$$

This method has the drawback to require the computation of the eigenvalues and eigenvectors of an $(L+1)^2\times(L+1)^2$ order matrix with entries given by (3.5) that requires a quadrature method to compute approximate values of these.

Method 2

This method was studied by Miranian in [40]. In Section 3.2 we develop an efficient computational method which uses the Gauss-Legendre quadrature and it is based on the method of Miranian.

We define the integral operator $\mathcal{T}$ over the region $\Theta\subset\mathbb{S}$:

$$(\mathcal{T}f)(u) = \int_\Theta\sum_{n=0}^{L}P_n(\langle u,u'\rangle_\Theta)f(u')\mathrm{d}u' = \int_\Theta\sum_{n=0}^{L}\sum_{m=-n}^{n}Y_{nm}(u)\overline{Y}_{nm}(u')f(u')\mathrm{d}u',\ u\in\Theta$$

with:

$$\int_0^{2\pi}\int_{-1}^{1}Y_{nm}(x,\phi)\overline{Y}_{nm}(x,\phi)\mathrm{d}x\mathrm{d}\phi = 1,\ x=\cos\theta$$

where $\overline{Y}_{nm}$ are the conjugate of (2.32).

For a particular region Θ as a polar cap or two symmetrically caps (one at each pole) defined by $\Theta: b\le\cos\theta\le 1$ or $0\le\theta\le\arccos b, 0\le\phi\le 2\pi$, the Sturm Liouville operator $\mathcal{S}$:

$$\mathcal{S} = \frac{\mathrm{d}}{\mathrm{d}x}[(1-x^2)(b-x)\frac{\mathrm{d}}{\mathrm{d}x}] - L(L+2)x - \frac{m^2(b-x)}{1-x^2} \tag{3.10}$$

defined on the interval $[b,1]$ commutes with the operator $\mathcal{T}$ on the spaces of functions whose dependence on ϕ is of the form $\mathrm{e}^{im\phi}$. We denote these spaces by H_m with:

$$H_m = \{g | g(u) = g(\theta, \phi) = f(\cos\theta)\mathrm{e}^{im\phi}, u \in \Theta\}$$

Definition 3.1.2. *The operator $\mathcal{T}_m$ is the restriction of the operator $\mathcal{T}$ on the space H_m, $m = 0, \ldots, L$.*

When the studied region is not anymore a polar cap, but a region with less symmetry, spherical belt bounded by two parallels, etc., with $\Theta : a \leq \cos\theta \leq b$ or $\arccos a \leq \theta \leq \arccos b$ with $\theta_0 = \arccos a, \theta_1 = \arccos b$ we can always consider the integral operator $\mathcal{T}_m$, but to get the commuting local operator is not simple.

In the following, let consider a function $g \in H_m$, $g(\theta, \phi) = f(\cos\theta)\mathrm{e}^{im\phi}$, $x = \cos\theta$ and apply it to the operator $\mathcal{T}$, see [40]:

$$\begin{aligned}
(\mathcal{T}_m)g(u) &= \int_\Theta (\sum_{l=0}^{L}\sum_{p=-l}^{l} Y_{lp}(u)\overline{Y}_{lp}(u'))g(u')\mathrm{d}u' \\
&= \int_\Theta \sum_{l=0}^{L}\sum_{p=-l}^{l} Y_{lp}(x,\phi)\overline{Y}_{lp}(x',\phi')f(x')\mathrm{e}^{im\phi'}\mathrm{d}x'\mathrm{d}\phi' \\
&= \int_0^{2\pi}\int_a^b \Big(\sum_{l=0}^{L}\sum_{p=-l}^{l} \frac{2l+1}{4\pi}\frac{(l-p)!}{(l+p)!}P_{lp}(x)\mathrm{e}^{ip\phi}P_{lp}(x')e^{-ip\phi'}\Big)f(x')\mathrm{e}^{im\phi'}\mathrm{d}x'\mathrm{d}\phi' \\
&= \int_a^b \sum_{l=0}^{L}\sum_{p=-l}^{l} \frac{2l+1}{4\pi}\frac{(l-p)!}{(l+p)!}P_{lp}(x)P_{lp}(x')f(x')\Big(\mathrm{e}^{ip\phi}\int_0^{2\pi} e^{i\phi'(-p+m)}\mathrm{d}\phi'\Big)\mathrm{d}x' \\
&= \mathrm{e}^{im\phi}\int_a^b \sum_{l=|m|}^{L} \frac{2l+1}{2\pi}\frac{(l-|m|)!}{(l+|m|)!}P_{lm}(x)P_{lm}(x')f(x')\mathrm{d}x'.
\end{aligned}$$

Remark 3.1.1. *By applying the operator $\mathcal{T}$ to a function $g \in H_m$, the result still belongs to H_m.*

We denote by K_m the kernel of the operator $\mathcal{T}_m$ in the space H_m:

$$K_m(x,x') = \sum_{n=|m|}^{L} \frac{2n+1}{2\pi}\frac{(n-|m|)!}{(n+|m|)!}P_{nm}(x)P_{nm}(x'). \tag{3.11}$$

Here, the problem (3.8) is reduced to the following eigenproblem:

$$\int_a^b K_m(x,x')\psi_{n,m}(x')\mathrm{d}x' = \mu_n(m)\psi_{n,m}(x),\ \forall x \in [a,b]. \tag{3.12}$$

with $\psi_{n,m}$ the eigenfunctions of the operator $\mathcal{T}_m$. The rank of $\mathcal{T}_m$ is $L - |m| + 1$ and so it admits $L - |m| + 1$ eigenvalues and $L - |m| + 1$ eigenfunctions, they are concentrated in the studied region, the remaining are zero. In the following is given the spectral study of the operator $\mathcal{T}_m$, see [40]:

Proposition 3.1.1. *Let us consider the finite $(L+1)^2$ operator $\mathcal{T}_m$. Then:*

- *There are $L+1$ linearly independent orthogonal eigenfunctions of $\mathcal{T}_0$ that belong to the space H_0; consequently, $\mathcal{T}_0$ has only $L+1$ distinct non-zeros eigenvalues that correspond to eigenfunctions in H_0.*
- *The $\frac{L(L+1)}{2}$ non zero eigenvalues of $\mathcal{T}_m$ have multiplicity 2: in both subspaces H_m and H_{-m}, $\mathcal{T}_m$ has $L-m+1$ non-zero distinct eigenvalues, where $m = 1, \ldots, L-1$.*
- *$L-|m|+1$ eigenfunctions of $\mathcal{T}_m$ belong to H_m for all $|m| = 1, \ldots, L-1$ and are orthogonal.*

The method used by Simons asks to compute the matrix $\mathbf{D}$ whose elements are given by (3.5). For L very big, this computation can occupy a lot of memory and time. In Section 3.2, we give a new practical method for computing the Slepian basis and their associated eigenvalues. This method uses Gauss-Legendre quadrature and it is based on the method proposed by Miranian.

Shifted Legendre polynomials

In the previous paragraph, we saw that the Sturm-Liouville operator $\mathcal{S}$ defined on the interval $[b, 1]$ commutes with the operator $\mathcal{T}_m$ for those functions which have a dependence on ϕ of the form $\mathrm{e}^{im\phi}$. In order to compute the eigenfunctions of $\mathcal{S}$ we use the shifted Legendre polynomials [40]. Once, we have the eigenfunctions denoted by ψ_n of the operator $\mathcal{S}$, the Slepian functions are obtained by the multiplication with $\mathrm{e}^{im\phi}$. The shifted Legendre polynomials are defined to be the solutions of the following second-order differential equation:

$$(b-x)(1-x)S_n'' + 2(x-b_1)S_n' - n(n+1)S_n = 0 \tag{3.13}$$

with

$$b_1 = (1+b)/2, \; b_2 = (1-b)/2.$$

Proposition 3.1.2. *Properties of shifted Legendre polynomials:*

Recursion formula:

$$xS_n = b_1 S_n + \frac{b_2(n+1)}{2n+1} S_{n+1} + \frac{b_2 n}{2n+1} S_{n-1}. \tag{3.14}$$

Derivative:

$$(1-x)(b-x)S_n' = b_2\frac{n(n+1)}{2n+1}(S_{n+1} - S_{n-1}). \tag{3.15}$$

Normalized shifted Legendre polynomials:

$$\overline{S}_n = S_n\sqrt{(2n+1)/2b_2}.$$

In this case, to solve the problem $\mathcal{S}\psi_n = \mu_n\psi_n$ with $m = 0$ and $m > 0$, we use the shifted Legendre polynomials [40].

For $m = 0$ the problem is reduced to the problem of computing eigenvectors of a certain symmetric tridiagonal matrix.
We have:

$$\Big(\frac{\mathrm{d}}{\mathrm{d}x}\Big[(1-x^2)(b-x)\frac{\mathrm{d}}{\mathrm{d}x}\Big] - L(L+2)x\Big)\psi_n = \mu_n\psi_n. \tag{3.16}$$

We express ψ_n in terms of shifted Legendre polynomials:

$$\psi_n = \sum_{k=0}^{\infty} a_k^n S_k.$$

In the case $m > 0$, the problem will be reduced to a generalized matrix eigenproblem $Ax = \mu_n Bx$ with A, B two matrices, x their eigenfunctions and μ_n their eigenvalues.

3.2 New constructive method of Slepian functions on the sphere

This method is based on the Gaussian quadrature formula applied to an eigenproblem of the form (3.12) for functions which belong to H_m for $x \in [a, b]$.

In this paragraph, we describe our Gaussian quadrature based technique for the accurate and efficient computation of the Slepian functions on the sphere. Moreover, we will provide the reader with the analysis of this method in computing the values of the $\psi_{n,m}$ as well as in computing the associated eigenvalues. This method is based on discretizing (3.12) by using an N-point quadrature formula associated with a Legendre polynomial $P_N(x)$ that is an orthogonal family over $[a, b] \subset [-1, 1]$. Hence, (3.12) is approximated by the following eigensystem:

$$\sum_{j=1}^{N} w_j K_m(x_i, x_j)\psi_{n,m}(x_j) = \mu_n(m)\psi_{n,m}(x_i),\ 1 \leq i \leq N. \tag{3.17}$$

Here, the w_i, x_i are the weights and the nodes of the N-point Gaussian quadrature that are easily computed by the techniques of the paragraph Orthogonality of spherical harmonics from Chapter 3.

3.2.1 Main results

We recall the substitutions and the notations:

$$x = \cos\theta,\ x' = \cos\theta',\ x_i = \cos\theta_i \tag{3.18}$$

and

$$\theta_0 = \arccos a,\ \theta_1 = \arccos b. \tag{3.19}$$

Hence, (3.12) is rewritten as follows:

$$\sum_{j=1}^{N} w_j K_m(\cos\theta_i, \cos\theta_j)\psi_{n,m}(\cos\theta_j) = \mu_n(m)\psi_{n,m}(\cos\theta_i),\ 1 \leq i \leq N. \tag{3.20}$$

We give the two main theorem results of this section:

Theorem 3.2.1. *Given an integer $0 \leq n \leq L - m$ and an arbitrary real number $0 < \epsilon < 1$ $\exists\ N(\epsilon, |\mu_n(m)|) \in \mathbb{N}$ such that $\forall N \geqslant N(\epsilon, |\mu_n(m)|)$ we have:*

$$\sup_{a\leq\theta\leq b} \left| \psi_{n,m}(\cos\theta) - \frac{1}{\mu_n(m)} \sum_{j=1}^{N} w_j \psi_{n,m}(\cos\varphi_j) K_m(\cos\theta, \cos\varphi_j) \right| < \epsilon. \tag{3.21}$$

The w_j are the weights associated with the Legendre polynomial $P_N(x)$.

The error analysis of our quadrature method for computing the eigenvalues of $\mathcal{T}_m$ is given by the following theorem. We should note that this theorem is an adaptation of a similar theorem given in the case of classical prolate spheroidal wave functions in [32].

Theorem 3.2.2. *Let $m > 0$ be a positive real number and let consider N an integer with $1 < N \leq L - m + 1$. Let $(\mu_i(m))_{0\leq i\leq N-1}$ denote the first N eigenvalues of the integral operator $\mathcal{T}_m$ arranged in decreasing order of their magnitudes. Let $x_1, \ldots, x_N \in [a, b]$ and $w_1, \ldots, w_N$ be the N different nodes and weights corresponding to the N-th degree Legendre polynomial. Assume that*

$$\sup_{0\leq n\leq N-1} \sup_{1\leq l\leq N} |\psi_{n,m}(x_l) - \frac{1}{\mu_n(m)} \sum_{j=1}^{N} w_j K_m(x_l, y_j)\psi_{n,m}(x_j)| \leq \epsilon. \tag{3.22}$$

Moreover, assume that the matrix $B = [\psi_{l-1,m}(x_j)]_{1\leq l,j\leq N}$ is nonsingular. Consider the matrix $\widetilde{A}_N = [w_j K_m(x_l, y_j)]_{1\leq l,j\leq N}$; then we have:

$$\max_{0\leq j\leq N-1} |\mu_j(\widetilde{A}_N) - \mu_j(\mathcal{T}_m)| \leq \frac{\epsilon\sqrt{N(L-m+1)}}{\pi}. \tag{3.23}$$

3.2.2 Bounds of associated Legendre functions and its derivatives

Before to give the proof of these two theorems we introduce the following results concerning the associated Legendre functions.

We consider $\mathcal{P}_n(\mathbb{R})$ the set of all algebraic polynomials of degree at most n with real coefficients. The following theorem is due to A.A. Markov [4]:

Theorem 3.2.3. *If $p \in \mathcal{P}_n(\mathbb{R})$ and $\|p\|_{[-1,1]} := \max_{-1\leq t\leq 1} |p(t)| \leq 1$, then:*

$$\|p'\|_{[-1,1]} \leq n^2. \tag{3.24}$$

The following theorem gives us a bound for the kth derivative of an algebraic polynomial:

Theorem 3.2.4. *[4] **V.A. Markov**: For $1 \leq k \leq n$, if $p \in \mathcal{P}_n(\mathbb{R})$ and $\|p'\|_{[-1,1]} \leq 1$, we have:*

$$\|p^{(k)}\|_{[-1,1]} \leq T_n^{(k)}(1) \cdot \|p\|_{[-1,1]} = \frac{n^2(n^2-1^2)\cdot\ldots\cdot(n^2-(k-1)^2)}{1\cdot 3\cdot\ldots\cdot(2k-1)} \cdot \|p\|_{[-1,1]}, \tag{3.25}$$

where T_n is the nth Chebyshev polynomial of the first kind.

Proposition 3.2.1. *For real θ, we have:*

$$|P_n(\cos\theta)| \leq 1 \tag{3.26}$$

and

$$|P_n'(\cos\theta)| \leq \frac{1}{2}n(n+1) \tag{3.27}$$

from what one may deduce the bound of the kth derivative of P_n:

$$|P_n^{(k)}(\cos\theta)| \leq \frac{(n+k)!}{(n-k)!k!2^k}, \tag{3.28}$$

for $0 \leq k \leq n$.

Note that in [28], (3.28) is given without proof. To prove this inequality, we proceed as follows:

Proof. We recall the relation (2.16) the derivative of Legendre polynomials P_n in function of the Jacobi polynomials $P_n^{(\alpha,\beta)}$:

$$\frac{\mathrm{d}^k}{\mathrm{d}x^k}P_n(x) = \frac{n+1}{2}\cdot\frac{n+2}{2}\cdot\ldots\cdot\frac{n+k}{2}P_{n-k}^{(k,k)}(x). \tag{3.29}$$

From (3.29), we have:

$$|P_n^{(k)}(\cos\theta)| = \Big|\frac{n+1}{2}\cdot\frac{n+2}{2}\cdot\ldots\cdot\frac{n+k}{2}P_{n-k}^{(k,k)}(x)\Big| \leq \frac{(n+1)_n}{2^k}\cdot\max|P_{n-k}^{(k,k)}(x)|.$$

or

$$|P_n^{(k)}(\cos\theta)| = \Big|\frac{n+1}{2}\cdot\frac{n+2}{2}\cdot\ldots\cdot\frac{n+k}{2}P_{n-k}^{(k,k)}(x)\Big| \leq \frac{(n+k)!}{2^k n!}\cdot\max|P_{n-k}^{(k,k)}(x)|.$$

Proposition 3.2.2.

$$\max_{-1\leq x\leq 1}|P_n^{(\alpha,\beta)}(x)| = \frac{(q+1)_n}{n!},\ q = \max(\alpha,\beta) \geq -1/2, \tag{3.30}$$

where $(a)_n$ denotes the shifted factorial defined by:

$$(a)_n = a(a+1)\ldots(a+n-1),\ \textit{for } n > 0, (a)_0 = 1, a \in \mathbb{R}.$$

Remark 3.2.1. *We have:*

$$x! = \frac{(x+n)!}{(x+1)_n}. \tag{3.31}$$

Using (3.30),

$$\max_{-1\leq x\leq 1} |P_{n-k}^{(k,k)}(x)| = \frac{(k+1)_{n-k}}{(n-k)!}.$$

From (3.31),

$$(k+1)_{n-k} = \frac{(k+n-k)!}{k!} = \frac{n!}{k!}.$$

Hence,

$$\max_{-1\leq x\leq 1} |P_{n-k}^{(k,k)}(x)| = \frac{n!}{k!(n-k)!}.$$

Therefore,

$$|P_n^{(k)}(\cos\theta)| \leq \frac{(n+k)!}{2^k n!} \cdot \frac{n!}{k!(n-k)!}. \tag{3.32}$$

$$|P_n^{(k)}(\cos\theta)| \leq \frac{(n+k)!}{2^k n!} \frac{n!}{k!(n-k)!} = \frac{(n+k)!}{(n-k)!k!2^k}.$$

□

From the definition of Legendre associated functions (2.19) and the previous bound (3.28), it has been mentioned in [28] that:

$$|P_{nm}(\cos\theta)| \leq |P_n^{(m)}(\cos\theta)| \leq \frac{(n+m)!}{(n-m)!m!2^m}.$$

A better bound is given in [28] by using the addition theorem for Legendre polynomials (see Theorem 2.3.4) and letting $\theta = \theta'$ and $\phi = \phi'$ in (2.21). Hence, one gets:

$$1 = P_n(1) = (P_n(\cos\theta))^2 + 2\sum_{m=1}^{n} \frac{(n-m)!}{(n+m)!}(P_{nm}(\cos\theta))^2. \tag{3.33}$$

Because the right side is a sum of positive terms, then each term of (3.33) is bounded by 1. Therefore, we obtain:

$$|P_{nm}(\cos\theta)| \leq \left[\frac{1}{2}\frac{(n+m)!}{(n-m)!}\right]^{\frac{1}{2}}. \tag{3.34}$$

Till now we introduced the bounds of P_n and its derivatives. Bounds of the associated Legendre functions P_{nm} and its derivatives are obtained in a similar way. Let $\phi' = \phi$ and obtain:

$$P_n(\cos(\theta-\theta')) = P_n(\cos\theta)P_n(\cos\theta') + 2\sum_{m=1}^{n} \frac{(n-m)!}{(n+m)!}P_{nm}(\cos\theta)P_{nm}(\cos\theta'). \tag{3.35}$$

Now, if we differentiate (3.35) with respect to θ and also θ' and then set $\theta = \theta'$, this gives:

$$P_n'(1) = \Big(\frac{\mathrm{d}}{\mathrm{d}\theta}P_n(\cos\theta)\Big)^2 + 2\sum_{m=1}^{n}\frac{(n-m)!}{(n+m)!}\Big(\frac{\mathrm{d}}{\mathrm{d}\theta}P_{nm}(\cos\theta)\Big)^2. \tag{3.36}$$

Now, because the right side is a sum of positive terms and the left side is bounded by (3.27) we obtain:

$$\Big|\frac{\mathrm{d}}{\mathrm{d}\theta}P_{nm}(\cos\theta)\Big| \le \Big[\frac{1}{2}n(n+1)\frac{(n+m)!}{2(n-m)!}\Big]^{\frac{1}{2}} \tag{3.37}$$

for $1 \le m \le n$. Iterating the above process, it is shown in [28] that:

$$\Big|\Big(\frac{\mathrm{d}}{\mathrm{d}\theta}\Big)^k P_{nm}(\cos\theta)\Big| \le Mn^k\Big[\frac{(n+m)!}{(n-m)!}\Big]^{\frac{1}{2}} \tag{3.38}$$

for $0 \le m \le n$, where M is a constant independent of θ, m and n. To show the next inequality we use all the previous inequalities.

Proposition 3.2.3. *For any integer $k \ge 0$, $0 \le m \le n$, $\arccos a \le \theta \le \arccos b, \arccos a \le \theta' \le \arccos b$, we have the following inequality:*

$$\Big|\frac{\mathrm{d}^k K_m(\cos\theta, \cos\theta')}{\mathrm{d}\theta^k}\Big| \le \frac{2n}{k+2}[(L+1)^{k+2} - m^{k+1}].$$

Proof. We have:

$$K_m(\cos\theta, \cos\theta') = \sum_{n=|m|}^{L}\frac{2n+1}{2\pi}\frac{(n-|m|)!}{(n+|m|)!}P_{nm}(\cos\theta)P_{nm}(\cos\theta'),$$

$$\frac{\mathrm{d}^k K_m(\cos\theta, \cos\theta')}{\mathrm{d}\theta^k} = \sum_{n=|m|}^{L}\frac{2n+1}{2\pi}\frac{(n-|m|)!}{(n+|m|)!}\frac{\mathrm{d}^k P_{nm}(\cos\theta)}{\mathrm{d}\theta^k}P_{nm}(\cos\theta').$$

$$\begin{aligned}\Big|\frac{\mathrm{d}^k K_m(\cos\theta,\cos\theta')}{\mathrm{d}\theta^k}\Big| &\le \Big|\sum_{n=m}^{L}\frac{2n+1}{2\pi}\frac{(n-m)!}{(n+m)!}\frac{\mathrm{d}^k P_{nm}(\cos\theta)}{\mathrm{d}\theta^k}P_{nm}(\cos\theta')\Big| \\ &\le \sum_{n=m}^{L}\frac{2n+1}{2\pi}\Big|\frac{(n-m)!}{(n+m)!}Mn^k\Big[\frac{(n+m)!}{(n-m)!}\Big]^{\frac{1}{2}}\Big[\frac{1}{2}\frac{(n+m)!}{(n-m)!}\Big]^{\frac{1}{2}}\Big| \\ &= M\sum_{n=m}^{L}n^k\Big(n+\frac{1}{2}\Big) \\ &\le M\Big[\frac{1}{k+2}((L+1)^{k+2}-m^{k+2})+\frac{1}{2(k+1)}((L+1)^{k+1}-m^{k+1})\Big] \qquad (3.39) \\ &\le \frac{2M}{k+2}[(L+1)^{k+2}-m^{k+1}].\end{aligned}$$

Note that to get (3.39), we have used the bound $\sum_{n=1}^{L} n^k \le \int_1^{L+1} x^k \mathrm{d}x$. □

3.2.3 Proof of main results

In the following, we give the proof of our first result.

Proof of Theorem 3.2.1:

Since from (3.12), we have:

$$\int_{\theta_0}^{\theta_1} K_m(\cos\theta,\cos\varphi)\psi_{n,m}(\cos\varphi)\sin\varphi\mathrm{d}\varphi = \mu_n(m)\psi_{n,m}(\cos\theta). \qquad (3.40)$$

From (3.40), we get the relation:

$$\begin{aligned}\psi_{n,m}(\cos\theta) &= \frac{1}{\mu_n(m)}\int_{\theta_0}^{\theta_1} K_m(\cos\theta,\cos\varphi)\psi_{n,m}(\cos\varphi)\sin\varphi\mathrm{d}\varphi \qquad (3.41) \\ &= \frac{1}{(\mu_n(m))^2}\int_{\theta_0}^{\theta_1}\int_{\theta_0}^{\theta_1} K_m(\cos\theta,\cos\varphi)K_m(\cos\varphi,\cos\theta')\psi_{n,m}(\cos\theta')\sin\theta'\sin\varphi\mathrm{d}\theta'\mathrm{d}\varphi.\end{aligned}$$

By using (3.41), to write $\psi_{n,m}(\cos\varphi_j)$, one gets:

$$\frac{1}{\mu_n(m)}\sum_{j=1}^{N} w_j\psi_{n,m}(\cos\varphi_j)K(m,\cos\theta,\cos\varphi_j)$$
$$= \frac{1}{(\mu_n(m))^2}\int_{\theta_0}^{\theta_1}\sum_{j=1}^{N} w_j K_m(\cos\theta,\cos\varphi_j)K_m(\cos\varphi_j,\cos\theta')\psi_{n,m}(\cos\theta')\sin\theta'\mathrm{d}\theta'.$$

Hence, one gets:

$$\left|\psi_{n,m}(\cos\theta) - \frac{1}{\mu_n(m)}\sum_{j=1}^{N} w_j\psi_{n,m}(\cos\varphi_j)K_m(\cos\theta,\cos\varphi_j)\right|$$
$$\leq \frac{1}{|\mu_n(m)|^2}\int_{\theta_0}^{\theta_1}\left|\int_{\theta_0}^{\theta_1} K_m(\cos\theta,\cos\varphi)K_m(\cos\varphi,\cos\theta')\sin\varphi\mathrm{d}\varphi\right.$$
$$\left.-\sum_{j=1}^{N} w_j K_m(\cos\theta,\cos\varphi_j)K_m(\cos\varphi_j,\cos\theta')\right|\cdot|\psi_{n,m}(\cos\theta')|\sin\theta'\mathrm{d}\theta'.$$

We denote by I the interior of the first integral:

$$I = \int_{\theta_0}^{\theta_1} K_m(\cos\theta,\cos\varphi)K_m(\cos\varphi,\cos\theta')\mathrm{d}\cos\varphi - \sum_{j=1}^{N} w_j K_m(\cos\theta,\cos\varphi_j)K_m(\cos\varphi_j,\cos\theta').$$

We apply the Gaussian quadrature error given via the following equation:

$$\int_a^b f(x)\mathrm{d}x = \sum_{k=1}^{n} w_k f(x_k) + \frac{1}{a_n^2}\frac{f^{(2n)}(\eta)}{(2n)!}\int_a^b P_n^2(x)\mathrm{d}x, a\leq\eta\leq b. \tag{3.42}$$

In terms of the substitutions (3.19) and in the case where $f(x)$ is substituted with

$$K_m(\cos\theta,\cos\varphi)K_m(\cos\varphi,\cos\theta')$$

and (3.42) is rewritten as follows:

$$\int_{\theta_0}^{\theta_1} K_m(\cos\theta,\cos\varphi)K_m(\cos\varphi,\cos\theta')\sin\varphi\mathrm{d}\varphi$$
$$= \sum_{k=1}^{n} w_k K_m(\cos\theta,\cos\varphi_k)K_m(\cos\varphi_k,\cos\theta')$$
$$+ \frac{1}{a_N^2(2N)!}\frac{\partial^{2N}}{\partial\varphi^{2N}}K_m(\cos\theta,\cos\varphi)K_m(\cos\varphi,\cos\theta')\Big|_{\varphi=\eta}\cdot\int_{\theta_0}^{\theta_1} P_n^2(\cos\theta)\sin\theta\mathrm{d}\theta.$$

with $\theta_0 \leq \eta \leq \theta_1$.

To abreviate the notation, we will write:

$$K_m(\theta, \varphi, \theta) = K_m(\cos\theta, \cos\varphi) K_m(\cos\varphi, \cos\theta').$$

For computing the $2N$th derivative of $K_m(\theta, \varphi, \theta)$, we apply the Leibnitz formula:

$$\frac{\mathrm{d}^{2N}}{\mathrm{d}\varphi^{2N}}[K_m(\theta, \varphi, \theta')] = \sum_{l=0}^{k} C_k^l \frac{\mathrm{d}^l}{\mathrm{d}\varphi^l}[K_m(\cos\theta, \cos\varphi)] \frac{\mathrm{d}^{k-l}}{\mathrm{d}\varphi^{k-l}}[K_m(\cos\varphi, \cos\theta')].$$

For $k = 2N$ and using the fact that the kernel K_m is symmetric, we obtain:

$$\begin{aligned}
&\frac{\mathrm{d}^{2N}}{\mathrm{d}\varphi^{2N}}[K_m(\cos\theta, \cos\varphi) K_m(\cos\varphi, \cos\theta')] \leq M^2 \sum_{l=0}^{2N} C_{2N}^l \sum_{n=m}^{L} n^{2N} \Big(n + \frac{1}{2}\Big)^2 \\
&\quad = M^2 \sum_{l=0}^{2N} C_{2N}^l \sum_{n=m}^{L} (n^{2N+2} + n^{2N+1} + \frac{n^{2N}}{4}) \leq M^2 \cdot 4^N \Big[\frac{1}{2N+3}((L+1)^{2N+3} - m^{2N+3}) \\
&\quad + \frac{1}{2N+2}((L+1)^{2N+2} - m^{2N+2}) + \frac{1}{4(2N+1)}((L+1)^{2N+1} - m^{2N+1})\Big] \\
&\quad \leq \frac{M^2 4^N 4}{2N+3}\Big[(L+1)^{2N+3} - m^{2N+1}\Big] = \frac{(2^{N+1}M)^2}{2N+3}\Big[(L+1)^{2N+3} - m^{2N+1}\Big] = C_{M,N,L},
\end{aligned}$$

where

$$\sum_{l=0}^{2N} C_{2N}^l = \frac{(2N)!}{l!(2N-l)!} = 2^{2N} \quad .$$

$$I \leq \frac{1}{|\mu_n(m)|^2} \cdot \frac{C_{M,N,L}}{(2N)! a_N^2} \|\psi_{n,m}\|_{2,[a,b]} \leq \frac{1}{|\mu_n(m)|^2} \frac{C_{M,N,L}}{(2N)! a_N^2} |\mu_n(m)| = \frac{C_{M,N,L}}{(2N)! a_N^2} \frac{1}{|\mu_n(m)|}$$

with:

$$a_N = \frac{(2N)! h_N}{N!}, \; h_N = \frac{\sqrt{2N+1}}{(b-a)^{N+\frac{1}{2}} N!}. \tag{3.43}$$

We call the Weyl's perturbation theorem used in error analysis study:

Theorem 3.2.5. *Let A and B be two hermitian matrices of order n, where $\|\cdot\|$ is the norm defined on the space $n \times n$ size of matrices $\mathcal{M}(\mathbb{R}^n \times \mathbb{R}^n)$. Then:*

$$\max_{0 \leq j \leq n-1} |\mu_j(A) - \mu_j(B)| \leq \|A - B\|.$$

Here, μ_j are the eigenvalues of A and B, respectively and

$$\{|\mu_0(A)| \geq |\mu_1(A)| \geq \dots |\mu_{n-1}(A)|\},\ \{|\mu_0(B)| \geq |\mu_1(B)| \geq \dots |\mu_{n-1}(B)|\}$$

are their rearrangements.

We give the proof of the second result.

Proof of Theorem 3.2.2:

We build the Hilbert space E_N defined by

$$E_N = Span\{\psi_{0,m}, \psi_{1,m}, \dots, \psi_{N-1,m}\}.$$

Let $\mathcal{T}_{N,m}, \widetilde{\mathcal{T}}_{N,m} : E_N \to \mathbb{R}^N$ be two operators defined by:

$$\mathcal{T}_{N,m}(f) = \Big[\int_a^b K_m(x_j, y) f(y) \mathrm{d}y\Big]_{1\leq j\leq N}^t.$$

$$\widetilde{\mathcal{T}}_{N,m}(f) = \Big[\sum_{k=1}^N w_k K_m(x_j, y_k) f(y_k)\Big]_{1\leq j\leq N}^t.$$

$\mathcal{T}_{N,m}, \widetilde{\mathcal{T}}_{N,m}$ We have:

$$\mathcal{T}_{N,m}(\psi_{i,m}) = \mu_i(m)\Psi_i,\ 0 \leq i \leq N-1,$$

where $\Psi_i = [\psi_{i,m}(x_1), \dots, \psi_{i,m}(x_N)]^t \in \mathbb{R}^N$. Note that, by assumption,

$$B = \{\Psi_0, \Psi_1, \dots, \Psi_{N-1}\}$$

is a basis of $\mathbb{R}^N$. Moreover, since:

$$\widetilde{\mathcal{T}}_{N,m}(\psi_{l,m}) = \Big[\sum_{k=1}^N w_k K_m(x_j, x_k)\psi_{l,m}(x_k)\Big]_{1\leq j\leq N}^t = \widetilde{A}_N \psi_{l,m},\ 0 \leq l \leq N-1,$$

where $\widetilde{A}_N$ is the matrix representation of $\widetilde{\mathcal{T}}_{N,m}$. Then, we have:

$$\|\mathcal{T}_{N,m} - \widetilde{\mathcal{T}}_{N,m}\|^2 \leq \sum_{l=0}^{N-1} |\mu_l(m)|^2 \cdot \sum_{j=1}^N \Big[\psi_{l,m}(x_j) - \frac{1}{\mu_l(m)} \sum_{k=1}^N w_k K_m(x_j, x_k)\psi_{l,m}(x_k)\Big]^2$$

$$\leq \sum_{0\leq l\leq N-1} N\epsilon^2 |\mu_l(m)|^2 \leq N\epsilon^2 \sum_{l\geq 0} |\mu_l(m)|^2. \tag{3.44}$$

We compute $\sum_{l\geq 0}|\mu_l(m)|^2$:

$$\|\mathcal{T}_m\|^2=\sum_{l\geq 0}|\mu_l(m)|^2=\int_a^b\int_a^b|K_m(x,y)|^2\mathrm{d}x\mathrm{d}y,$$

$$=\int_a^b\int_a^b\sum_{n=m}^{L}\sum_{p=m}^{L}\frac{2n+1}{2\pi}\frac{(n-m)!}{(n+m)!}P_{nm}(x)P_{nm}(y)\frac{2p+1}{2\pi}\frac{(p-m)!}{(p+m)!}P_{pm}(x)P_{pm}(y)\mathrm{d}x\mathrm{d}y,$$

$$\begin{aligned}&=\sum_{n,p=m}^{L}\frac{(2n+1)(2p+1)}{4\pi^2}\int_a^b(P_{nm}(x)P_{pm}(x))\mathrm{d}x\int_a^b(P_{nm}(y)P_{pm}(y))\mathrm{d}y\\&\leq\sum_{n=m}^{L}\frac{(2n+1)^2}{4\pi^2}\int_{-1}^{1}(P_{nm}(x))^2)\mathrm{d}x\int_{-1}^{1}(P_{nm}(y))^2)\mathrm{d}y\\&=\sum_{n=m}^{L}\frac{(2n+1)^2}{4\pi^2}\frac{2^2}{(2n+1)^2}=\frac{L-m+1}{\pi^2},\end{aligned}$$

then we have:

$$\|\mathcal{T}_{N,m}-\widetilde{\mathcal{T}}_{N,m}\|^2\leq\frac{N\epsilon^2(L-m+1)}{\pi^2}.$$

Because

$$\mu(\widetilde{\mathcal{T}}_{N,m})=\mu(\widetilde{A}_N)$$

and

$$\mu_j(\mathcal{T}_{N,m})=|\mu_j(m)|,\ j=0,\ldots,N-1,$$

then, by using Weyl's perturbation theorem and the previous inequality, we get:

$$\begin{aligned}\max_{1\leq j\leq N}|\mu_j(\mathcal{T}_{N,m})-\mu_j(\widetilde{\mathcal{T}}_{N,m})|&=\max_{1\leq j\leq N}\Big||\mu_j(m)|-\mu_j(\widetilde{A}_N)\Big|\\&\leq\|\mathcal{T}_{N,m}-\widetilde{\mathcal{T}}_{N,m}\|\leq\frac{\epsilon\sqrt{N(L-m+1)}}{\pi}\end{aligned}$$

3.3 Numerical illustrations

To compute the Slepian functions by using Gauss-Legendre quadrature, we need the weights and the nodes in that we evaluate them. An example of the computed nodes and weights of the Gauss-Legendre quadrature over the sphere are given in Annexe (see Fig.1). In the next figure we show the distribution of these nodes that we took over the sphere and in which the potential is computed:

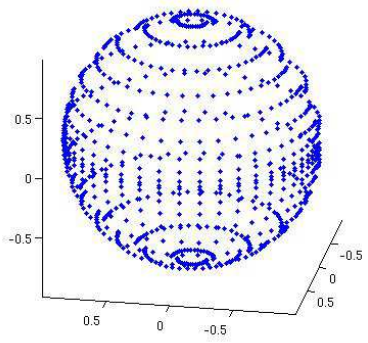

Figure 3.1: *Distribution of nodes on the sphere*

Eigenvalues of $\mathcal{T}_m$ operator

In this paragraph we illustrate the eigenvalues of the problem (3.12):

$$1 > \mu_1 \geq \mu_2 \geq \ldots \geq \mu_{(L+1)^2} > 0. \tag{3.45}$$

For $m = 0$, the operator $\mathcal{T}_m$ has L+1 distinct non-zeros eigenvalues. For $m \neq 0$, $\mathcal{T}_m$ has $\frac{L(L+1)}{2}$ non-zeros eigenvalues of multiplicity 2.

The next figures illustrate the eigenvalues of the operator $\mathcal{T}_m$ for different values of the bandwidth L ($L = 5, 10, 15$) and concentrated within the belt of angle $\theta \in [0, 90]$.

The eigenvalues λ measure the quality of the eigenfunctions concentration: the band-limited function that is most concentrated inside Θ is ψ_1 with λ_1 the largest associated eigenvalue and so on. The insignificant eigenvalues ($\lambda \approx 0$) determine excluded eigenfunctions and for the significant eigenvalues $\lambda \approx 1$, we have well concentrated eigenfunctions. The eigenfunctions with significant eigenvalues ($\lambda \approx 1$) provide an uniform coverage of the region Θ.

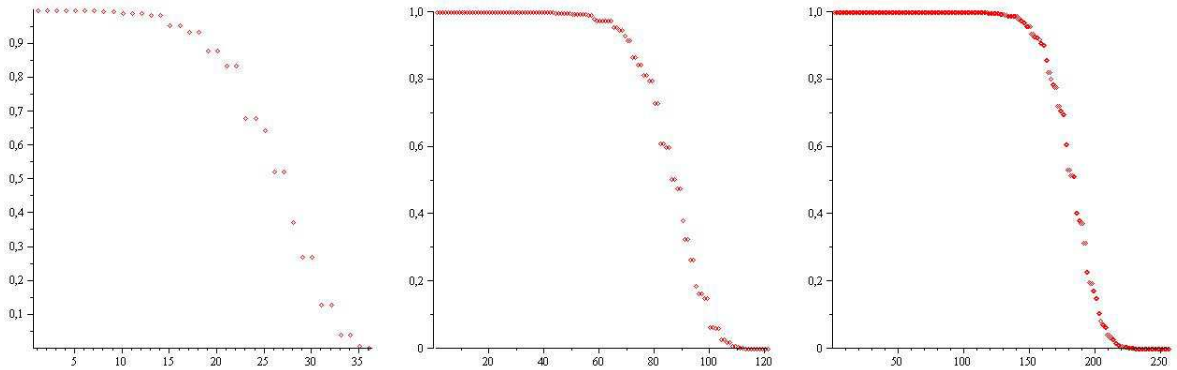

Figure 3.2: *Rearanged eigenvalues for* $L = 5$, $L = 10$ *and* $L = 15$

Below we present the eigenfunctions of the operator $\mathcal{T}_m$ for $L = 3$:

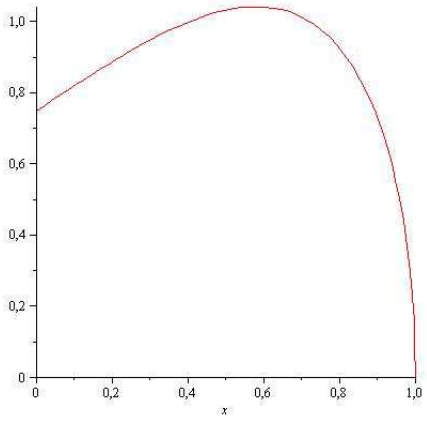

Figure 3.3: *L=3, m=1*

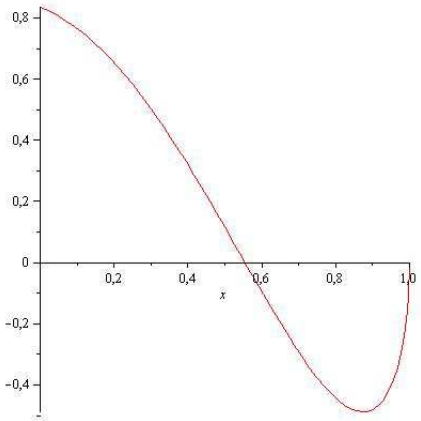

Figure 3.4: *L=3, m=2*

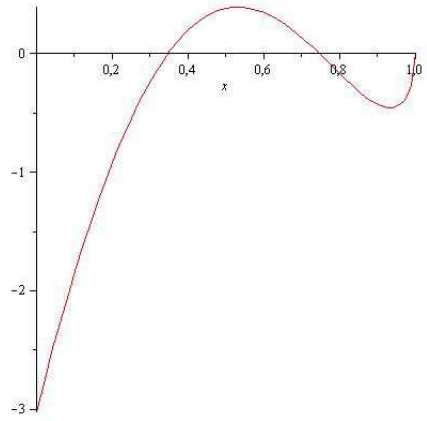

Figure 3.5: *L=3, m=3*

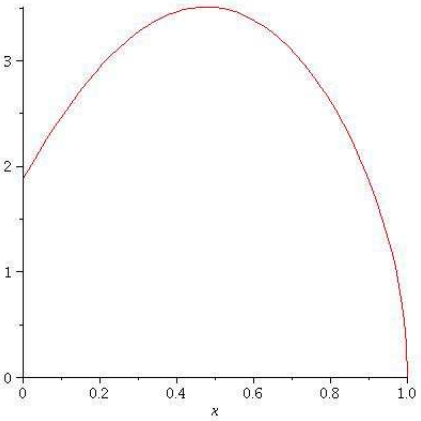

Figure 3.6: *L=3, m=4*

Figure 3.7: *Eigenfunctions obtained by using the integral operator $\mathcal{T}_m$ for m=1, 2, 3, 4. Functions presented can be numeroted according to the number of roots.*

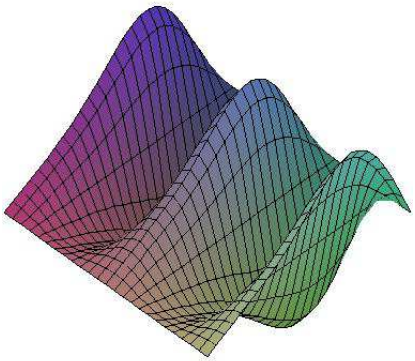

Figure 3.8: *L=3, m=1*

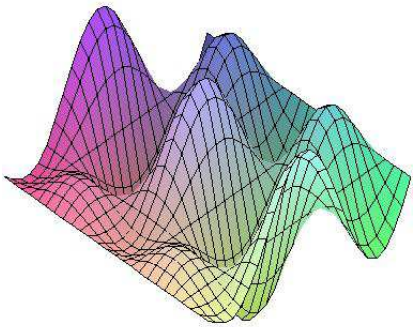

Figure 3.9: *L=3, m=2*

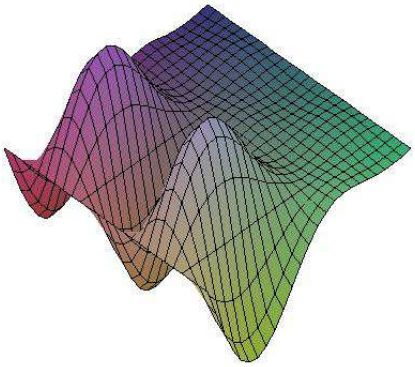

Figure 3.10: *L=3, m=3,n=2*

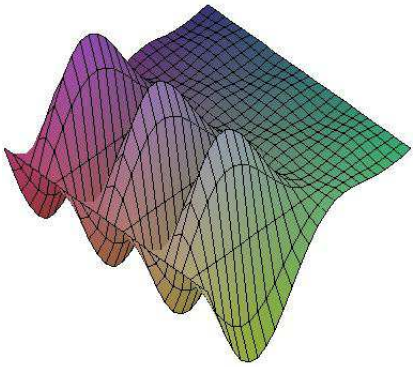

Figure 3.11: *L=3, m=3, n=3*

Figure 3.12: *Slepian functions associated to the previous eigenfunctions*

.

Chapter 4

Potentials estimation on the sphere

4.1 Statement of the problem

In this chapter the problem that we consider to be solved is the estimation of the potential (such as gravitational potential or electromagnetic potential) over the whole unit sphere $\mathbb{S}$ from noise contaminated observations over regions $\Theta \subset \mathbb{S}$. For this, Slepian functions form a natural basis for the expansion and the estimation of the potential data on the unit sphere. In practice, we can dispose also of values of first derivative or Hessian of the potential. These inverse problems are related to direct Dirichlet, Neumann and Robin problems, whose solutions can be computed by using the double-layer potential, see [14].
The unit sphere $\mathbb{S}$ is parametrized in terms of the spherical coordinates, colatitude θ and longitude ϕ. In the sequel, the region where the data is considered and its complemantary region will be denoted by Θ and $\Theta^e = \mathbb{S} \setminus \Theta$, respectively, see the figure:

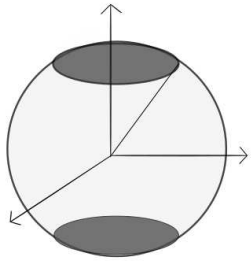

Figure 4.1: *Spherical caps*

4.2 Noisy measurements

We consider the signal [46]:

$$s(\sigma) = \underbrace{\sum_{nm}^{L} s_{nm} Y_{nm}(\sigma)}_{\text{bandlimited component}} + \underbrace{\sum_{nm>L}^{\infty} s_{nm} Y_{nm}(\sigma)}_{\text{non bandlimited component}} \qquad \sigma = (\theta, \phi) \in \mathbb{S} \quad (4.1)$$

with the coefficients of the signal spherical harmonic expansion given by:

$$s_{nm} = \int_{\mathbb{S}} s(\sigma) Y_{nm}(\sigma) \mathrm{d}\omega(\sigma). \quad (4.2)$$

The data over the covered region Θ is given by (4.1), but they are contamined by noise. Thus, a satellites measures:

$$d(\sigma) = s(\sigma) + n(\sigma), \text{ if } \sigma \in \Theta, \Theta \subset \mathbb{S} \quad (4.3)$$

We assume that the noise is modelled by a function $n \in L^2(\Theta)$ with the norm $\|n\|_\Theta$ small.

4.3 Signal field estimation

Being given the noisy data d taken by the satellites over an incomplete region Θ, we look to estimate the signal s, that gives rise to these observations. Although the signal has an infinite bandwidth, we will be able, practically, only to make bandlimited estimates of it, which we denote by $\hat{s}$. The limitation to the bandwidth L as well as the spatial restriction of the observations to the region Θ motivates to seek an estimate in terms of Slepian basis that are well concentrated in the considered region, rather than using the non-localized spherical harmonics Y_{nm}. In this manner, the signal is given by:

$$s(\sigma) = \sum_{\alpha}^{(L+1)^2} s_\alpha g_\alpha(\sigma) + \sum_{nm>L}^{\infty} s_{nm} Y_{nm}(\sigma), \ \sigma = (\theta, \phi) \in \mathbb{S}$$

whereas the estimated signal $\hat{s}(\sigma)$ is given on $\mathbb{S}$ by:

$$\hat{s}(\sigma) = \sum_{nm}^{L} \hat{s}_{nm} Y_{nm}(\sigma) = \sum_{\alpha=1}^{(L+1)^2} \hat{s}_\alpha g_\alpha(\sigma), \quad (4.4)$$

where $(g_\alpha)_{1\leq\alpha\leq(L+1)^2}$, $\alpha = \alpha(n,m)$ are the Slepian functions on the sphere $\mathbb{S}$ that are concentrated on the region Θ and associated with the bandwidth $L > 0$, see (3.7) (after the computation method used by Miranian, we have $\psi_{n,m}(\theta)\sin m\phi$, $\psi_{n,m}(\theta)\cos m\phi, 0 \leq n \leq L, m \leq n \leq L$ for Slepian functions).

The Slepian functions g_α verify:

$$g_\alpha(\sigma) = \sum_{nm}^{L} g_{\alpha,nm} Y_{nm}(\sigma), \sigma \in \mathbb{S} \tag{4.5}$$

$$g_{\alpha,nm} = \int_{\mathbb{S}} g_\alpha(\sigma) Y_{nm}(\sigma) \mathrm{d}\omega(\sigma). \tag{4.6}$$

Using (4.1) and (4.6) we get:

$$\hat{s}_{nm} = \sum_{\alpha=1}^{(L+1)^2} g_{\alpha,nm}\hat{s}_\alpha \tag{4.7}$$

and

$$\hat{s}_\alpha = \sum_{nm}^{L} g_{\alpha,nm}\hat{s}_{nm}. \tag{4.8}$$

The Slepian functions $g_1(\sigma), \ldots, g_{(L+1)^2}(\sigma)$ are defined on the part Θ of the unit sphere $\mathbb{S}$.

Now, if we index g_α in terms of an index $\beta(n,m)$, between α and β there exists a bijective mapping such that $\alpha = \beta(n,m)$.
Using the Miranian computational method, the Slepian functions are given by

$$\psi^L_{\beta(n,m)}(\theta)(\eta_{n,m}\cos m\phi + (1-\eta_{n,m})\sin m\phi).$$

where

$$\eta_{n,m} = \begin{cases} 1 & \text{if } 1 \leq n \leq (L-m+1) \\ 0 & \text{if } L-m+2 \leq n \leq 2(L-m+1) \end{cases}$$

$$\sum_{\alpha=1}^{(L+1)^2} \hat{s}_\alpha g_\alpha = \sum_{n=0}^{L+1} \hat{s}^L_{\beta(n,0)}\psi^L_{\beta(n,0)}(\theta)\cos m\phi + \sum_{m=1}^{L}\sum_{n=1}^{2(L-m+1)} \hat{s}^L_{\beta(n,m)}\psi^L_{\beta(n,m)}(\theta)(\eta_{n,m}\cos m\phi + (1-\eta_{n,m})\sin m\phi)$$

with

$$\beta_{n,m} = \begin{cases} n & \text{if } 1 \leq n \leq (L+1), m = 0 \\ (L+1) + (m-1)(2L-(m-2)) + n & \text{if } 1 \leq n \leq 2(L-m+1), 1 \leq m \leq L. \end{cases}$$

The coefficients of the Slepian functions can be computed by:

$$s^L_{\beta(n,m)} = \langle s, \psi^L_{\beta(n,m)}(\theta)(\eta_{n,m}\cos m\phi + (1-\eta_{n,m})\sin m\phi)\rangle_\Theta. \tag{4.9}$$

For simplicity, in what follows, the Slepian functions $\psi^L_{\beta(n,m)}(\theta)(\eta_{n,m}\cos m\phi + (1-\eta_{n,m})\sin m\phi)$ will be denoted by $\Psi_{n,m}(\theta,\phi)$ or $\Psi_{n,m}(\sigma)$. The normalized Slepian functions are denoted by $\tilde{\Psi}_{n,m}$. They are orthonormal over the sphere and orthogonal over the region Θ:

$$\int_{\mathbb{S}} \tilde{\Psi}_{n,m}(\sigma)\tilde{\Psi}_{n',m'}(\sigma)\mathrm{d}\omega(\sigma) = \delta_{n,n'}\delta_{m,m'} \tag{4.10}$$

$$\int_{\Theta} \tilde{\Psi}_{n,m}(\sigma)\tilde{\Psi}_{n',m'}(\sigma)\mathrm{d}\omega(\sigma) = \mu_{nm}\delta_{n,n'}\delta_{m,m'} \tag{4.11}$$

The inverse problem which consists to estimate the signal $\hat{s}$ over the whole sphere $\mathbb{S}$ from measurements of the noisy data d on the region Θ, becomes to minimize:

$$\int_{\Theta} (\hat{s}(\sigma) - d(\sigma))^2 \mathrm{d}\omega(\sigma). \tag{4.12}$$

In [46], the estimate of the field coefficients is given by:

$$\hat{s}_{nm} = \sum_{n'm'}^{L} D^{-1}_{nm,n'm'} \int_{\Theta} d(\sigma) Y_{n',m'}(\sigma)\mathrm{d}\omega(\sigma), \tag{4.13}$$

where $D_{nm,n'm'}$ is given by (3.5).
Because $\mathbf{D}$ composed by the elements $D_{nm,n'm'}$, see (3.5) has a low condition number, finding a stable inverse $\mathbf{D^{-1}}$ is problematic, hence the problem is ill-conditioned. To stabilize the solution it was included a weighted norm to the minimization problem (4.12):

$$\int_{\Theta} (\hat{s} - d(\sigma))^2 \mathrm{d}\omega(\sigma) + \eta \int_{\Theta^e} \hat{s}^2 \mathrm{d}\omega(\sigma), \tag{4.14}$$

where $\eta > 0$ is a damping parameter.
Involving (4.4) and (3.5), we get:

$$\hat{s}_{nm} = \sum_{n'm'}^{L} (D_{nm,n'm'} + \eta\tilde{D}_{nm,n'm'})^{-1} \times \int_{\Theta} d(\sigma) Y_{n',m'}(\sigma)\mathrm{d}\omega(\sigma) \tag{4.15}$$

with

$$\tilde{D}_{nm,n'm'} = \int_{\Theta^e} Y_{nm} Y_{n',m'} \mathrm{d}w = \delta_{nn'}\delta_{mm'} - D_{nm,n'm'}. \tag{4.16}$$

The relation (4.15) holds for $n \leq L$, since, when $n > L$, no estimate is available, $\hat{s}_{nm} = 0$. The case where $n = 1$, for which $\mathbf{D} + \tilde{\mathbf{D}} = \mathbf{I}$, the identity matrix, was treated by Sneeuw and Gelderen [50].

By substituting the equation (4.3) and using (4.4), (3.5), the integral over the data in (4.15) becomes:

$$\int_\Theta d(\sigma) Y_{n',m'}(\sigma) \mathrm{d}\omega(\sigma) = \sum_{n'm'} D_{nm,n'm'} s_{n'm'} + \int_\Theta n(\sigma) Y_{nm}(\sigma) \mathrm{d}\omega(\sigma). \tag{4.17}$$

After we compute $\int_\Theta d(\sigma) Y_{n',m'}(\sigma) \mathrm{d}\omega(\sigma)$, we get the coefficients $\hat{s}_{nm}$ and consequently the signal $\hat{s}$. Now, if we use the Slepian expansion of $\hat{s}$:

$$\hat{s} = \sum_{\alpha=1}^{(L+1)^2} \hat{s}_\alpha g_\alpha, \tag{4.18}$$

the coefficients $\hat{s}_\alpha$ are computed according to (4.8). A Slepian basis expansion of the observations, combining (4.1), (4.3), (4.4), is given by:

$$d(\sigma) = \sum_{\alpha=1}^{(L+1)^2} \hat{s}_\alpha g_\alpha + \sum_{nm>L}^{\infty} s_{nm} Y_{nm}(\sigma) + n(\sigma). \tag{4.19}$$

This equation allows us to find an alternative expression for the data integral (4.17), for which we also use (4.5), (3.5) and (3.6):

$$\int_\Theta d(\sigma) Y_{nm} \mathrm{d}\omega(\sigma) = \sum_{\alpha=1}^{(L+1)^2} g_{\alpha,nm} (\mu_\alpha s_\alpha + \int_\Theta n g_\alpha \mathrm{d}\omega(\sigma)) + \sum_{n'm'>L}^{\infty} D_{nm,n'm'} s_{n'm'}. \tag{4.20}$$

where μ_α are the eigenvalues associated to the eigenfunctions g_α, see (3.6). Inserting (4.7), (4.14), (4.20) into (4.4), we get the following formula for the computation of $\hat{s}$:

$$\hat{s}(\sigma) = \sum_{\alpha=1}^{(L+1)^2} \mu_\alpha^*(\eta) g_\alpha(\sigma) \times \Big(\mu_\alpha s_\alpha + \int_\Theta n(\sigma) g_\alpha \mathrm{d}\omega + \sum_{nm>L}^{\infty} D_{nm,n'm'} s_{n'm'} \Big)$$

with

$$\mu_\alpha^*(\eta) = [\mu_\alpha + \eta(1 - \mu_\alpha)]^{-1}.$$

Remark 4.3.1. *In practice, the data is measured by satellites at an altitude a from the unit sphere* $\mathbb{S}$*. In this case, instead to consider the data on* $\mathbb{S}$ *it can be supposed known at the surface of* $\mathbb{S}_{1+a}$*,* $R = 1 + a$*.*

Then, at the altitude a above the unit sphere, the signal is given by:

$$s^u(\sigma) = \sum_{nm}^{L} s^u_{nm} Y_{nm}(\sigma) + \sum_{nm>L}^{\infty} s^u_{nm} Y_{nm}(\sigma), \tag{4.21}$$

where

$$s^u_{nm} = (1+a)^{-(n+1)} s_{nm}. \tag{4.22}$$

where the index u denotes the upward component.

Remark 4.3.2. *The estimation problem (4.14) can be also formulated in terms of best constrained approximation problems (BEP), see [5].*

4.4 Bandlimited signals expansion

Given $s_L \in B_L$ a bandlimited function on the sphere, we have that $s_L(\sigma)$ has the following Slepian functions expansion on the region Θ and the sphere $\mathbb{S}$:

On the sphere $\mathbb{S}$:

$$s_L(\sigma) = \sum_{m=0}^{L} \sum_{n=1}^{2(L-m+1)} a_{nm} \tilde{\Psi}_{n,m}(\sigma) = \sum_{m=0}^{L} \sum_{n=1}^{2(L-m+1)} a_{nm} \sqrt{\mu_{nm}} \Psi_{n,m}(\sigma), \tag{4.23}$$

where $\tilde{\Psi}_{n,m}(\sigma)$ are the normalized Slepian functions introduced in (4.9).
Using (4.10) and (4.11), we have:

$$\int_{\Theta} |\Psi_{n,m}(\sigma)|^2 \mathrm{d}\omega(\sigma) = 1 \tag{4.24}$$

and

$$\int_{\mathbb{S}} |\Psi_{n,m}(\sigma)|^2 \mathrm{d}\omega(\sigma) = \frac{1}{\mu_{nm}}, \tag{4.25}$$

where the μ_{nm} are the eigenvalues associated to the eigenfunctions of the operator $\mathcal{T}_m$.

On the region Θ:

$$s_L(\sigma) = \sum_{m=0}^{L} \sum_{n=1}^{2(L-m+1)} b_{nm} \Psi_{n,m}(\sigma), \tag{4.26}$$

$\Psi_{n,m}(\sigma)$ is a basis for $L^2(\mathbb{R}) \cap B_L$, where:

$$B_L = \{s \in L^2(\mathbb{S}), s \text{ is an } L - \text{bandlimited function}\}. \tag{4.27}$$

On the region Θ, the equations (4.23) and (4.26) hold simultaneously, that is:

$$b_{n,m} = \sqrt{\mu_{nm}} a_{nm},\ 1 \leq n \leq 2(L - m + 1). \tag{4.28}$$

Moreover, we have from (4.23):

$$\|s_L\|_{\mathbb{S}}^2 = \sum_{m=0}^{L} \sum_{n=1}^{2(L-m+1)} |a_{nm}|^2. \tag{4.29}$$

Hence,

$$\frac{|b_{nm}|}{\sqrt{\mu_{nm}}} = |a_{nm}| \leq \|s_L\|_{\mathbb{S}}, \forall n, m. \tag{4.30}$$

By combining, (4.28) and (4.30), we conclude that the $|b_{nm}|^2$ have the same decay as the sequence of eigenvalues $\mu_{nm}, 0 \leq m \leq L, 1 \leq n \leq 2(L - m + 1)$. They have also a faster decay than the spherical harmonic coefficients.

Example:

In this example, we consider a particular signal, the gravitational potential V, defined on $\mathbb{S}$ by:

$$V(X) = \sum_{k=1}^{N} \frac{m_k}{|X - S_k|}, \tag{4.31}$$

where S_k are monopolar sources and m_k their masses. We define also the region $\Theta = \{(\theta, \phi), \theta \in [0, 90], \phi \in [0, 2\pi]\}$. Then, the first spherical harmonic coefficients expansion of V and the corresponding Slepian functions expansion coefficients are given by the next table. The gravitational potential V is supposed to be generated by the monopolar source $S = (-0.06, 0.42, 0.25)$ of masse $m = 0.6$.

Table 4.1: *Slepian and spherical harmonic coefficients*

Slepian coefficients	Sph. harmonic coeffs.
1.34735025892288	2.12694462108036
1.18133457989493	0.52281646393469
0.45997548109045	-0.3108172255903
-0.0252840301636	0.08394471836205
0.03100363169295	0.04794941680222
-0.0299892861079	0.17753951636619
0.00548231227261	-0.0274923910878
-0.1930938528012	0.02850618855291
0.18677640267095	-0.1454675460986
-0.0341444128050	-0.0452532233219
-0.0512831282433	0.02293579710826
0.04474925300979	0.01473934291648
-0.0169040872483	0.04371476066204
0.01475037313615	0.00236658574342
0.01656191070438	-0.0695819541854
-0.0319988610750	-0.0234220787321

Now, using these coefficients, we express the gravitational potential V in Slepian (in red) and the spherical harmonic basis (in blue). We plot their behavior with respect to the exact simulated potential in green (4.31):

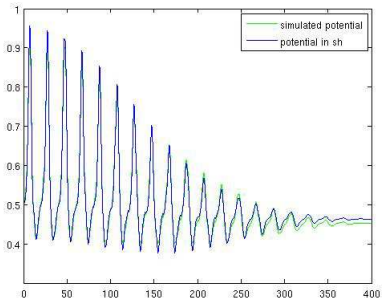

Figure 4.2: *Spherical harmonic expansion*

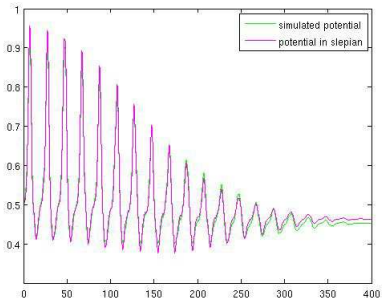

Figure 4.3: *Slepian expansion*

Choice of bandwidth L

The bandwidth L plays an important role in the approximation of a signal s by its truncated approximant s_L as well as in source localization error. Let us consider the monopolar sources $S_k, k = 1, \ldots, N$ located at (r_k, θ_k, ϕ_k) and with masses m_k. We take $\beta = \max |\frac{r_k}{R}| < 1, R \geq 1, r_k < R$ and let us consider $\beta < \gamma < 1$. Then, $\forall \gamma > \beta$, we have $s \in L^2(\mathbb{S}_\gamma)$ and its expansion on spherical harmonic basis there is:

$$s(\theta, \phi) = \sum_{n \geq 0, m} s_{nm} \gamma^{-n} Y_{nm}(\theta, \phi) \text{ on } \mathbb{S}_\gamma. \tag{4.32}$$

with s harmonic at $\mathbb{B}^e_\gamma$.
From Parseval equality, we have:

$$\|s\|^2_{\mathbb{S}} = \sum_{n \geq 0}^{\infty} \sum_{m=-n}^{n} |\gamma^{-n} s_{nm}|^2,$$

we have:

$$\sum_{n > L} \sum_{m=-n}^{n} |\gamma^{-n} s_{nm}|^2 \leq \|s\|^2_{\mathbb{S}_\gamma}.$$

Hence,

$$|s_{nm}|^2 \leq \gamma^n \|s\|^2_{\mathbb{S}_\gamma}.$$

and then:

$$\begin{aligned}
\|s - s_L\|^2_{\mathbb{S}} &= \sum_{n \geq L+1} \sum_{m=-n}^{n} |s_{nm}|^2 \\
&\leq \|s\|^2_{\mathbb{S}_\gamma} \sum_{n \geq L+1} \sum_{m=-n}^{n} \gamma^{2n} \\
&\leq \|s\|^2_{\mathbb{S}_\gamma} \sum_{n \geq L+1} (2n+1)\gamma^{2n} \\
&= \|s\|^2_{\mathbb{S}_\gamma} \frac{\mathrm{d}(\sum_{n \geq L+1} \gamma^{2n+1})}{\mathrm{d}\gamma} \\
&= \|s\|^2_{\mathbb{S}_\gamma} \cdot \frac{\gamma^{2L+2}(2L+3-(2L+1)\gamma^2)}{(1-\gamma^2)^2}
\end{aligned}$$

$$\frac{\|s - s_L\|^2_{\mathbb{S}}}{\|s\|^2_{\mathbb{S}_\gamma}} \leq \epsilon_L(\gamma) \to 0 \text{ for } L \to \infty,$$

where

$$\begin{aligned}\epsilon_L(\gamma) &= \frac{\gamma^{2L+2}(2L+3-(2L+1)\gamma^2)}{(1-\gamma^2)^2} \\ &= \frac{\gamma^2}{(1-\gamma^2)^2} L\gamma^{2L}(2+\frac{3}{L}-(2+\frac{1}{L})\gamma^2) \\ &\simeq \frac{2\gamma^2}{1-\gamma^2} L\gamma^{2L} \to 0, L \to \infty, |\gamma| < 1\end{aligned}$$

with

$$L\gamma^{2L} = L\mathrm{e}^{-2L(\ln(\frac{1}{\gamma}))}.$$

We have used:

$$L\mathrm{e}^{-\alpha L} \to 0 \text{ for } L \to \infty, \alpha > 0.$$

Chapter 5

Singularities of the potential in the ball

The aim of this chapter is the resolution of the density recovery (DR) problem and singularity recovery (SR) problem when the disposed data is the gravitational potential and the electrical potential, respectively (monopolar and dipolar sources, respectively). The unified mathematical formulation of these two potential problems is expressed by [6, 22]:

$$\Delta Pot = \rho \text{ in } \mathbb{B}, \tag{5.1}$$

where Pot can be the gravitational or the electrical potential and the density ρ can be approximated by a discrete combination of monopolar and dipolar density given as follows:

$$f = \sum_{k=1}^{N} m_k \delta_{S_k} + \sum_{k=1}^{N} p_k . \nabla \delta_{C_k}, \tag{5.2}$$

$f \simeq \rho$, where S_k are monopolar sources, C_k are the dipolar sources, m_k the masses of S_k and p_k the moments of C_k. For $p_k = 0$ the problem becomes a monopolar geodesy inverse problem and for $m_k = 0$ we have a dipolar EEG inverse problem. We recall the (DR) and (SR) problems for geodesy and EEG:

(DR): *Being given boundary data $Pot_{\mathbb{S}}$ associated to a solution Pot of (5.1) on $\mathbb{S}$ (i.e. $Pot_{|_{\mathbb{S}}} = Pot_{\mathbb{S}}$), find a related density ρ in $\mathbb{B}$* (uniqueness properties will be discussed).

(SR): *Being given on $\mathbb{S}$ measurements $Pot_{\mathbb{S}}$, find a pointwise discrete distribution ρ_N of (a given number) N pointwise monopolar or dipolar sources located inside $\mathbb{B}$, such that the associated potential Pot_N best approximates Pot in quadratic norm on $\mathbb{S}$.*

In [22] an important identifiability result associated with the problem (5.1) and (5.2) is given. The identifiability result permits us to know if the inverse problem is well posed in the following sense: if two measured potentials Pot_1 and Pot_2 coincide on Γ_* (a convenient subset of the sphere $\mathbb{S}$), then they are generated by the same sources. In other words, identifiability means the uniqueness of the inverse problem, see Theorem 5.2.1. Related to the geodesy and EEG inverse problems, well-posedness properties discussions intervene naturally. This chapter is organized as follows. In Section 5.1, we give the mathematical formulation for some direct and inverse geodesy and EEG problems, then in Section 5.2 some well-posedness results are introduced. We end by Section 5.3 where the best quadratic approximation method is presented as algorithm for the resolution of both (DR) inverse problems, see [8, 17].

5.1 Density models

The mathematical formulation for the direct and the inverse problems related to the geodesy and M/EEG that we consider in this thesis is given by the equations:

$$-\Delta V = \rho \text{ in } \mathbb{B}\,,\ \Delta V = 0 \text{ in } \mathbb{B}^e = \mathbb{R}^3 \setminus \mathbb{B}, \tag{5.3}$$

where $V \in L^2(\mathbb{R}^3)$ and $\rho \in L^2(\mathbb{B})$ are the gravitational potential and the gravitational density, respectively. In this section, we study the inverse density recovery problems. In fact, the *density recovery problem* (DR) consists of approximately computing the density $\rho \in L^2(\mathbb{B})$ inside the ball by solving the (SR) problem. For the solution of this later, we apply the rational approximation techniques given in [8, 17]. More precisely, given $V_{|\mathbb{S}}$ on $\mathbb{S}$, we build the "discrete" problem (SR) as an intermediary step for the (DR) resolution problem [6, 10]. At this level, we will describe the algorithm that allows us to go from the data on the sphere to the singularities in the ball $\mathbb{B}$. Hence, the recovery of the discrete density is accomplished. In fact, we are interested in a density of the following form (relation (5.2) with $p_k = 0$):

$$\rho_N = \sum_{k=1}^{N} m_k \delta_{S_k}, \tag{5.4}$$

which leads to the associated approximated potential V_N such that ρ_N approximates ρ and it is solution of:

$$-\Delta V_N = \rho_N \text{ in } \mathbb{B},\ \Delta V_N = 0 \text{ in } \mathbb{B}^e \text{ and } V_N \text{ best approximates } V \text{ on } L^2(\mathbb{S}) \text{ norm}. \tag{5.5}$$

The discrete density ρ_N can be approximated by a density ρ_χ which characterize inclusions zones of the Earth with high concentration. Recall that, when it comes to applications, the surface $\mathbb{S}$ of $\mathbb{B}$ could be either the Earth boundary, or the scalp of the head. We assume here that the given data $V_{\mathbb{S}}$ on $\mathbb{S}$ is given via its harmonic spherical expansion coefficients. In this thesis, we use the available data on $\mathbb{S}$ or part of $\mathbb{S}$ and we apply our proposed Gaussian quadrature method on the sphere to get accurate approximations of these coefficients.

Density recovery problem

Related to the inverse problem is the direct (forward) problem, which consists in finding the values on $\mathbb{S}$ of the potential V solution to (5.3), from the internal density ρ in $\mathbb{B}$. The relation between the density ρ on $\mathbb{B}$ and V on $\mathbb{S}$ is expressed by the forward operator T:

$$(T\rho)(y) = \int_{\mathbb{B}} \frac{\rho(x)}{|x-y|} \mathrm{d}x \text{ for } y \in \mathbb{S}, \tag{5.6}$$

so that $T\rho = V_{|\mathbb{S}}$ for V solution to (5.3) or T_e (for data taken on $\mathbb{S}_R, R > 1$):

$$(T_e\rho)(y) = \int_{\mathbb{B}} \frac{\rho(x)}{|x-y|} \mathrm{d}x \text{ for } y \in \mathbb{B}^e, \tag{5.7}$$

whence $(T_e\rho)_{|\mathbb{S}} = T\rho$. From this, it is easy to see that minimizing the potential in $L^2(\mathbb{S})$ comes to minimize $\|\rho\|_{\mathbb{S}}$. This last problem was studied in [12, 39]. Under a harmonicity constraint, a unique minimizer of ρ is given.

In [16, 51], the authors have given local and global methods for the density approximation in the Earth. In [39] and [38] under a constraint of harmonicity a kernel or a scaling function is proposed for the density approximation.

In the following, we give a proposition for the existence of the direct problem, and continuity properties of the forward operator T:

Proposition 5.1.1. *[39, Thm 2.1] Whenever $\rho \in L^2(\mathbb{B})$, then V is a solution to (5.3) if and only if $V = T_e\rho$, see (5.7).*

Remark 5.1.1. *The previous Proposition is also valid for pointwise densities ρ_N given by (5.4), see [39]. Moreover, it remains true for $\rho \in L^1(\mathbb{B})$ with $\operatorname{supp}\rho \subset \mathbb{B}_r \subset \mathbb{B}$ the ball centered at 0 and of radius $r < 1$.*

Note that in [39], it has been shown that the operator T maps $L^2(\mathbb{B}) \to L^2(\mathbb{S})$ continuously and

$$\|T\rho\|_{L^2(\mathbb{S})} \leq 4\pi \|\rho\|_{L^2(\mathbb{B})}.$$

Another important property of the operator T_e is given by the following proposition:

Proposition 5.1.2. *Whenever $\rho \in L^2(\mathbb{B})$ with $\operatorname{supp}\rho \subset \mathbb{B}_r, r < 1$, then $T_e\rho$ is a continuous function on $\overline{\mathbb{B}}^e$.*

Proof. Put $T_e\rho = V$. Let $y_1, y_2 \in \overline{\mathbb{B}}^e$:

$$\begin{aligned} |V(y_2) - V(y_1)| &= |\int_{\mathbb{B}_r} \frac{\rho(x)}{|x-y_2|}\mathrm{d}x - \int_{\mathbb{B}_r} \frac{\rho(x)}{|x-y_1|}\mathrm{d}x| \\ &= |\int_{\mathbb{B}_r} \rho(x)\left[\frac{1}{|x-y_2|} - \frac{1}{|x-y_1|}\right]\mathrm{d}x| = |\int_{\mathbb{B}_r} \rho(x)\left[\frac{|x-y_1|-|x-y_2|}{|x-y_1||x-y_2|}\right]\mathrm{d}x| \\ &\leq \int_{\mathbb{B}_r} |\rho(x)|\left[\frac{|y_1-y_2|}{|x-y_1||x-y_2|}\right]\mathrm{d}x, \end{aligned}$$

because $\rho \in L^2(\mathbb{B}_r)$ and $|x-y| \geq 1-r$ for $y \in \mathbb{B}^e$.
So,

$$|V(y_2) - V(y_1)| \leq c\,\|\rho\|_{L^2(\mathbb{B})}\,|y_1 - y_2|,$$

with $c = c_r = (1-r)^2$.
Hence, $|V(y_2) - V(y_1)| \longrightarrow 0$ for $|y_1 - y_2| \longrightarrow 0$. □

Remark 5.1.2. *The previous Proposition remains true for $\rho \in L^1(\mathbb{B})$ and $\operatorname{supp}\rho \subset \mathbb{B}_r, r < 1$ and for pointwise densities ρ_N given by (5.4).*

In the following, we give other properties of the density ρ and the operator T:
The density $\rho \in L^2(\mathbb{B})$ can be decomposed into a harmonic and an anti-harmonic part $\rho = \rho_{harm} + \rho_{anharm}$ such that [39]:

$$\|\rho\|^2_{\mathbb{B}} = \|\rho_{harm}\|^2_{\mathbb{B}} + \|\rho_{anharm}\|^2_{\mathbb{B}}.$$

To show this relation we use the next proposition:

Proposition 5.1.3. *[39] $L^2(\mathbb{B})$ is written as the following direct sum:*

$$L^2(\mathbb{B}) = \mathrm{Harm}(\mathbb{B}) \oplus \mathrm{Anharm}(\mathbb{B}), \tag{5.8}$$

where

$$\mathrm{Harm}(\mathbb{B}) = \{H \in C^2(\mathbb{B}) |\, \Delta H = 0 \text{ in } \mathbb{B}\},$$
$$\mathrm{Anharm}(\mathbb{B}) = \{F \in L^2(\mathbb{B}) |\, \langle F, H\rangle_{\mathbb{B}} = 0, \forall H \in \mathrm{Harm}(\mathbb{B})\}.$$

Proposition 5.1.4. *An equivalent decomposition is also given as follows:*

$$L^2(\mathbb{B}) = \mathrm{Harm}(\mathbb{B}) \oplus \Delta\, W_0^{2,2}(\mathbb{B}). \tag{5.9}$$

The space of "anharmonic functions" coincides with those density functions ρ which have vanishing associated potential V_ρ in $\mathbb{B}^e$:

$$\mathrm{Anharm}(\mathbb{B}) = \{\rho \in L^2(\mathbb{B}) \,|\, T_e\rho = 0\}.$$

Proof. First, we show that $\text{Anharm}(\mathbb{B}) \subset \{\rho \in L^2(\mathbb{B}) \,|\, T_e\rho = 0\}$.
The equality $T_e\rho(y) = 0$ means:

$$\int_{\mathbb{B}} \frac{\rho(x)}{|y-x|}\mathrm{d}x = (\rho * E_3)(y) = \int_{\mathbb{B}} \rho(x)E_3(y-x)\mathrm{d}x = \langle \rho, E_3(y-x)\rangle_{\mathbb{B}} = 0,$$

where $E_3(y-x)$ is the fundamental solution of Laplace equation.

Let $g \in \Delta W_0^{2,2}(\mathbb{B})$, so $g = \Delta v, v \in W_0^{2,2}(\mathbb{B})$. Using the second Green's formula, we have:

$$\langle g, E_3(y-x)\rangle_{\mathbb{B}} = \int_{\mathbb{S}} \frac{\partial v(x)}{\partial n} E_3(y-x)\mathrm{d}x - \int_{\mathbb{S}} v(x)\frac{\partial E_3(y-x)}{\partial n}\mathrm{d}x = 0,$$

because $\Delta_x E_3(y-x) = 0$ in $\mathbb{B}$ if $y \in \mathbb{B}^e$ and $v \in W_0^{2,2}$. Hence, $\text{Anharm}(\mathbb{B}) \subset \{\rho \in L^2(\mathbb{B}) \,|\, T_e\rho = 0\}$.

Secondly, we show that $\text{Anharm}(\mathbb{B}) \supset \{\rho \in L^2(\mathbb{B}) \,|\, T_e\rho = 0\}$.
Let $\rho \in L^2(\mathbb{B})$ such as $T_e\rho = 0$. This is equivalent to say that $\langle \rho, E_3(y-x)\rangle_{\mathbb{B}} = 0$ for $y \in \mathbb{B}^e$. Because $E_3(y-x)$ is harmonic for $y \in \mathbb{B}^e$, we have $\rho \in \text{Anharm}(\mathbb{B})$. □

This proposition is equivalent to say that only the harmonic part of the density generates a non nul exterior potential.

Remark 5.1.3. *$KerT_e = KerT = \text{Anharm}(\mathbb{B}) = \{\rho \in L^2(\mathbb{B}) \,|\, T_e\rho = 0\}$ with the topological supplement* $\text{Harm}(\mathbb{B})$ *in* $L^2(\mathbb{B})$.

Source recovery problem

(SR) problem has been considered for example in [1] and consists in finding a discrete density in $\mathbb{B}$ denoted by ρ_N, such that $T\rho_N = V_{N|_{\mathbb{S}}}$ is close to a given function $V_{\mathbb{S}}$ on $\mathbb{S}$, in a sense to be made precise. Note that whenever $V_{\mathbb{S}} = V_{|_{\mathbb{S}}}$ for some solution $V = T\rho$ to (5.3), then (SR) leads to a discretization V_N of the potential V (and to the related discrete density ρ_N, approximating ρ).
Given $V_{\mathbb{S}}$ on $\mathbb{S}$, we thus introduce the functional $\mathcal{F}_N$ defined on $\mathbb{B}^N \times \mathbb{R}^N$ which depends on two families of parameters (vectors) $(\mathbf{S}, \mathbf{m})$ representing the positions and masses associated with N monopolar sources, that is:

$$\mathcal{F}_N(\mathbf{S}, \mathbf{m}) = \|V_{\mathbb{S}} - V_N\|_{\mathbb{S}}^2, \tag{5.10}$$

where $V_N = V(N, \mathbf{S}, \mathbf{m})$, $\mathbf{S} = (S_k) \in \mathbb{B}^N$, $0 < r_1 \leq |S_k| \leq r_2 < 1$, $\mathbf{m} = (m_k) \in \mathbb{R}^N$, $M \geq m_k \geq \mathbf{m} > 0$, for $k = 1, \ldots, N$, where M is the mass of the Earth and

$$V_N(y) = \sum_{k=1}^{N} \frac{m_k}{|y - S_k|}, \forall\ y \neq S_k. \tag{5.11}$$

Then, with $\rho_N = \sum_{k=1}^{N} m_k \delta_{S_k}$, we have that V_N is a solution to (5.3) associated to ρ_N, with $V_N = T\rho_N$.

Remark 5.1.4. *Though the Earth density possesses localized zones of high concentration, they can though be approximated by pointwise masses or by inclusions [10].*

In geophysics literature, the inverse geodesy problem (DR) was intensively studied, see for example [1, 38, 39, 51].

Next, the inverse problem of density recovery related to EEG that we consider in this thesis is modeled by the equations (2.50). We note in this case that the surface $\mathbb{S}$ of $\mathbb{B}$ is the scalp of the head and after a preliminary cortical mapping step of data transmission, we end up with a "filtered" part of the electrical potential which satisfies $\Delta U = 0$ in $\mathbb{B}^e$.
In the same way as for the monopolar case, we can formulate the direct and the inverse (DR) EEG problem.

The *direct problem* associated to (SR) is: *being given the density* $\rho_N = \sum_{k=1}^{N} p_k.\nabla\delta_{C_k}$ *inside the ball* $\mathbb{B}$, *find the exterior generated potential* U *at* $\mathbb{S}$.

The density recovery problem (SR) is: *being given boundary data* $U_{\mathbb{S}}$ *associated to a solution* U *of (2.50) on* $\mathbb{S}$ *(i.e.* $U_{|_{\mathbb{S}}} = U_{\mathbb{S}}$*), find the related density* ρ_N *in* $\mathbb{B}$.

Links between (DR) and (SR) problem

To have an approximation of the (DR) problem, we solve the source recovery problem (SR) supposing the discrete density given by a monopolar or dipolar sources distribution. In the geodesy case, because of the non uniformed repartition of the density (different levels of concentration on the Earth), this can be modeled by agglomerations of monopolar/dipolar sources contained in small inclusions parametrized by a small radius ϵ, see Section 5.4.

5.2 Existence, uniqueness and stability results

We recall the (SR) inverse geodesy problem with ρ_N given by (5.4), supposing that $M \geq m_k \geq m > 0$, and the sources considered inside the spherical shell $\mathcal{B} = \mathcal{B}(r_1, r_2)$: $0 < r_1 \leq |S_k| \leq r_2 < 1$. Before solving this problem, we give some existence, uniqueness and stability results. The point-masses determination problem (5.10) was introduced in [1]. In order to study the well-posedeness of the problem, we introduce details on the existence property.

Problem (SR): For a fixed N

$$\text{find } V_N \text{ (alternatively, } (\mathbf{S}, \mathbf{m})) \text{ that minimizes (5.10).} \tag{5.10$'$}$$

In the following we give a proof of the existence of this problem:

Proposition 5.2.1. *For any set of measurements of V, there exists a density ρ such that $T\rho = V \in L^2(\mathbb{S})$.*

Proof. The existence of solutions V_N to problem (5.10$'$) is ensured by continuity properties. The expansion of V, measured at the surface of the unit sphere, in terms of the spherical harmonic basis is given by:

$$V(1, \theta, \phi) = \sum_{n=0}^{\infty} \sum_{m=-n}^{n} c_{nm} Y_{nm}(\theta, \phi), \tag{5.12}$$

The potential generated by N sources is the sum of the potentials generated by the considered point masses.

$$V_N(1, \theta, \phi) = \sum_{k=1}^{N} m_k \sum_{n=0}^{\infty} \sum_{m=-n}^{n} r_k^n \frac{4\pi}{2n+1} Y_{nm}(\theta_k, \phi_k) Y_{nm}(\theta, \phi), \tag{5.13}$$

with c_{nm} the coefficients of the development of V in spherical harmonic basis. For getting the spherical harmonic expansion of the discrete gravitational potential (5.11) we denote by l_k the Euclidean distance between X and S_k with

$$l_k = \sqrt{1 - 2r_k \cos\psi_k + r_k^2}, \tag{5.14}$$

where ψ_k is the spherical distance between X and S_k. Then, we have:

$$\frac{1}{l_k} = \frac{1}{\sqrt{1 - 2r_k \cos\psi_k + r_k^2}} = \frac{1}{r_k} \sum_{n=0}^{\infty} r_k^{n+1} P_n(cos\psi_k). \tag{5.15}$$

Using the addition formula for spherical harmonics (2.38), we get:

$$\frac{1}{l_k} = \sum_{n=0}^{\infty} r_k^n \frac{4\pi}{2n+1} Y_{nm}(\theta_k, \phi_k) Y_{nm}(\theta, \phi). \tag{5.16}$$

Then, we obtain (5.13). Using the development of V and V_N on the spherical harmonic basis, the functional $\mathcal{F}_N(\mathbf{S}, \mathbf{m}) = \|V_{\mathbb{S}} - V_N\|_{\mathbb{S}}^2$ becomes:

$$\min_{\mathbf{S}\in\mathbb{B}^N, \mathbf{m}\in\mathbb{R}^N} \|b - A(\mathbf{S})\mathbf{m}\|_{\mathbb{S}}^2, \tag{5.17}$$

where, the entries of b and $A(\mathbf{S})$ are given by:

$$b_{I(n,m)} = c_{nm}\Big(\frac{1}{R}\Big)^n, \quad I(n,m) = 1, 2, \ldots,$$

$$A_{I(n,m)k}(\mathbf{S}) = \frac{4\pi}{(2n+1)} r_k^n Y_{nm}(\theta_k, \phi_k), \quad I(n,m) = 1, 2 \ldots, \quad k = 1, \ldots, N,$$

with $I(n,m) = \sum_{l=0}^{n}(2l+1) - n + m = n^2 + n - m + 1$, $-n \leq m \leq n$. We note that the functional $\mathcal{F}_N$ is continuous on the ball $\mathbb{B}^N \times [0, M]^N$, $0 \leq \sum_{k=1}^{N} m_k \leq M$.

□

The problem (5.5) is ill posed. A condition on this problem such that the solution exists is the next compatibility condition:

$$\int_{\mathbb{S}} g \mathrm{d}\omega = -\sum_{k=1}^{N} m_k,$$

with $g = \frac{\partial V}{\partial n}$. Then, the solution is unique up to an additive constant.

For the (SR) problem, the uniqueness (i.e. identifiability) of the solution of (5.10) is establish in [22], see the next theorem for $p_k = 0$ in (5.2):

Theorem 5.2.1. *[22] Let $V_i, i = 1, 2$ be the solution of the problems*

$$\begin{cases} \Delta V_i = F^i \text{ in } \mathbb{B} \\ \frac{\partial V_i}{\partial n} = g \text{ on } \mathbb{S} \\ V = f \text{ on } \mathbb{S} \end{cases} \tag{5.18}$$

such that $V_1 = V_2$ on Γ_* which is a subset with non-void interior of $\mathbb{S}$. Then $V_1 = V_2$, i.e.

$$S_k^{(1)} = S_k^{(2)}, m_k^{(1)} = m_k^{(2)}, k = 1, \ldots, N.$$

where S_k are monopolar sources and m_k their masses.

A general stability result is given by Theorem 2.2.1. Next, we give some existence and stability results associated with the EEG problem. The identifiability Theorem 5.2.1 remains valid for $m_k = 0$ and $p_k \neq 0$. The direct problem (2.50) is well-posed on the Hilbert quotient space $W^{1,2}(\mathbb{B})/\mathbb{R}$ under the compatibility condition [22]:

$$\int_\Gamma g \mathrm{d}\omega = \int_\Gamma \frac{\partial U}{\partial n} \mathrm{d}\omega = \langle \rho_N, 1 \rangle_{\mathbb{B}} \tag{5.19}$$

where $W^{1,2}$ is the Sobolev space, U the electrical potential. Note that if $f_1, f_2 \in W^{1,2}(\mathbb{B})$ with $f_1 = f_2 + constant$, then $f_1 = f_2$ in $W^{1,2}(\mathbb{B})/\mathbb{R}$.

Another result is given in [6].

Proposition 5.2.2. *Given a dipolar source distribution $C_k, k = 1, \ldots, N$ of moments p_k, the potential U generated by this distribution verifies (2.50), where the current flux belongs to $W^{-\frac{1}{2},2}(\Gamma)$ with*

$$\int_{\mathbb{S}} g \mathrm{d}\omega = 0.$$

Then, the direct EEG problem (2.50) admits a unique solution up to an additive constant and the solution U belongs to $W^{\frac{1}{2},2}(\mathbb{S})$.

The identifiability Theorem 5.2.1 can be seen as a uniqueness result [22, 55]: if two measured potentials U_1 and U_2 coincide on Γ_*, a non void-interior subset of $\mathbb{S}$, then they are generated by the same sources.

Stability: If two potentials generated by two distributions of N dipolar sources have close values on the boundary $\mathbb{S}$, then the corresponded distributions are also close rapported to a distance [22, 53]. A local stability for EEG problem is given in [21]:

Theorem 5.2.2. *If $\varphi^h = (p_k, C_k)_{1 \leq k \leq N} \in (\mathbb{R}^3 \times \mathbb{B})^N$ such that $\varphi^h \to \varphi$ if $h \to 0$ and if we denote by f^h the data on Γ_* corresponding to φ^h, then:*

$$\lim_{h \to 0} \frac{\|f - f^h\|_{\Gamma_*}}{|h|} > 0.$$

5.3 Resolution schemes

A short description of some resolution methods was introduced in Chapter 1. In this thesis, the (SR) problem is solved by using the best quadratic approximation on 2D combined with our scheme for the extrapolation of the potential to whole sphere via Slepian functions basis and the computation of spherical harmonic expansion coefficients of this later.

Our resolution procedure

Once the data is estimated over the whole sphere $\mathbb{S}$ (geodesy, M/EEG) by solving (TP), the next step in the resolution of the inverse problem (IP), is the source recovery problem (SR). The resolution of (SR) problem in the ball $\mathbb{B}$ involves 3 steps:

- Planar sections
  The ball $\mathbb{B}$ is sliced along a family of parallel sections, perpendicular to a chosen axis. The intersection between $\mathbb{B}$ and the planar sections gives us a family of disks where we apply the best quadratic rational approximation.
- Best quadratic rational approximation on circles
  The 2D approximation techniques are used to find the planar singularities on the disks obtained in the previous step.
- 3D sources localization
  The sources are localized in 3D by analyzing the planar singularities induced by sources or masses which are superposed.

Remark 5.3.1. *In order to get more accuracy on the localization process and to separate the sources, the detection step must be performed with several slicing directions.*

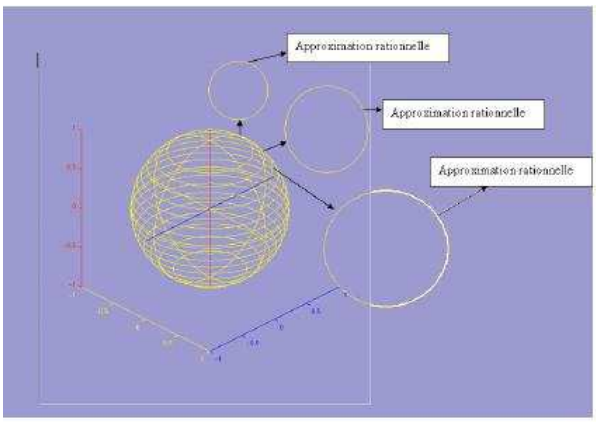

Figure 5.1: *Rational approximation from 3D to 2D*

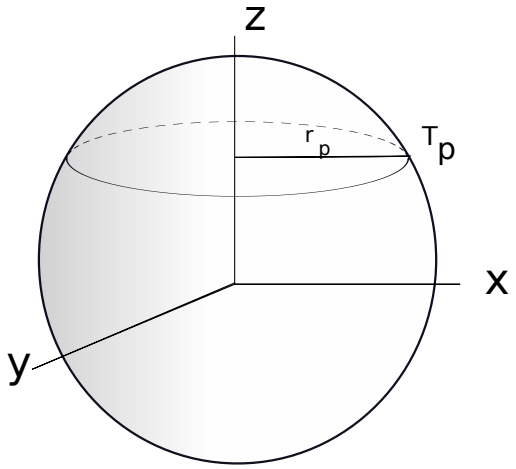

Figure 5.2: *One section of* $\mathbb{S}$

Planar sections

We suppose that the data is given over the whole sphere $\mathbb{S}$ and it is harmonic at the exterior of the ball. The ball $\mathbb{B}$ is sliced along a family of planes $\Pi_p, p = 1, \cdots, P$. The intersection between $\mathbb{B}$ and Π_p are disks D_p whose boundaries are circles T_p of radius r_p centered at a point of the chosen axis. From V_p on T_p (the restriction of

the potential V on the circles T_p, i.e. $V \setminus T_p$), we build the complex rational variable function f_p on the unit circle T_p. Due to the N sources C_k, f_p has N singularities $z^-_{k,p}$ (related to the positions of C_k) inside the disk D_p (as well as N related singularities $z^+_{k,p}$ outside the closed disk $\overline{D}_p$). The data f_p is assumed to be given either by a number of its pointwise values on T_p or by a number of its Fourier coefficients, using the spherical harmonics expansions of $V_{\mathbb{S}}$.

Remark 5.3.2. *For building the function f_p on the circles, we use the relation $\overline{z} = \frac{r_p^2}{z}$, with z the affix of the points where we take the measurements, see [8].*

Remark 5.3.3. *In [8, 17], the data is available over whole the sphere $\mathbb{S}$ and the coefficients of the spherical harmonic expansion of the data are computed by solving a linear system of equations that might be unstable. Our proposed method works with data potential known only in a region of the sphere, like belt or spherical caps. Also, the coefficients are computed by using the Gauss-Legendre quadrature.*

Once we can localize the singularities $z^-_{k,p}$, this leads to an estimate of C_k. The relation between the singularities $z^-_{k,p}$ and the sources C_k is given by the next proposition [56]:

Proposition 5.3.1. *We suppose $z_k \neq 0, k \in \{1, \dots n\}$. Then:*

$$arg(z^-_{k,p}) = arg(z_k) \text{ and } \max_{p=1\dots P} |z^-_{k,p}| = z_k$$

This allows us to determine the number N of sources.

The function f_p has the following properties:

1. If there exists just one source ($N = 1$), then f_p is a rational function with a pole (single or triple) in D_p at $z_{1,p}$.

2. If there are more than one source ($N \geq 2$), f_p is not anymore a rational function. In this case, f_p can still be approximated on the boundary T_p by a rational function with poles in D_p [8, 9].

Best quadratic rational approximation on circles

At the origin, the rational approximation was mainly used in systems theory, control theory and signal treatment [11]. The software used for the inverse source problem identification (Matlab software RARL2, see [37]) was first implemented for the resolution of frequencies filters identification problems in signal [21]. These problems consist in approximating the transfer function of a system by a rational

function with poles in $\mathbb{D}$, given pointwise values of the transfer function on the unit circle $\mathbb{T}$ of $\mathbb{C}$. Before describing the algorithm we need to introduce $\mathcal{R}_m$ to be the set of rational functions R_m with less than m poles in the unit disk $\mathbb{D}$:

$$R_m = \Big\{ \frac{p_m}{q_m}, \text{ where } p_m, q_m \text{ are polynomials such that } \deg p_m < \deg q_m \leq m, \text{roots of } q_m \text{belong to } \mathbb{D} \Big\}$$

A best quadratic rational approximant to f_p in $\mathcal{R}_m$ is a function $R_m^* \in \mathcal{R}_m$ which verify:

$$\|f_p - R_m^*\|_{\mathbb{T}} = \min_{R_m \in \mathcal{R}_m} \|f_p - R_m\|_{\mathbb{T}} \tag{5.20}$$

for the $L^2(\mathbb{T})$ norm. As we see in the previous step, the function f_p is computed on each circle T_p. To apply the best quadratic rational approximant of f_p we need to get the norm L^2 on the unit circle $\mathbb{T}$. For this, a normalization step of f_p is required. Existence and uniqueness in problem (5.20) are studied in [26]. For each section p, we compute the best meromorphic approximant of the function f_p and the singularities $z_{k,p}$ are approximated by the poles of the best approximant of f_p. This step is repeated for each section and the poles are gathered in groups which give us an estimation of the number N of sources and of their positions C_k.

Remark 5.3.4. *If the function f_p to be approximated is a rational function of degree m', the best approximant of f_p of degree m coincides with f_p for $m \geq m'$.*

3D source localization

This step "from 2D to 3D" consists in superposing all the estimated singularities and estimating the positions of sources. To each k fixed and each axis section, is associated a singularity line which connects together the singularities $z_{k,p}$ of f_p when p varies for k fixed. When the sources are "well separated", the convergence of the poles of the best approximant is better for the sections close to the sources. Closer we are to the section where the source is located, better the poles of the rational approximant gather towards the induced singularity. From this remark, in order to get more accuracy on the localization process, it is indicated to take several slicing directions. Each line l_k is associated with one of the sources C_k and has the following theoretical properties [17]:

- l_k lies in a half-plane containing C_k and orthogonal to the slicing plane Π.
- l_k goes through its associated source C_k. If we look to the ball $\mathbb{B}$ from the top of the slicing axis, the source C_k is found at the maximum modulus of singularities.

The singularity lines l_k associated to various slicing directions Π intersect at the sources which allows to better estimate their positions.

Remark 5.3.5. *For both cases i.e. monopolar (geodesy inverse problem) and dipolar density (EEG inverse problem, see [17]), the same approximation scheme can be used in order to solve the discretization issue (SR) of the initial (DR) problem. In other words, using the best quadratic rational approximantion we solve the (SR) problem for geodesy and EEG and the solution of this problem gives us an approximant of the (DR) problem.*

5.4 Others density models

Due to different levels of concentration of the Earth density, it can be approximated by different models. As we already saw, one of the appropriate model is that one of the monopolar masses. In the following, we describe briefly a case when the (Earth) potential V is generated by a density denoted by $c_\omega \chi_\omega$ which is concentrated inside a ball ω of radius ϵ and centered in y_0 contained in the unit ball $\mathbb{B}$ which model the Earth [10, 25]. This new model of density allows us to compute an approximant for (DR) problem. In the complementary part of the ball, $\mathbb{B} \setminus \overline{\omega}$, the corresponded density has the constant value c_T.
We have the equation :

$$\Delta V = \left\{ \begin{array}{ll} 0, & \mathbb{R}^3 \setminus \mathbb{B} \\ c_T, & in\ \mathbb{B} \setminus \omega \\ c_\omega, & in\ \omega \end{array} \right\} = \rho_\chi,$$

with $c_\omega, c_T \in \mathbb{R}_+, c_\omega >> c_T$.

$$\Delta V = c_T \chi_{\mathbb{B}\setminus\overline{\omega}} + c_\omega \chi_\omega = c_T \chi_{\mathbb{B}} + (c_\omega - c_T)\chi_\omega = \rho_\chi.$$

For subsets $\mathcal{A} \subset \mathbb{R}^n$, $\chi_{\mathcal{A}}$ is the indicator function with:

$$\chi_{\mathcal{A}}(x) = \left\{ \begin{array}{ll} 1 & \text{if } x \in \mathcal{A}; \\ 0 & \text{if } x \notin \mathcal{A}. \end{array} \right.$$

Proposition 5.4.1. *The potential generated by the above density $\rho \in L^2(\mathbb{B})$ coincides, up to an additive constant, with a potential issued from a pointwise mass at y_0.*

Proof. We have:

$$V(x) = \int_{\mathbb{B}} \frac{c_T + \chi_\omega(y)(c_\omega - c_T)\mathrm{d}y}{|x-y|},$$

$$V(x) = c_T \int_{\mathbb{B}} \frac{\mathrm{d}y}{|x-y|} + (c_\omega - c_T)\int_\omega \frac{\mathrm{d}y}{|x-y|}. \tag{5.21}$$

Now, if we take

$$U(y) = U_x(y) = \frac{1}{|x-y|} = E_3(x-y) \text{ with } \Delta_y U_x = 0 \text{ in } \mathbb{B}.$$

applying the Theorem 2.2.3 of mean-value property, we have:

$$\frac{1}{\frac{4}{3}\pi}\int_{\mathbb{B}} \frac{\mathrm{d}y}{|x-y|} = U_x(y=0) = \frac{1}{|x|} = 1, |x| = 1 \text{ (unit ball)}. \tag{5.22}$$

Consequently, we have:

$$\int_{\mathbb{B}} \frac{\mathrm{d}y}{|x-y|} = \frac{4\pi}{3}.$$

For the ball denoted by $\omega = \omega(y_0, \epsilon)$, we obtain:

$$\frac{1}{\frac{4}{3}\pi\epsilon^3}\int_\omega \frac{\mathrm{d}y}{|x-y|} = U_x(y=y_0) = \frac{1}{|x-y_0|} = E_3(x-y_0), \tag{5.23}$$

$$\int_\omega \frac{\mathrm{d}y}{|x-y|} = \frac{\epsilon^3 4\pi}{3|x-y_0|} = \frac{\epsilon^3 4\pi}{3} E_3(x-y_0).$$

From (5.21), (5.22) and (5.23) we obtain:

$$V(x) = \frac{4\pi}{3}\Big[c_T + \epsilon^3(c_\omega - c_T)E_3(x-y_0)\Big]. \tag{5.24}$$

□

In the case when the density of the Earth is model by 6 dipoles (or a finite number of point masses) placed inside a small ball $\omega(x_0, \epsilon)$, the associated potential is the sum of the individual contributions. For solving the inverse problem we use the rational approximation technique described in Section 5.3. The unit ball $\mathbb{B}$ is intersected by 5 parallel planes orthogonal to the z-th axis, so that we obtain a family of $2D$ disks $D_p, p = -5, \ldots, 5$. The next image represents the approximation result on the 5-th section: the blue points are the poles of the approximant and those in red the true singularities of sources. The next two images represent a 3D visualization of the sphere after we apply the best meromorphic approximant on each circle. On the first figure we can see the poles of each $2D$-approximant (in blue) for the 6 sources (in green). In the second case, the figure is seen from above.

Figure 5.3: *2D-approximation on the 4th and 5th section*

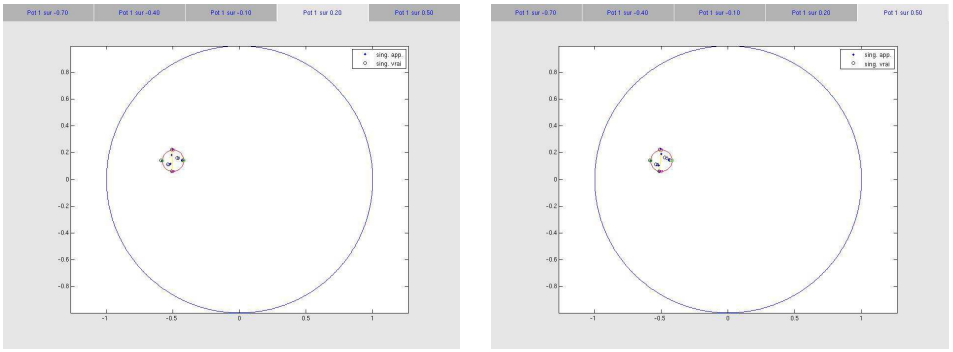

Figure 5.4: *Six sources*

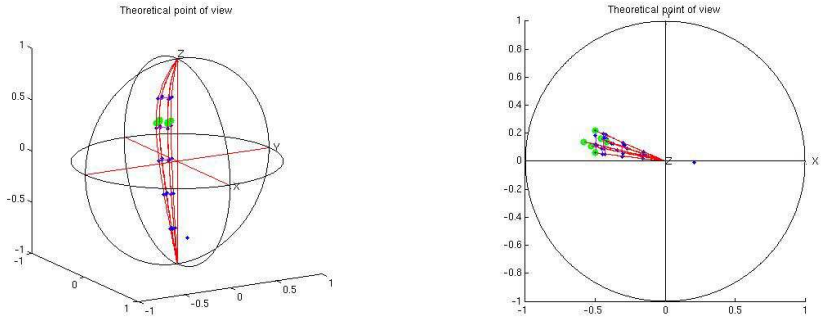

Now, we suppose that the density of the Earth is contained inside an union of 3 balls $w = \cup_{i=1}^{3} \mathbb{B}(x_i, \epsilon)$. In this case, we compute the potential by the explicit formula (5.24). This figure represents the approximation result on the third section, where the blue points are the poles of the approximant and the black ones the true singularities of the sources. We give as example the results that we obtain for the $3th$ and $4th$ sections of the unit sphere where we apply the best rational approximant.

Figure 5.5: *2D-approximation on the 3th and 4th section*

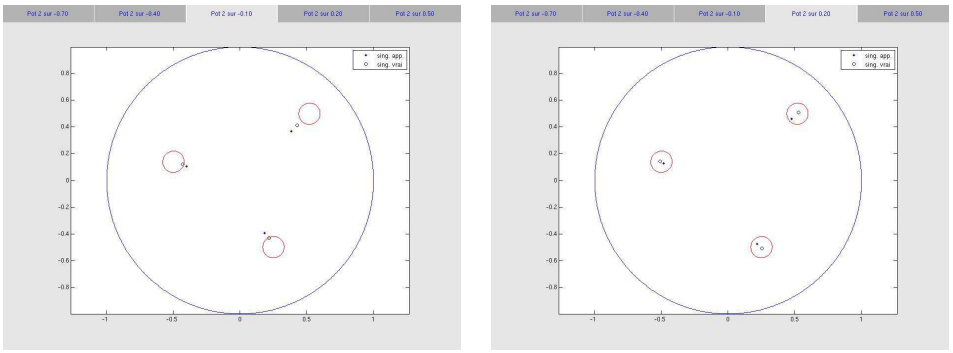

After superposing the sections we get the $3D$ source localization. In the next figure we have in blue the poles of each $2D$-approximant and in green the estimated sources.

Figure 5.6: *Localization of three sources*

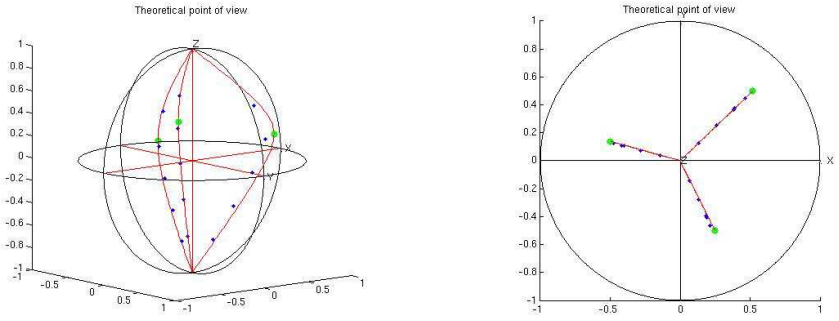

More numerical results concerning the monopolar and dipolar source localization will be presented in Chapter 6.

Chapter 6

Numerical results

In this chapter, we give various examples that illustrate the results of this thesis. The scheme used to obtain these numerical results is explained in the following. We already saw that the resolution of the inverse problem (IP) involves the resolution of two problems: the transmission data problem (TP) and density recovery (DR) problem. In practice, as we know, the data is available just on some regions as the north hemisphere of the head (M/EEG) or above continents, spherical caps, etc. (geodesy). To represent these data, we have build a new adaptive basis. The **Chapter 3** provides a new efficient method for building the convenient Slepian basis. This method is based on Gauss-Legendre quadrature. The step which consists in passing from the partial data expressed in the new Slepian basis, towards the complete data over the whole sphere $\mathbb{S}$ and expressed in spherical harmonic basis, is called the transmission data problem (TP). For more details, see **Chapter 4**. For (DR) resolution problem via the best quadratic rational approximation on 2D on sections, we need the coefficients of the spherical harmonic expansion of the data over the sphere. In this thesis we have given an accurate method based on Gauss-Legendre quadrature, for the computation of the coefficients of the spherical harmonic development. This passage involves some steps and it was implemented in MAPLE:

- We compute the spherical harmonic expansion of the potential (gravitational or electrical) truncated up to a bandwidth L. For this, informations as bandwidth, angles of spherical caps (belts) and positions of sources are read from a file called input.txt;

- Once we know the potential and the Slepian basis, we compute the coefficients of its Slepian expansion (as integrals over the region Θ between the potential

and Slepian basis, see **Chapter 4**, relation (4.9));

- Knowing the coefficients of the Slepian expansion and Slepian functions, we have to built the potential by using the Slepian basis;
- We compute the coefficients of the spherical harmonic expansion as integral over the sphere between the potential and the spherical harmonic basis.

The output data furnished by this MATLAB software will give informations which serve as input for the MATLAB software FindSources3D. This output data will be exported from MAPLE as a file called output.txt and it contains the truncation bandwidth of the potential, the angles associated with the the region (spherical caps, belts), the spherical harmonic coefficients and the nodes on which the potential data was evaluated over the whole sphere. For a better organization of files, the name of output.txt will change in function of the variables values.
The next step of the (IP) resolution problem is the density recovery (DR) problem solved by FindSources3D (INRIA, APICS team, see [24]) that uses the best quadratic approximation on 2D planar sections, see **Chapter 5**. **Chapter 6** is presented such that to illustrate numerical tests which was obtained by using the MAPLE and MATLAB codes and which corresponds to (TP) and (DR) problems. Firstly, we introduce the monopolar case of geodesy masses model and in a second time we consider the dipolar case for EEG.
Choice of the bandwidth L
The truncated spherical harmonics expansion of the potential data represents an approximation of the real potential. The choice of the bandwidth L affects the reconstruction of the data and the precision of the source localization. We make different choices of the bandwidth L in order to show the fact that greater the bandwidth L is, better we localize the sources. We introduce some symbols:

- the singularities $z_{k,p}$ of f_p are represented by green points.
- the sources C_k are marked by red points.

6.1 Monopolar case

6.1.1 Simulations parameters

For these numerical simulations we will consider in a first time the gravitational potential V (monopolar case) given by:

$$V(X) = \sum_{k=1}^{N} \frac{m_k}{|X - S_k|},\ X \in \mathbb{S}. \tag{6.1}$$

where S_k are the sources, m_k their masses. Secondly, we consider the electrical potential generated by a dipolar distribution of sources:

$$U(X) = \sum_{k=1}^{N} \frac{\langle p_k, X - C_k \rangle}{|X - C_k|^3},\ X \in \mathbb{S}.$$

with C_k dipolar masses, p_k their moments. Our simulations will be done for one and two sources. We start with the data known on different belts or parts Θ of the unit sphere (see Chapter 3 and 4). These data will be approximated by truncated Slepian series expansion of the form:

$$\sum_{m=0}^{L} \sum_{n=1}^{2(L-m+1)} a_{n,m} \Psi_{n,m}(\theta, \phi)$$

The bandwidth L will be changed in order to see its influence on the sources localization. Hence, by using the Gauss-Legendre quadrature, we compute the coefficients of the spherical harmonic expansion of the gravitational or electrical potential. In order to find the estimates values of the source (monopolar or dipolar), i.e. to solve the source localization inverse problem, these coefficients will be read on planar sections where the best quadratic approximation method is applied.

Remark 6.1.1. *The slicing axis is [0z) and the singularities $z_{k,p}$ from each section are approximated by a simple pole.*

This scheme will be used for each case that we consider in this chapter. In the output figures, we can see in green the singularities and in red the true source.

6.1.2 Monopolar case

Example 1.1:

In this first example, we illustrate our scheme for a first monopolar sources localization. For this purpose, we consider the exact source $S = (-0.06, 0.42, 0.25)$ in Cartesian coordinates and the associated mass $m = 6$. The associated potential is given by (6.1):

First, we consider the free noise data V known on the belt Θ of the unit sphere:

$$\Theta = \{X = (1, \theta, \phi), \theta \in [0, 90], \phi \in [0, 2\pi]\} \tag{6.2}$$

In the following table, we present the positions of the true and estimated source and

Figure 6.1: *L=3, belt=[0, 90]*

the error between them.

	positions		
true sources	-0.06	0.42	0.25
estimated sources	-0.002	0.42	0.22
L^2 relative error	0.040		

Table 6.1: *True vs estimated sources*

Example 1.2:

Here, we take the same source S and we add a Gaussian noise of amplitude $\sigma = 0.02$. In the following table we give the real positions of the source S and the

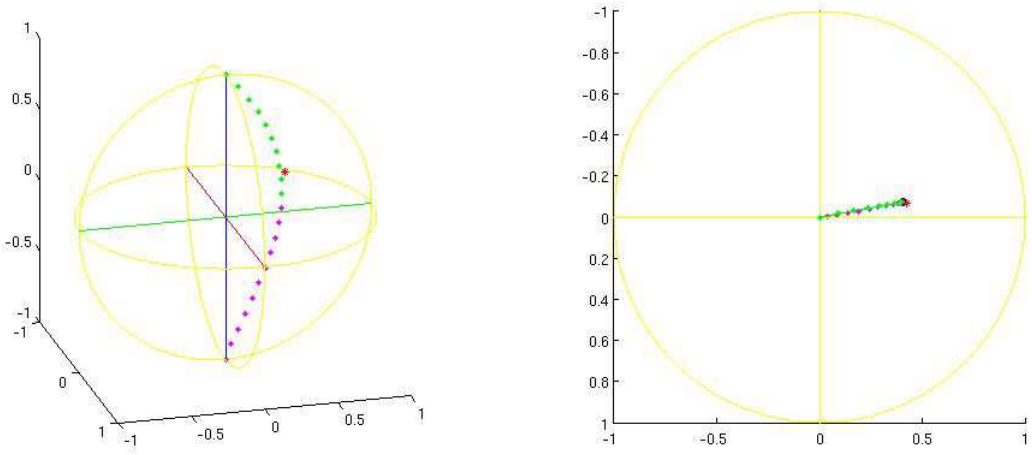

Figure 6.2: *L=3, belt=[0, 90], noise: 2%*

positions of the estimated one after we add the noise. We can compare the values of the estimated source for free and noisy data. We can remark that after adding a

	positions		
true sources	-0.06	0.42	0.25
estimated sources	-0.067	0.404	0.151
L^2 relative error	0.18		

Table 6.2: *True vs estimated sources*

noise, the source S is less well localized.

Example 1.3:

In this example we consider $L = 6$, $\theta \in [0, 90]$. When the data is available over the north hemisphere $\theta \in [0, 90]$, we notice that for bigger L, the source is better localized. The data is supposed without noise. Comparing to the numerical test

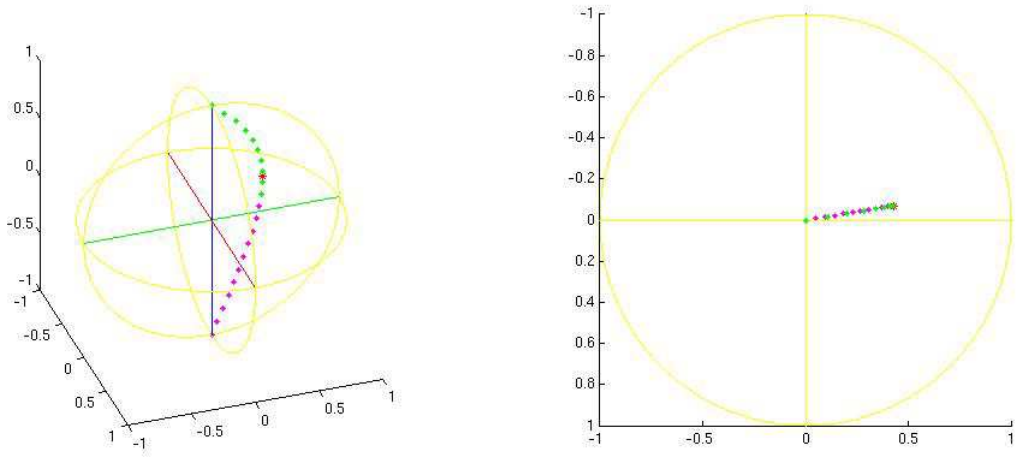

Figure 6.3: *L=6, belt=[0, 90]*

	positions		
true sources	-0.06	0.42	0.25
estimated sources	-0.06	0.42	0.23
L^2 relative error	0.00061		

Table 6.3: *True vs estimated sources*

for $L = 3$, when we obtained an error localization of order 10^{-2}, for $L = 6$ we have a better localization with an error of order 10^{-4}.

Example 1.4:

In this example we consider the same source $S = (-0.06, 0.42, 0.25)$, $m = 0.6$, $L = 3$ with the data over the whole sphere $\mathbb{S}$. The corresponded table for the sources

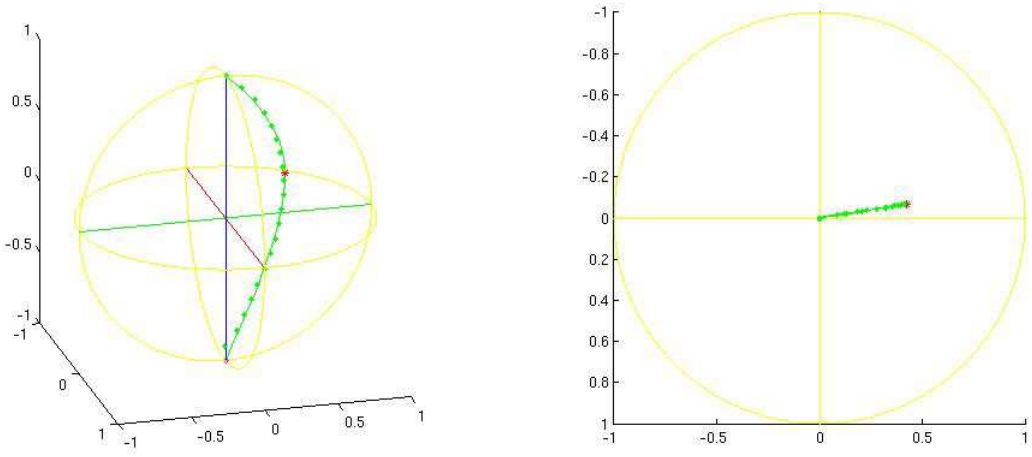

Figure 6.4: *L=3, [0,180]*

positions as well the L^2 relative error of localization is:

	positions		
true sources	-0.06	0.42	0.25
estimated sources	-0.06	0.42	0.25
L^2 relative error	0.0409		

Table 6.4: *True vs estimated source*

Example 1.5:

We change the positions of the source. Let us consider the monopolar source:

$$S = (0.23, 0.57, 0.31) \text{ and } m = 0.6$$

We take $L = 10$, and the belt Θ defined by $\theta \in [0, 90]$. The corresponded table for

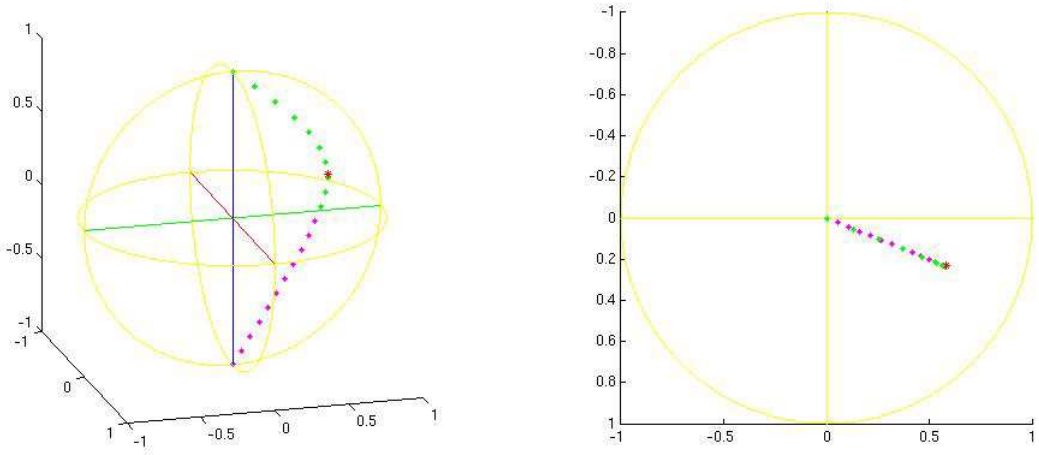

Figure 6.5: *L=10, belt=[0, 90]*

the sources positions as well the L^2 relative error of localization is:

	positions
true sources	0.23 0.57 0.317
estimated sources	0.23 0.57 0.316
L^2 relative error	0.002

Table 6.5: *True vs estimated source*

Remark 6.1.2. *For this example, we notice that for $L = 10$ the source S is better localized than for $L = 3$. If we compare its localization with that for $S = (-0.06, 0.42, 0.25)$, this last was well localized even for $L = 3$.*

2 sources

Example 1.1:

In this example we consider a numerical result concerning the localization of 2 sources whose positions are given in cartesian coordinates with the truncation bandwidth $L = 3$ and the belt $\theta \in [0, 90]$. The associated potential is given by:

$$V(X) = \frac{m_1}{|X - C_1|} + \frac{m_2}{|X - C_2|}, \; X \in \mathbb{S} \tag{6.3}$$

In the table we give the positions and the estimation error of the considered sources:

$$C_1 = (-0.06, 0.42, 0.25), \; m_1 = 0.6$$
$$C_2 = (-0.31, -0.07, -0.23), \; m_2 = 0.7$$

Figure 6.6: *L=3, belt=[0, 90]*

	positions		
true sources	-0.06	0.42	0.25
	-0.31	-0.07	-0.23
estimated sources	-0.03	0.17	0.34
	-0.26	-0.12	0.25
L^2 relative error	0.496		
	0.918		

Table 6.6: *True vs estimated sources*

Comparing to the case when the potential is generated by a single source, the localization is less good when we consider two sources. This is due to the cross product which appears when we compute the power of (6.3). We remember that we compute for each section of the sphere a best meromorphic approximate to the function V^2, see Section (5.3).

Example 1.2:

In this example we consider the same sources, $\theta \in [0, 90]$ and $L = 10$. We

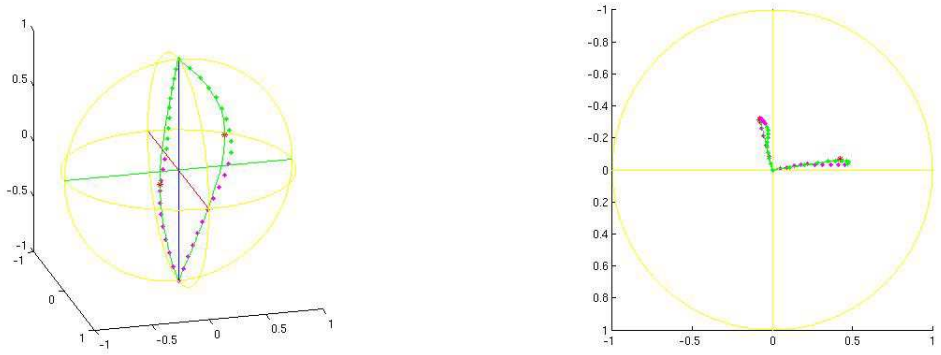

Figure 6.7: *L=10, belt=[0, 90]*

	positions		
true sources	-0.06	0.42	0.25
	-0.31	-0.07	-0.23
estimated sources	-0.06	0.42	0.25
	-0.31	-0.07	-0.23
L^2 relative error	0.0098		
	0.0067		

Table 6.7: *True vs estimated sources*

remark a better localization for $L = 10$ for both sources.

Example 1.3:

We retake the previous example and we add a noise of amplitude $\sigma = 0.01$. The

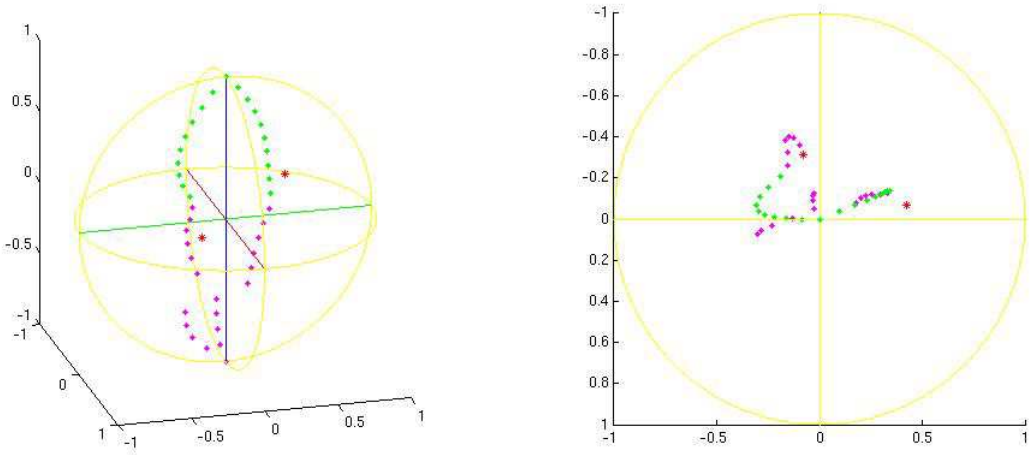

Figure 6.8: *L=3, belt=[0, 90], noise: 1%*

corresponded table for these two sources:

	positions		
true sources	-0.06	0.42	0.25
	-0.31	-0.07	-0.23
estimated sources	-0.12	0.28	0.39
	-0.16	-0.29	-0.12
L^2 relative error	0.386		
	0.527		

Table 6.8: *True vs estimated sources*

Example 1.4:

This case illustrates and localize two sources placed in different hemispheres. Consequently, when the data is available over the belt $[0, 90]$, one source is placed inside the belt and the other one at the exterior.

$$C_1 = (-0.06, 0.42, 0.25),\ m_1 = 0.6$$
$$C_2 = (-0.34, -0.08, -0.18),\ m_2 = 0.6$$

Figure 6.9: *L=3, belt=[0, 90], without and with noise 2%*

The corresponded table of the true and estimated sources, as well the error of localization is:

	positions		
true sources	-0.06	0.42	0.25
	-0.34	-0.08	-0.18
estimated sources(free noise)	-0.01	0.13	0.16
	-0.19	-0.10	-0.04
estimated sources(noise)	-0.06	0.23	0.40
	-0.31	-0.12	-0.10
L^2 relative error(free noise)	0.586		
	0.384		
L^2 relative error(noise)	0.453		
	0.561		

Table 6.9: *True vs estimated sources*

6.2 Dipolar case

1 source

Example 1.1:

In [23], the author has developed a scheme for the source localization. This scheme is based on the use of an initial guess of the exact locations of the sources combined with the boundary element method to calculate a cost function J and its gradient associated with the (SR) problem. Then, an iterative minimization algorithm is used to compute the approximate location of the sources.

In [23], it was applied the previous scheme for one dipolar source with $C_{true} = (0.12, 0.12, 0.12)$, $p_{true} = (0.70, 0, 0.70)$ and taking two different starting points $C_0^1 = (0.63, 0.1, 0.75)$, $p_0^1 = (0.4, 0, 0.2)$ and $C_0^2 = (0.5, 0.3, 0.9)$, $p_0^2 = (0.4, 0.3, -0.2)$. The first value is closer to the exact solution than the second one. The data are considered to be known on the whole boundary of the sphere, with no added noise.

In the case when the data are considered known just on the belt $\Theta = [0, 90]$, we use the method of Simons [46] to have the data expansion on Slepian basis. After, we use FindSource3D software for source localization and we find the estimated source $C_{estim} = (0.118, 0.117, 0.132)$ with the L^2 relative error equal to 0.0579. We note that although the scheme introduced in [23] gives a slightly better result (an error of order 10^{-5} and 10^{-4} for the initial guess C_0^1, respectively C_0^2), our method has the advantage to not require an initial accurate guess of the source localization. Also, we have repeated the previous example with an added Gaussian noise with $\sigma = 0.02$ and truncation bandwidth $L = 10$ and find the location of the source $C_{estim} = (0.121, 0.117, 0.151)$ and an error equal to 0.149. The following numerical tests are done by using the method of Simons when we dispose of partial data on the sphere.

Example 1.2:

$$C = (-0.06, 0.42, 0.25), p = (0.7, 0, 0.7)$$

In this example we suppose the data given on the belt $\Theta = [0, 90]$ and the bandwidth $L = 10$. The corresponded table of the true and estimated source, as well the relative

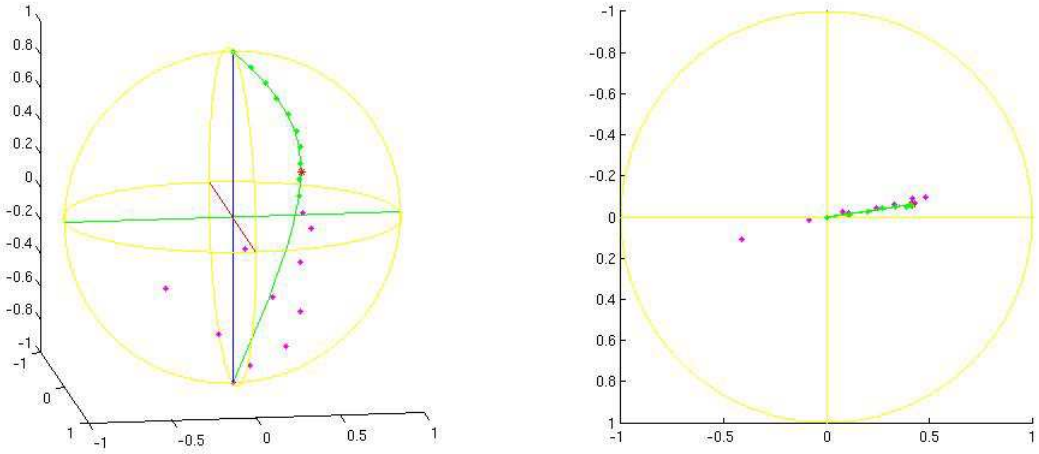

Figure 6.10: *L=10, belt=[0, 90], without noise*

error of localization is:

	positions		
true sources	-0.06	0.42	0.25
estimated sources	-0.061	0.417	0.253
L^2 relative error	0.00897		

Table 6.10: *True vs estimated sources*

Example 1.3:

We add a noise of amplitude $\sigma = 0.02$ for the previous example:

$$C = (-0.06, 0.42, 0.25), p = (0.7, 0, 0.7)$$

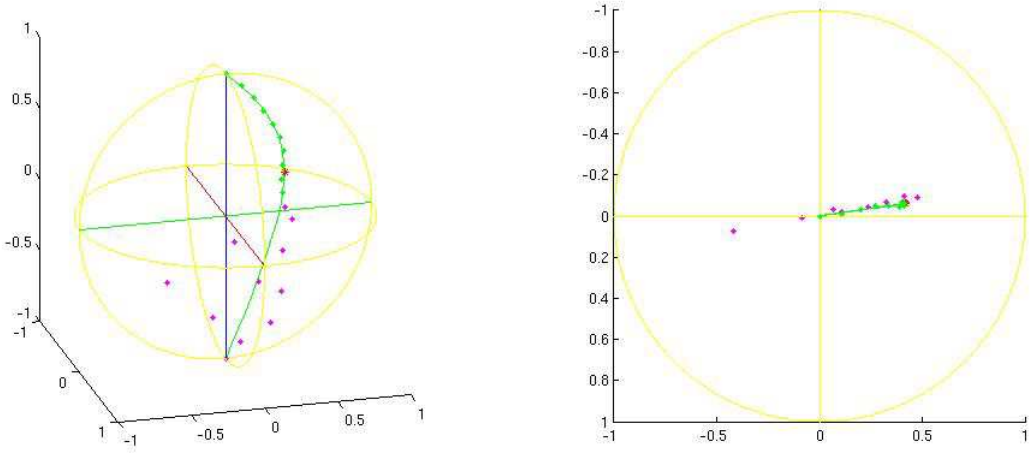

Figure 6.11: *L=10, belt=[0, 90], with noise: 2%*

The corresponded table of the true and estimated source, as well the relative error of localization is: Comparing to the previous example, the source is less well

	positions		
true sources	-0.06	0.42	0.25
estimated sources	-0.061	0.417	0.259
L^2 relative error	0.019		

Table 6.11: *True vs estimated sources*

localized with an error localization of order 10^{-2} instead of 10^{-3}.

Example 1.4:

In this example we consider the same positions of sources and the data is available on the belt $\Theta = [45, 135]$.

$$C = (-0.06, 0.42, 0.25), p = (0.7, 0, 0.7)$$

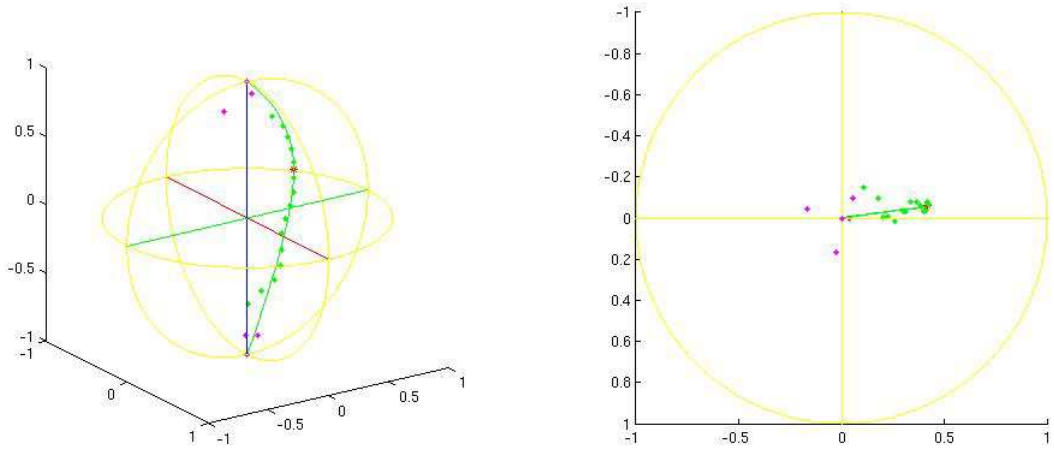

Figure 6.12: *L=10, belt=[45,135], without noise*

The corresponded table of the true and estimated source, as well the relative error of localization is: Where the data covers a part of the nord hemisphere where the

	positions		
true sources	-0.06	0.42	0.25
estimated sources	-0.058	0.421	0.258
L^2 relative error	0.0172		

Table 6.12: *True vs estimated sources*

source is placed and a part of the sud hemisphere (where we do not dispose of data), the source is less well localized comparing with the Example 1.2 when the data is given just on the belt $[0, 90]$ where the source is placed.

Example 1.5:

$$C = (-0.06, 0.42, 0.25), p = (0.7, 0, 0.7)$$

For the previous example, we add a noise of amplitude $\sigma = 0.02$. The following table

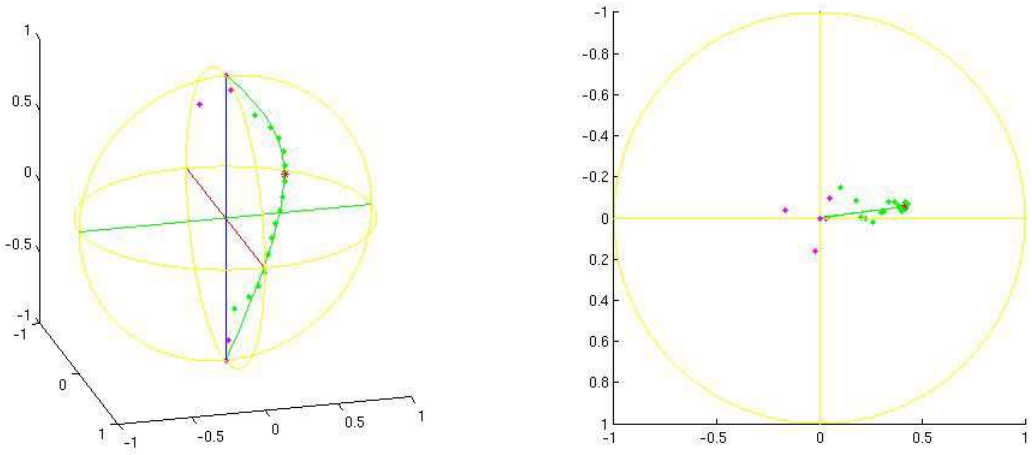

Figure 6.13: *L=10, belt=[45,135], with noise 2%*

gives us the positions of the true and estimated source, as well the relative error of localization: The same remark: adding a noise, the error localization increases.

	positions		
true sources	-0.06	0.42	0.25
estimated sources	-0.055	0.416	0.242
L^2 relative error	0.0206		

Table 6.13: *True vs estimated sources*

Example 1.6:

Now, if we change the positions of sources,

$$C = (0.23, 0.57, 0.31), p = (0.7, 0, 0.7)$$

we get the localization, see Fig. 6.14. The corresponded table of the true and

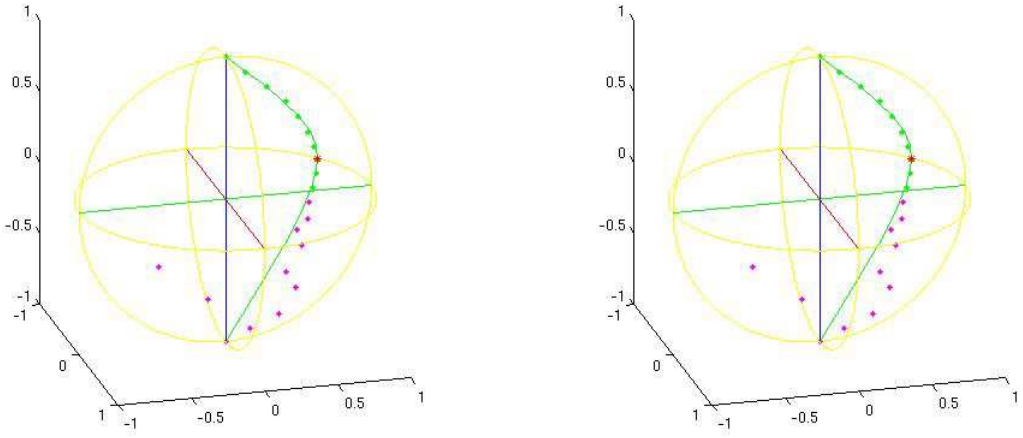

Figure 6.14: *L=10, belt=[0,90], without noise*

estimated source, as well the relative error of localization is:

	positions		
true sources	0.23	0.57	0.31
estimated sources	0.223	0.568	0.311
L^2 relative error	0.0111		

Table 6.14: *True vs estimated sources*

Example 1.7:

In this example we add a noise of amplitude $\sigma = 0.02$:

$$C = (0.23, 0.57, 0.31), p = (0.7, 0, 0.7)$$

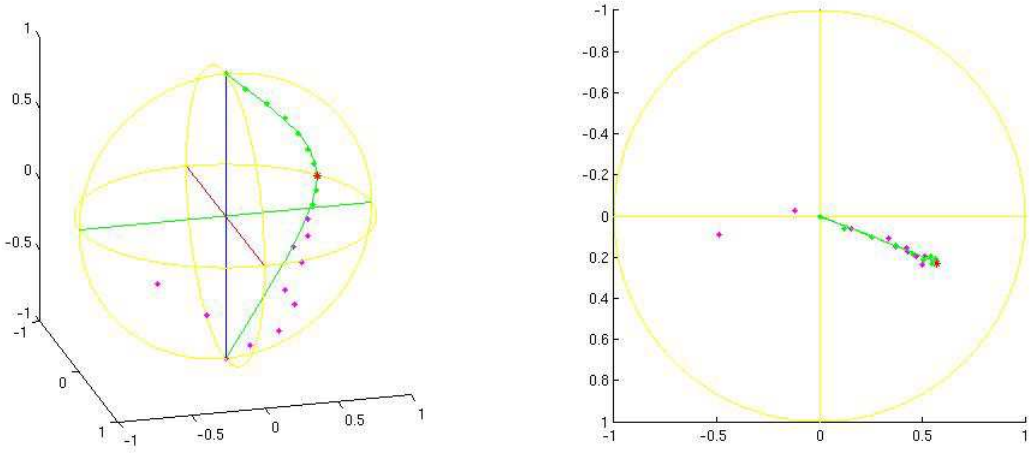

Figure 6.15: *L=10, belt=[0,90], with noise 2%*

The corresponded table of the true and estimated source, as well the error of localization. Comparing with the previous example, we remark that the error increases

	positions		
true sources	0.23	0.57	0.31
estimated sources	0.222	0.567	0.308
L^2 relative error	0.0126		

Table 6.15: *True vs estimated sources*

by adding a noise.

2 sources

Example 1.1:

We consider the sources:

$$C_1 = (-0.06, 0.42, 0.25),\ p_1 = (0.7, 0, 0.7)$$
$$C_2 = (-0.31, -0.07, -0.23),\ p_2 = (0.7, 0, 0.7)$$

Figure 6.16: *L=10, belt=[0,90], without noise*

The corresponded table of the true and estimated sources, as well the error of localization is:

	positions		
true sources	-0.06	0.42	0.25
	-0.31	-0.07	-0.23
estimated sources(free noise)	-0.061	0.424	0.351
	-0.294	-0.051	-0.237
estimated sources(noise)	-0.051	0.41	0.241
	-0.289	-0.065	-0.276
L^2 relative error(free noise)	0.190		
	0.048		
L^2 relative error(noise)	0.0320		
	0.0962		

Table 6.16: *True vs estimated sources*

Figure 6.17: *L=10, belt=[0,90], with noise 2%*

Example 1.2:

We change the moment for the second source. The data is supposed over the belt $\theta \in [45, 135]$ for $L = 10$:

$$C_1 = (-0.06, 0.42, 0.25),\ p_1 = (0.7, 0, 0.7)$$
$$C_2 = (-0.31, -0.07, -0.23),\ p_2 = (0.2, -0.1, 0.1)$$

We give the corresponded table of the true and estimated sources, as well the error of localization. We notice that we have a better localization when the sources have

	positions		
true sources	-0.06	0.42	0.25
	-0.31	-0.07	-0.23
estimated sources	-0.069	0.369	0.478
	-0.208	0.116	0.114
L^2 relative error	0.142		
	0.765		

Table 6.17: *True vs estimated sources*

the same coordinates of moments.

Example 1.3:

We consider the two sources and the data are available over the whole sphere.

$$C_1 = (-0.06, 0.42, 0.25),\ p_1 = (0.7, 0, 0.7)$$
$$C_2 = (-0.31, -0.07, -0.23),\ p_2 = (0.7, 0, 0.7)$$

Figure 6.18: *L=10, belt=[0,180], without noise*

The corresponded table of the true and estimated sources, as well the error of localization is: Comparing this example with the previous one, when the data is available

	positions		
true sources	-0.06	0.42	0.25
	-0.31	-0.07	-0.23
estimated sources(free noise)	-0.058	0.418	0.236
	-0.313	-0.067	-0.223
estimated sources(noise 2%)	-0.064	0.404	0.262
	-0.300	-0.105	0.019
L^2 relative error(free noise)	0.0276		
	0.0151		
L^2 relative error(noise 2%)	0.0387		
	0.476		

Table 6.18: *True vs estimated sources*

just over the north hemisphere, the localization is better because the data is available over the entire sphere.

General remarks:

1. The bandwidth L plays an important role in the source localization: bigger the L is, smaller the error localization becomes.

2. The localization depends also on the positions of the sources with respect to the belt, i.e. if the sources are placed or not in the covered region.

3. The localization is also improved when the data is considered over the whole sphere.

Chapter 7

Conclusion

This thesis is developped around the representation of data on the sphere and approximation, for transmission and recovery problems concerning some Laplace partial differential equations.

The resolution of the associated inverse problems requires a first transmission data step, from the considered region to the whole boundary sphere, and in a second time, the recovery of the sources in the domain [17].

The use of families like spherical harmonics and Slepian bases is of special interest for the resolution of such inverse problems in geodesy and EEG, when we dispose of partial boundary data.

When we dispose of different types of heterogeneous data, as the gravitational potential measured at the surface of the Earth and its derivative or Hessian measured on sattelite orbits, for their expansion we can use different bases like Slepian [46], wavelets [13] or other functions families.

Suitable functions families here are given by Slepian bases that allow to represent partially available data on sphere, whenever these come from almost band-limited functions (this is numerically the case; however, further error bounds should be established concerning the above potentials with pointwise or localized singularities in the ball, following Chapter 4). For the computation of such a Slepian basis, an efficient scheme has been proposed, using Gauss-Legendre quadrature methods [33]. The comparison between zonal spherical harmonics and Slepian functions would be interesting particularly when the studied region is a belt, contained between two parallels of the sphere.

In practice, the nodes location is imposed (they are not chosen as suitable nodes, as for Gauss-Legendre quadrature) and consequently, the study of different quadrature methods (as points of a cubature rule on the sphere, see [49]) which could give

more flexibility on the choice of the nodes (location of electrodes or satellites) is suitable.

The considered data could be gravitational or electrical potential measured at points on the boundary sphere (from electrodes on the scalp, or by gravimeters on the Earth surface) or some other sphere (for satellite measurements, or for MEG).

For the case when we dispose of partial data over particular regions of the sphere, the estimation of the data over all the sphere can be formulated in terms of best constrained approximation problems [5], boundary elements methods or other regularization techniques [17].

For the second sources recovery step of the inverse problem, from data now available on a whole sphere, we used best quadratic rational approximation methods on planar sections [8, 17]. It furnishes good localization results for monopolar and dipolar sources type. The source localization results could be improved using several directions of planar sections, technique called of "clustering". This procedure yields a family of estimations of the sources at the intersection of the axis [17].

Concerning EEG issues, simultaneous measurements from MEG could be used for a better source localization (this will be done through the software FindSources3D, [24]).

To complete the resolution of the inverse problem, masses and moments identification is further required [43].

Similar inverse problems come from other physical and non destructive control issues, like paleomagnetism [7], determination of the thickness of glaciers and soils, exploration of subsoils, etc.

Bibliography

[1] A. Abdelmoula, M. Moakher, and B. Philippe, *Localized spectral analysis for an inverse problem in geodesy*, CARI, (2008).

[2] A. Albertella, F. Anso, and N. Neeuw, *Band-limited functions on a bounded spherical domain: the Slepian problem on the sphere*, Journal Geodesy, 73 (1999), pp. 436–447.

[3] M. Alfaro, J. Dehesa, F. Marcellan, J. R. de Francia, and J. Vinuesa, *Orthogonal Polynomials and their Applications*, SIAM, 1988.

[4] G. Andrews, R. Askey, and R. Roy, *Special functions*, 2011.

[5] B. Atfeh, L. Baratchart, J. Leblond, and J. Partington, *Bounded extremal and Cauchy-Laplace problems on the sphere and shell*, The Journal of Fourier Analysis and Applications, 16 (2010), pp. 177–203.

[6] L. Baratchart, A. Ben Abda, F. Ben Hassen, and J. Leblond, *Recovery of pointwise sources or small inclusions in 2D domains and rational approximation*, Inverse problems, 21 (2005), pp. 51–74.

[7] L. Baratchart, D. Hardin, E. Lima, E. Saff, and B. Weiss, *Inverse magnetization problems for a two-dimensional slab and generalizations of hodge decompositions*, *V* Bell Syst. Tech. J., (30 September, 2011).

[8] L. Baratchart, J. Leblond, and J.-P. Marmorat, *Inverse source problem in a 3D ball from best meromorphic approximation on 2D slices*, ETNA, 25 (2006), pp. 41–53.

[9] L. Baratchart and M. Yattselev, *Meromorphic approximants to complex Cauchy transforms with polar singularities*, Mat. Sb., 200 (2009), pp. 3–40.

[10] F. Ben Hassen and E. Bonnetier, *Asymptotic formulas for the voltage potential in a composite medium containing close or touching disks of small diameter*, Multiscale Model. Simul., 4 (2005), pp. 250–277.

[11] A. Bultheel and B. D. Moor, *Rational approximation in linear system and control*, Journal of Computation and Applied Mathematics, 121 (2000), pp. 355–378.

[12] F. Chambat and Y. Ricard, *Empirical 3D basis for the internal density of a planet*, Geophysical Journal International, 162 (2005), pp. 32–35.

[13] A. Chambodut, I. Panet, M. Mandea, D. Diament, M. Holschneider, and O. Jamet, *Wavelet frames: an alternative to spherical harmonic representation of potential fields*, Geophys. J. Int., 163 (2005), pp. 857–899.

[14] G. Chen and J. Zhou, *Boundary element methods*, Academic Press London, 1992.

[15] M. Chung, K. Dalton, A. Evans, and R. Davidson, *Tensor-based cortical surface morphometry via weighted spherical harmonic representation*, IEEE. Trans. Med. Imag., (2007).

[16] S. Claessens, W. Featherstone, and F. Barthelmes, *Experiences with point-mass gravity field modelling in the Perth region*, Geomatics Research Australasia, 75 (2001), pp. 53–86.

[17] M. Clerc, J.Leblond, J.-P. Marmorat, and T. Papadopoulo, *Source localization using rational approximation on plane sections.* Research Report, submitted, 2011.

[18] B. Cuffin, *A method for localizing EEG sources in realistic head models*, IEEE TransBiomed Eng., 42 (1995), pp. 68–71.

[19] R. Dautray and J. Lions, *Analyse Mathématique et Calcul Numerique pour les Sciences et les techniques*, vol. 3, Masson, 1988.

[20] P. Davis and P. Rabinowitz, *Methods of Numerical Integration*, Academic Press Inc, second ed., 1984.

[21] A. El Badia, *Summary of some results on an EEG inverse problem*, Neurology and Clinical Neurophysiology, 104 (2004).

[22] A. El Badia and T. Duong, *An inverse source problem in potential analysis*, Inverse Problems, 16 (2000), pp. 651–663.

[23] A. El Badia and M. Farah, *A stable recovering of dipole sources from partial boundary measurements*, Inverse Problems, 26 (2010).

[24] FindSources3D, *Guide utilisateur, url: http://www-sop.inria.fr/apics/FindSources3D*, INRIA, APICS-ATHENA, 2009.

[25] A. Friedman and M. Vogelius, *Identification of small inhomogeneities of extreme conductivity by boundary measurements: a theorem on continuous dependence*, Arch. Rat. Mech. Anal., 105 (1989), pp. 299–326.

[26] E. Gilbert and D. Slepian, *Existence and generic properties of l^2 approximants of linear systems*, IMA Journal of Mathematical Control and Information, 3 (1986), pp. 89–101.

[27] K. Gorski, E. Hivon, A. Banday, B. Wandelt, F. Hansen, M. Reinecke, and M. Bantelman, *A framework for high-resolution discretization and fast analysis of data distributed on the sphere*, Astroph. J., 622 (2005), pp. 759–771.

[28] R. Gregory, *Uniform bounds for $P_n^m(\cos\theta)$ and the absolute convergence of series expansions in spherical surface harmonics*, Quartely Journal of Mechanics and Applied Mathematics, 50 (1997), pp. 467–479.

[29] V. Isakov, *Inverse problems for partial differential equations*, Springer-Verlag, Berlin, 1998.

[30] J. Jackson, *Classical Electrodynamics*, Academic Press Inc, third ed., 1984.

[31] K. Jerbi, J. Mosher, S. Baillet, and R. Leahy, *On MEG forward modelling using multipolar expansions*, Physics in Medicine and Biology, 47 (2002), pp. 523–555.

[32] A. Karoui, *Recent developments in fractals and related fields. Based on the international conference on fractals and related fields, Uncertainty principles, prolate spheroidal wave functions, and applications*, Springer Science+Business Media, 2010.

[33] A. Karoui, J. Leblond, and A.-M. Nicu, *Slepian functions on the sphere with applications to signal recovery and inverse source problems*, in preparation, (2012).

[34] J. Keiner and D. Potts, *Fast evaluation of quadrature formulae on the sphere*, Mathematics and Computation, 77 (2008), pp. 397–419.

[35] A. Krall, *Hilbert Space Boundary Value Problems and Orthogonal Polynomials*, Birkhauser Verlag, 2002.

[36] H. Landau and H. Pollak, *Prolate spheroidal wave functions, Fourier analysis and uncertainty ii*, Bell Syst. Tech. Journal., 40 (1961), pp. 65–84.

[37] J. Marmorat and M. Olivi, *The RARL2 software: Realizations and Rational Approximation in L^2-norm, url: http://www-sop.inria.fr/apics/RARL2/rarl2-eng.html*, Project APICS, INRIA, Sophia Antipolis.

[38] V. Michel, *Regularized wavelet-based multiresolution recovery of the harmonic mass density distribution from data of the Earth's gravitational field at satellite height*, Inverse problems, 21 (2005).

[39] V. Michel and A. Fokas, *A unified approach to various techniques for the non- uniqueness of the inverse gravimetric problem and wavelet-based methods*, Inverse problems, 24 (2008).

[40] L. Miranian, *Slepian functions on the sphere, generalized Gaussian quadrature rule*, Inverse Problems, 20 (2004).

[41] J. Mosher, P. Lewis, and R. Leahy, *Multiple dipole modelling and localizing from spatio-temporal meg data*, IEEE Transactions on Biomedical Engineering, 39 (1992), pp. 541–553.

[42] A. Nikiforov, *Special functions of mathematical physics*, Birkhauser Berlag Basel, 1988.

[43] H. Ouerghi, *Localization des sources ponctuelle dans une boule par approximation sur les sections planes: calcules des moments*, Master's thesis, Tunis, Tunisie, 2008.

[44] W. Rudin, *Analyse réelle et complexe*, Masson, 1975.

[45] J. Sarvas, *Basic mathematical and electromagnetic concepts of the biomagnetic inverse problem*, Physics in Medicine and Biology, 32 (1987), pp. 11–12.

[46] F. Simons and F. Dahlen, *Spherical Slepian functions and the polar gap in geodesy*, Geophysics Journal, 166 (2006), pp. 1039–1061.

[47] F. Simons, F. Dahlen, and M. Wieczorek, *Spatiospectral concentration on a sphere*, SIAM, 48 (2006), pp. 504–536.

[48] D. Slepian, *Prolate spheroidal wave functions, fourier analysis and uncertainty, V* Bell Syst. Tech. J., 57 (1978), pp. 1371–430.

[49] I. Sloan and R. Womersley, *Good approximation on the sphere, with application to geodesy and the scattering of sound*, Journal of Computational and Applied Mathematics, 149 (2002), pp. 227–237.

[50] N. Sneeuw and M. van Gelderen, *The polar gap*, vol. 65, Springer, 1997, pp. 559–568.

[51] D. Stromeyer and L. Ballani, *Uniqueness of the inverse gravimetric problem for point mass models*, Manuscr. Geodaet., 9 (1984), pp. 125–136.

[52] G. Szegö, *Orthogonal polynomials*, American Mathematical Society Colloquium Publications, Vol. 23. Revised ed, American Mathematical Society, 1959.

[53] S. Vessella, *Locations and strengths of point sources: Stability estimates*, Inverse Problems, 8 (1992), pp. 911–917.

[54] B. Wellenhof and H. Moritz, *Physical geodesy*, Springer-Verlag, Wien, second ed., 2006.

[55] N. Young, *An introduction to Hilbert space*, Cambridge Mathematical textbooks, (1998).

[56] M. Zghal, *Problèmes inverses pour l'équation de Laplace en dimension 3: Application à l'électroencéphalographie*, PhD thesis, ENIT LAMSIN, Tunis, Tunisie, 2010.

Annexe

MAPLE code

Slepian basis construction

As we already saw in the different chapters, the method that we use to build the Slepian functions in this thesis is based on a discretization of a certain integral operator by the use of a convenient Gaussian-Legendre quadrature. In the following, we give the Maple code which permits us to compute the Slepian basis functions as well as their corresponding eigenvalues. Also, it allows us to extrapolate a given signal to the whole sphere. Finally, it allows to compute the spherical harmonic expansion coefficients of a signal from their Slepian functions expansion coefficients.

```
######### QUADRATURE OVER (theta_0, theta_1) ######################
>theta_0_degres:=(theta_0*Pi)/180;
>theta_1_degres:=(theta_1*Pi)/180;
>Digits:=50:with(linalg):
a:=-evalf(sin(theta_1_degres)):
b:=evalf(sin(theta_0_degres)):
#N0 is the number of noeds taken on (theta_0,theta_1)
N0:=20:x:='x':
for n from N0 to N0+1 do
   hh:=evalf(sqrt(2*n+1)*1.0/((b-a)^(n+0.5)*n!)):
   Q[n]:=expand(diff((b-x)^(n)*(a-x)^n,x$n)*hh):
   k[n]:=coeff(Q[n],x,n):
od:
Q1:=expand(diff(Q[N0],x)):
## nodes and weights for (theta_0,theta_1)
```

```
#we build the matrix DD with eigenvalues being the nodes
DD:=array(1..N0,1..N0):
for i from 1 to N0 do
for j from 1 to N0 do
   DD[i,j]:=0.0:
od:
od:
for i from 1 to N0 do
  DD[i,i]:=0.5*(a+b):
od:
for i from 1 to N0-1 do
  DD[i,i+1]:=-evalf(i*(b-a)/(2.0*sqrt(2*i+1.0)*sqrt(2*i-1.0))):
  DD[i+1,i]:=DD[i,i+1]:
od:
#the nodes as eigenvalues of matrix DD and the corresponding weights
E:=evalf(eigenvals(DD)):
>for i from 1 to N0 do
  x:=E[i]:#the nodes for (theta_0,theta_1)
  W[i]:=-k[N0+1]/k[N0]*1.0/(Q1*Q[N0+1]):#the weights
od:
>with(linalg):a2:=arccos(b):b2:=arccos(a):NN1:=N0:x:='x':
#NN1 is the number of nodes over the belt (a2,b2)
for n from NN1 to NN1+1 do
  hhh:=evalf(sqrt(2*n+1.0)*1.0/(n!)*1.0/((b2-a2)^(n+1/2))):
  QQ[n]:=expand(diff((x-a2)^n*(x-b2)^(n),x$n)*hhh):
  ka[n]:=coeff(QQ[n],x,n):
od:
QQ1:=expand(diff(QQ[NN1],x)):
>DDD:=array(1..NN1,1..NN1):
for i from 1 to NN1 do
for j from 1 to NN1 do
  DDD[i,j]:=0.0:
od:
od:
for i from 1 to NN1 do
DDD[i,i]:=0.5*(a2+b2):
od:
for i from 1 to NN1-1 do
DDD[i,i+1]:=-evalf(i*(b2-a2)/(2.0*sqrt(2*i+1.0)*sqrt(2*i-1.0))):
DDD[i+1,i]:=DDD[i,i+1]:
od:
```

```
#the nodes as eigenvalues of matrix DDD
E2:=evalf(eigenvals(DDD)):
>for i from 1 to NN1 do
#nodes and weights over (arccos(theta_0),arccos(theta_1))
x:=E2[i]:W2[i]:=-ka[NN1+1]/ka[NN1]*1.0/(QQ1*QQ[NN1+1]):
od:
#########################################################################
```

We compute the nodes and the weights for the Gauss-Legendre quadrature applied to the interval $(0, \pi)$:

```
########### QUADRATURE OVER (0,Pi) ###################################
>with(linalg):a3:=0:b3:=evalf(Pi):NN1:=N0:x:='x':
for n from NN1 to NN1+1 do
  hhh:=evalf(sqrt(2*n+1.0)*1.0/(n!)*1.0/((b3-a3)^(n+1/2))):
  QQ[n]:=expand(diff((x-a3)^n*(x-b3)^(n),x$n)*hhh):
  ka[n]:=coeff(QQ[n],x,n):
od:
QQ1:=expand(diff(QQ[NN1],x)):
# nodes E3 and weights W3 for (0,Pi)
DDD:=array(1..NN1,1..NN1):
for i from 1 to NN1 do
for j from 1 to NN1 do
  DDD[i,j]:=0.0:
od:
od:
for i from 1 to NN1 do
  DDD[i,i]:=0.5*(a3+b3):
od:
for i from 1 to NN1-1 do
  DDD[i,i+1]:=-evalf(i*(b3-a3)/(2.0*sqrt(2*i+1.0)*sqrt(2*i-1.0))):
  DDD[i+1,i]:=DDD[i,i+1]:
od:
E3:=evalf(eigenvals(DDD)):# E3 are the nodes for (0,Pi)
>for i from 1 to NN1 do
  x:=E3[i]:W3[i]:=-ka[NN1+1]/ka[NN1]*1.0/(QQ1*QQ[NN1+1]):
od:
#########################################################################
####### QUADRATURE OVER (0,2pi) #######################################
>with(linalg):
aa:=0:bb:=evalf(2*Pi):NN0:=20:x:='x':
for n from NN0 to NN0+1 do
```

```
  hhh:=evalf(sqrt(2*n+1.0)*1.0/(n!)*1.0/(bb^(n+1/2))):
  QQ[n]:=expand(diff(x^n*(x-bb)^(n),x$n)*hhh):
  ka[n]:=coeff(QQ[n],x,n):
od:
QQ1:=expand(diff(QQ[NN0],x)):
# nodes EE and weights WW for (0,2PI)
DDD:=array(1..NN0,1..NN0):
for i from 1 to NN0 do
for j from 1 to NN0 do
  DDD[i,j]:=0.0:
od:od:
for i from 1 to NN0 do
  DDD[i,i]:=0.5*(aa+bb):
od:
for i from 1 to NN0-1 do
  DDD[i,i+1]:=-evalf(i*(bb-aa)/(2.0*sqrt(2*i+1.0)*sqrt(2*i-1.0))):
  DDD[i+1,i]:=DDD[i,i+1]:
od:
EE:=evalf(eigenvals(DDD)):
#### nodes and weights ######
>for i from 1 to NN0 do
  x:=EE[i]:
  WW[i]:=-ka[NN0+1]/ka[NN0]*1.0/(QQ1*QQ[NN0+1]):
od:
#####################################################################
```

We compute the kernel of the operator $\mathcal{T}_m$associated to Slepian functions

```
 ######### KERNEL  K(m,x,y) ######################################
>x:='x':y:='y':
>K:=proc(m,x,y)
  if (m=0) then evalf(sum((2*l+1.0)/(4.0*Pi)*1/(2^l*l!)
*(diff((x^2-1)^l,x$l))*1/(2^l*l!)*(diff((y^2-1)^l,y$l)),l=0..L)):
  else
 evalf(sum((2*l+1.0)/(4.0*Pi)*(((l-abs(m))!)/((l+abs(m))!)
*((1-x^2)^(m/2)*1/(2^l*l!)*diff(diff((x^2-1)^l,x$l),x$m)
*(1-y^2)^(m/2)*1/(2^l*l!)*diff(diff((y^2-1)^l,y$l),y$m))),l=abs(m)..L)):
 fi:
end:
#####################################################################
```

Using the quadrature Gauss-Legendre over the belt (θ_0, θ_1), we compute the eigenvalues and eigenfunctions of the kerner $K(m, x, y)$ evaluated at the nodes taken over the belt:

```
 ######## EIGENVALUES of K(m,x,y) ################################
>with(LinearAlgebra):mmm:='mmm':mmm:=L+1:i:=0:j:=0:
A:=Matrix(1..mmm*N0,1..N0):
for m from 0 to mmm-1 do
for i from 1 to N0 do
for j from 1 to N0 do
    A[m*N0+i,j]:=evalf(W[j]*subs(x=E[i],y=E[j],K(m,x,y))):x:='x':y:='y':
#we evaluate the kernel in the nodes "E" taken over the belt
od:od:od:
m:='m':
for m from 0 to mmm-1 do
   F[m]:=eigenvectors(SubMatrix(A,[m*N0+1..(m+1)*N0],[1..N0])):
od:
#####################################################################
######## SORTED EIGENVALUES ##########################################
#here, we sort ascending the eignevalues
beta:=Matrix(1..mmm,1..N0):
for m from 0 to mmm-1 do
for p from 1 to N0 do
  beta[m+1,p]:=abs(F[m][p][1]):
od:od:
for m from 0 to mmm-1 do
  X[m]:=Row(beta,m+1):Xsort[m]:=sort(X[m]):
od:
#####################################################################
######## EIGENVALUES READING #########################################
>for m from 0 to mmm-1 do
 for mm from 1 to N0 do
    R[m,mm]:=0:
 od:od:
for m from 0 to mmm-1 do
for i from 1 to N0 do
for j from 1 to N0 do
   if((abs(Xsort[m][i])-abs(F[m][j][1]))=0) then R[m,i]:=j:
   else R[m,j]:=R[m,j]+0:
   fi:
od:od:od:
#####################################################################
```

The approximate eigenfunctions of the integral operator with the kernel $K(m,x,y)$ by using Gauss-Legendre quadrature over the belt (θ_0,θ_1):

```
########## EIGENFUNCTIONS ########################################
>n:='n':m:='m':
>psi:=proc(n,m,x)
   evalf((1.0/F[m][R[m,N0+1-n]][1])*sum(W[kk]*subs(y=E[kk],K(m,x,y))
*F[m][R[m,N0+1-n]][3][1][kk],kk=1..N0)):
end:
#####################################################################
```

Multiplying the eigenfunctions of the operator $K(m,x,y)$ by $e^{im\phi}$, we compute the Slepian functions.

```
## NORMALIZATION CONSTANTE BY USING GAUSS-LEGENDRE QUADRATURE ##
>kk:='kk':
for m from 0 to mmm-1 do
for n from 1 to (L-m+1) do
    AA[n,m]:=evalf(sum(W[kk]*(F[m][R[m,N0+1-n]][3][1][kk])^2, kk=1..N0)):
od:od:
ppsi:=proc(n,m,x)
  evalf((1.0/sqrt(AA[n,m])*psi(n,m,x))):
end:
subs(x=3,ppsi(2,1,x));
#####################################################################
######## NORMALIZED SLEPIAN FUNCTIONS ###############################
>slepian:=proc(n,m,theta,phi)
   if (m<=L-1) then if(n<=L-m+1) then subs(x=cos(theta),
     evalf(1.0/sqrt(evalf(Pi)))*ppsi(n,m,x))*cos(m*phi)
   else
subs(x=cos(theta),evalf(1.0/sqrt(evalf(Pi)))*ppsi(n-L+m-1,m,x))*sin(m*phi)
   fi:
  else
  if(m=L) then
  if(n=1) then
    subs(x=cos(theta), evalf(1.0/sqrt(evalf(Pi)))*ppsi(1,L,x))*cos(L*phi)
  else
    subs(x=cos(theta),evalf(1.0/sqrt(evalf(Pi)))*ppsi(1,L,x))*sin(L*phi)
  fi:
  fi:
  fi:
end:
#####################################################################
```

We indroduce the matrix whose coefficients are the Slepian functions evaluated at the quadrature nodes:

```
# MATRIX T COMPUTATION WHOSE COEFFICIENTS ARE SLEPIAN FUNCTIONS ####
>T:=Matrix((L+1)*(L+2),N0*NN0):
iii:=0:
for m from 0 to L do
for n from 1 to 2*(L-m+1) do
  iii:=iii+1:jjj:=0:
for k from 1 to N0 do
for j from 1 to NN0 do:
  jjj:=jjj+1:T[iii,jjj]:=evalf(WW[j]*W2[k]*sin(E2[k])
  *slepian(n,m,E2[k],EE[j])):
od:od:
od:od:
#here, we put away zero slepian functions (for m=0 n=L+1..2*(L+m+1))##
T2:=Matrix((L+1)^2,N0*NN0):jjj:=0:
for k from 1 to N0 do
for j from 1 to NN0 do
  jjj:=jjj+1:T2[1..L+1,jjj]:=T[1..L+1,jjj]:T2[L+2..(L+1)^2,jjj]
:=T[2*(L+1)+
     1..(L+1)*(L+2),jjj]:
od:
od;
#########################################################################
```

By using this matrix, we compute the Slepian functions expansion coefficients of a given signal. By a matrix multiplication between the matrix T and the matrix associated to the signal (potential) computed in the nodes taken on the belt we get the coefficients. After having the Slepian functions and the coefficients, we can give the expansion of the signal over the sphere. Moreover, from this expansion we can get the spherical harmonic expansion coefficients of the signal. In the following, we consider as application a particular signal, the gravitational potential, and we give the code for the previous scheme. Note that the input data (the bandwith, the positions of sources, the angels which parametrize the belt) is given in a file which we call *data.txt*. The file will be opened for reading the data using basical file commands.

Spherical harmonic coefficients of a potential generated by a monopolar and dipolar sources distribution

```
\section
#################### READ DATA ###################################
>Restart;_EnvLegendreCut := 1 .. infinity;forget(evalf);
```

```
>#  we give the name of the input file
>name_file_to_read:=readstat("The name of the file");
>convert(name_file_to_read,string);
>#here, we open the file for reading the data
>f:=fopen("../datafiles/"||name_file_to_read||"."||txt,READ,TEXT);
>#we read each line
>i:=0:while ligne[i]<>0 do i:=i+1:ligne[i]:=readline(f) end do:fclose(f):
Ligne:=convert(ligne,list);whattype(Ligne);nops(Ligne):
>i:=0:
for i from 1 to nops(Ligne) do
   if Ligne[i]="# BELT"
      then t:=sscanf(Ligne[i+1], "%d%d"):
     theta_0:=t[1]:theta_1:=t[2]:position_belt:=i:
   fi:
   if Ligne[i]="# BANDWITH"
      then L0:=sscanf(Ligne[i+1], "%d");
      L:=L0[1]:
   fi:
   if Ligne[i]="# SOURCES"
      then
      position_source:=i:
   fi:
od:
>nbSources:=position_belt-position_source-1:
  source:=Array(1..nbSources,1..4):j:=0:
  for j from 1 to nbSources do
     s[j]:=sscanf(Ligne[position_source+j], "%f%f%f%f");
     source[j,1]:=s[j][1];
     source[j,2]:=s[j][2];
     source[j,3]:=s[j][3]:
     source[j,4]:=s[j][4]:
  od:
#############################################################################
```

We compute the real spherical harmonic basis:

```
############## SPHERICAL HARMONIC BASIS CONSTRUCTION ####################
>Y2:=proc(l,m,x,y)
  evalf(sqrt(2*(2*l+1)/(4*Pi)*(l-abs(m))!/(l+abs(m))!)
  *LegendreP(l,abs(m),x)*cos(m*y)):
end:
Y1:=proc(l,m,x,y)
```

```
  evalf(sqrt(2*(2*l+1)/(4*Pi)*(l-abs(m))!/(l+abs(m))!)
  *LegendreP(l,abs(m),x)*sin(m*y)):
end:
Y3:=proc(l,m,x,y)
  evalf(sqrt((2*l+1)/(4*Pi)))*(l-0)/(l+0)*diff(1/(2^l*l!)*(1-x^2)^l,x$l):
end:
Y:=proc(l,m,x,y)
  if   m>0 then Y2(l,m,x,y)
  elif m<0 then Y1(l,m,x,y)
  elif m=0 then Y3(l,m,x,y)
  fi:
end:
#############################################################################
################ QUADRATURE OVER (theta_0, theta_1) ########################
>theta_0_degres:=(theta_0*Pi)/180;
>theta_1_degres:=(theta_1*Pi)/180;
>Digits:=50:with(linalg):
a:=-evalf(sin(theta_1_degres)):
b:=evalf(sin(theta_0_degres)):
N0:=20:x:='x':
for n from N0 to N0+1 do
   hh:=evalf(sqrt(2*n+1)*1.0/((b-a)^(n+0.5)*n!)):
   Q[n]:=expand(diff((b-x)^(n)*(a-x)^n,x$n)*hh):
   k[n]:=coeff(Q[n],x,n):
od:
Q1:=expand(diff(Q[N0],x)):
#######the zeros of P_n as eigenvalues of DD matrix ###############
DD:=array(1..N0,1..N0):
for i from 1 to N0 do
for j from 1 to N0 do
   DD[i,j]:=0.0:
od:
od:
for i from 1 to N0 do
  DD[i,i]:=0.5*(a+b):
od:
for i from 1 to N0-1 do
  DD[i,i+1]:=-evalf(i*(b-a)/(2.0*sqrt(2*i+1.0)*sqrt(2*i-1.0))):
  DD[i+1,i]:=DD[i,i+1]:
od:
E:=evalf(eigenvals(DD)):
```

```
####### nodes and weights ########################################
>for i from 1 to N0 do
  x:=E[i]:#the nodes
  W[i]:=-k[N0+1]/k[N0]*1.0/(Q1*Q[N0+1]):#the weights
od:
>with(linalg):a2:=arccos(b):b2:=arccos(a):NN1:=N0:x:='x':
for n from NN1 to NN1+1 do
  hhh:=evalf(sqrt(2*n+1.0)*1.0/(n!)*1.0/((b2-a2)^(n+1/2))):
  QQ[n]:=expand(diff((x-a2)^n*(x-b2)^(n),x$n)*hhh):
  ka[n]:=coeff(QQ[n],x,n):
od:
QQ1:=expand(diff(QQ[NN1],x)):
>DDD:=array(1..NN1,1..NN1):
for i from 1 to NN1 do
for j from 1 to NN1 do
  DDD[i,j]:=0.0:
od:
od:
for i from 1 to NN1 do
DDD[i,i]:=0.5*(a2+b2):
od:
for i from 1 to NN1-1 do
DDD[i,i+1]:=-evalf(i*(b2-a2)/(2.0*sqrt(2*i+1.0)*sqrt(2*i-1.0))):
DDD[i+1,i]:=DDD[i,i+1]:
od:
E2:=evalf(eigenvals(DDD)):
>for i from 1 to NN1 do
x:=E2[i]:W2[i]:=-ka[NN1+1]/ka[NN1]*1.0/(QQ1*QQ[NN1+1]): #nodes and weights
od:
##########################################################################
########### QUADRATURE OVER (0,Pi) ########################################
>with(linalg):a3:=0:b3:=evalf(Pi):NN1:=N0:x:='x':
for n from NN1 to NN1+1 do
  hhh:=evalf(sqrt(2*n+1.0)*1.0/(n!)*1.0/((b3-a3)^(n+1/2))):
  QQ[n]:=expand(diff((x-a3)^n*(x-b3)^(n),x$n)*hhh):
  ka[n]:=coeff(QQ[n],x,n):
od:
QQ1:=expand(diff(QQ[NN1],x)):
DDD:=array(1..NN1,1..NN1):
for i from 1 to NN1 do
for j from 1 to NN1 do
```

```
  DDD[i,j]:=0.0:
od:
od:
for i from 1 to NN1 do
  DDD[i,i]:=0.5*(a3+b3):
od:
for i from 1 to NN1-1 do
  DDD[i,i+1]:=-evalf(i*(b3-a3)/(2.0*sqrt(2*i+1.0)*sqrt(2*i-1.0))):
  DDD[i+1,i]:=DDD[i,i+1]:
od:
E3:=evalf(eigenvals(DDD)):
# nodes and weights
>for i from 1 to NN1 do
  x:=E3[i]:W3[i]:=-ka[NN1+1]/ka[NN1]*1.0/(QQ1*QQ[NN1+1]):
od:
##########################################################################
########## QUADRATURE OVER (0,2pi) ########################################
>with(linalg):
aa:=0:bb:=evalf(2*Pi):NN0:=20:x:='x':
for n from NN0 to NN0+1 do
  hhh:=evalf(sqrt(2*n+1.0)*1.0/(n!)*1.0/(bb^(n+1/2))):
  QQ[n]:=expand(diff(x^n*(x-bb)^(n),x$n)*hhh):
  ka[n]:=coeff(QQ[n],x,n):
od:
QQ1:=expand(diff(QQ[NN0],x)):
les zeros du P_n comme des valeurs propres de la matrice DDD
DDD:=array(1..NN0,1..NN0):
for i from 1 to NN0 do
for j from 1 to NN0 do
  DDD[i,j]:=0.0:
od:od:
for i from 1 to NN0 do
  DDD[i,i]:=0.5*(aa+bb):
od:
for i from 1 to NN0-1 do
  DDD[i,i+1]:=-evalf(i*(bb-aa)/(2.0*sqrt(2*i+1.0)*sqrt(2*i-1.0))):
  DDD[i+1,i]:=DDD[i,i+1]:
od:
EE:=evalf(eigenvals(DDD)):
#### nodes and weights ######
>for i from 1 to NN0 do
```

```
  x:=EE[i]:
  WW[i]:=-ka[NNO+1]/ka[NNO]*1.0/(QQ1*QQ[NNO+1]):
od:
#######################################################################
######### KERNEL  K(m,x,y) ############################################
>x:='x':y:='y':
>K:=proc(m,x,y)
  if (m=0) then evalf(sum((2*l+1.0)/(4.0*Pi)*1/(2^l*l!)
*(diff((x^2-1)^l,x$l))*1/(2^l*l!)*(diff((y^2-1)^l,y$l)),l=0..L)):
  else
 evalf(sum((2*l+1.0)/(4.0*Pi)*(((l-abs(m))!)/((l+abs(m))!)
*((1-x^2)^(m/2)*1/(2^l*l!)*diff(diff((x^2-1)^l,x$l),x$m)
*(1-y^2)^(m/2)*1/(2^l*l!)*diff(diff((y^2-1)^l,y$l),y$m))),l=abs(m)..L)):
 fi:
end:
#######################################################################
######## EIGENVALUES of K(m,x,y) ######################################
>#the eigenvalues of K which is computed in nodes taken over the belt:
>with(LinearAlgebra):mmm:='mmm':mmm:=L+1:i:=0:j:=0:
A:=Matrix(1..mmm*NO,1..NO):
for m from 0 to mmm-1 do
for i from 1 to NO do
for j from 1 to NO do
    A[m*NO+i,j]:=evalf(W[j]*subs(x=E[i],y=E[j],K(m,x,y))):x:='x':y:='y':
od:od:od:
m:='m':
for m from 0 to mmm-1 do
   F[m]:=eigenvectors(SubMatrix(A,[m*NO+1..(m+1)*NO],[1..NO])):
od:
#######################################################################
######## SORTED EIGENVALUES ############################################
>ascendent sorted eigenvalues
>beta:=Matrix(1..mmm,1..NO):
for m from 0 to mmm-1 do
for p from 1 to NO do
  beta[m+1,p]:=abs(F[m][p][1]):
od:od:
for m from 0 to mmm-1 do
  X[m]:=Row(beta,m+1):Xsort[m]:=sort(X[m]):
od:
#######################################################################
```

```
######## EIGENVALUES INDEXATION ######################################
>for m from 0 to mmm-1 do
 for mm from 1 to N0 do
    R[m,mm]:=0:
 od:od:
for m from 0 to mmm-1 do
for i from 1 to N0 do
for j from 1 to N0 do
   if((abs(Xsort[m][i])-abs(F[m][j][1]))=0) then R[m,i]:=j:
   else R[m,j]:=R[m,j]+0:
   fi:
od:od:od:
#############################################################################
######### EIGENFUNCTIONS OF THE KERNEL K(m,x,y)##############################
#E are the nodes over the belt, W the weights of G-L quadrature of the belt
>n:='n':m:='m':
>psi:=proc(n,m,x)
   evalf((1.0/F[m][R[m,N0+1-n]][1])*sum(W[kk]*subs(y=E[kk],K(m,x,y))
*F[m][R[m,N0+1-n]][3][1][kk],kk=1..N0)):
end:
#############################################################################
##### NORMALIZATION CONSTANTE OF GAUSS-LEGENDRE QUADRATURE  ###############
>kk:='kk':
for m from 0 to mmm-1 do
for n from 1 to (L-m+1) do
    AA[n,m]:=evalf(sum(W[kk]*(F[m][R[m,N0+1-n]][3][1][kk])^2, kk=1..N0)):
od:od:
ppsi:=proc(n,m,x)
  evalf((1.0/sqrt(AA[n,m])*psi(n,m,x))):
end:
subs(x=3,ppsi(2,1,x));
#############################################################################
######## NORMALIZED SLEPIAN FUNCTIONS ###################################
#From eigenfunctions of K(m,x,y), we build the slepian functions
>slepian:=proc(n,m,theta,phi)
   if (m<=L-1) then if(n<=L-m+1) then subs(x=cos(theta),
     evalf(1.0/sqrt(evalf(Pi)))*ppsi(n,m,x))*cos(m*phi)
   else
subs(x=cos(theta),evalf(1.0/sqrt(evalf(Pi)))*ppsi(n-L+m-1,m,x))*sin(m*phi)
   fi:
  else
```

```
  if(m=L) then
  if(n=1) then
    subs(x=cos(theta), evalf(1.0/sqrt(evalf(Pi)))*ppsi(1,L,x))*cos(L*phi)
  else
    subs(x=cos(theta),evalf(1.0/sqrt(evalf(Pi)))*ppsi(1,L,x))*sin(L*phi)
  fi:
  fi:
  fi:
end:
#########################################################################
#EIGENVALUES COMPUTATION OF EIGENVALUES lambda[m,n],m=0..L,n=1..2(L-m+1)#
       ASSOCIATED TO SLEPIAN FUNCTIONS slepian(n,m,theta,phi)
> m := 0;
for n to L+1 do
 lambda[m, n] := evalf(2.0*Pi)*F[m][R[m, N0+1-n]][1]
od;
for m to L do
for n to L-m+1 do
 lambda[m, n] := evalf(2.0*Pi)*F[m][R[m, N0+1-n]][1]
od;
for n from L-m+2 to 2*(L-m+1) do
lambda[m, n] := lambda[m, n-L+m-1]
od:od
#########################################################################
####### PLOT THE EIGENVALUES ############################################
>lambda1:=Vector(1..(L+1)^2):i:=0:m:=0:
for n from 1 to (L+1) do
  i:=i+1:
  lambda1[i]:= evalf(2.0*Pi)*F[m][R[m,N0+1-n]][1]:
od:
i:=0:
for m from 1 to L do
for n from 1 to (L-m+1) do
  i:=i+1:lambda1[(L+1)+L*(L+1)/2+i]:=evalf(2.0*Pi)*F[m][R[m,N0+1-n]][1]:
  lambda1[L+1+i]:=evalf(2.0*Pi)*F[m][R[m,N0+1-n]][1]:
od:
od:
k:=0:
for k from 1 to (L+1)^2 do
  lambda1[k]
od:
```

```
P:=sort(lambda1,‘>‘):
k:=0:
for k from 1 to (L+1)^2 do
 P[k]
od:
plot([seq([k,P[k]],k=1..(L+1)^2)],style=point,color=red):
#########################################################################
########### PLOT THE EIGENVALUES ########################################
> plot(ppsi(1,3,x), x=0..1):
#########################################################################
######## PLOT THE SLEPIAN FUNCTIONS #####################################
>Slepian:=proc(n,m,theta,Phi)
evalf(subs(x=cos(theta),ppsi(n,m,x))*cos(m*phi)):
end;
plot3d(Slepian(1, 3, theta, Phi),theta = 0..evalf(Pi),phi = 0..evalf(2*Pi)):
#########################################################################
####### MATRIX T-COMPUTATION WHOSE COEFFICIENTS ARE SLEPIAN FUNCTIONS ####
>T:=Matrix((L+1)*(L+2),N0*NN0):
iii:=0:
for m from 0 to L do
for n from 1 to 2*(L-m+1) do
  iii:=iii+1:jjj:=0:
for k from 1 to N0 do
for j from 1 to NN0 do:
  jjj:=jjj+1:T[iii,jjj]:=evalf(WW[j]*W2[k]*sin(E2[k])*slepian(n,m,E2[k],EE[j])):
od:od:
od:od:
## here, we put away zero slepian functions (for m=0 n=L+1..2*(L+m+1)) ####
T2:=Matrix((L+1)^2,N0*NN0):jjj:=0:
for k from 1 to N0 do
for j from 1 to NN0 do
  jjj:=jjj+1:T2[1..L+1,jjj]:=T[1..L+1,jjj]:T2[L+2..(L+1)^2,jjj]
  :=T[2*(L+1)+1..(L+1)*(L+2),   jjj]:
od:
od;
#########################################################################
```

We give the bandlimited spherical harmonic developpement of the gravitational potential:

```
### GRAVITATIONAL POTENTIAL ##############################################
>pot_monopolar:=proc(theta,phi)
i:=0:a3:=0:
```

```
for i from 1 to nbSources do
 a3:=a3+evalf(source[i,4]): od:
for i from 1 to nbSources do
 for n from 1 to L do
 for m from -n to n do
  a3:=a3+evalf(source[i,4]*source[i,1]^n*((4*evalf(Pi))/(2*n+1))
   *subs(x=cos(source[i,2]),y=source[i,3],Y(n,m,x,y))
   *subs(x=cos(theta),y=phi,Y(n,m,x,y))):
  od:od:od:
end;
#######################################################################
```

We compute the potential in the nodes taken over the belt and we associate the corresponded matrix:

```
########## THE POTENTIAL MATRIX ASSOCIATED ##########################
>S1:=Matrix(N0*NN0,3):jjj:=0:
for k from  1 to N0 do
for j from 1 to NN0 do
  jjj:=jjj+1:
  S1[jjj,1]:=pot_monopolar((E2[k]),EE[j]):
  S1[jjj,2]:=E2[k]:
  S1[jjj,3]:=EE[j]:
od:
od:
>s1:=array(1..N0*NN0): ## the potential array
for i from 1 to N0*NN0 do
 s1[i]:= S1[i,1]:
od:
#######################################################################
```

We compute the coefficients of the potential developpement on Slepian basis:

```
###### THE COEFFS OF THE SLEPIAN POTENTIAL DEVELOPEMENT ################
>C1:=multiply(T2,S1):
#######################################################################
```

Having the Slepian basis and the corresponded coefficients of the potential Slepian basis developpement, we can express the potential in all points which belong to the sphere:

```
###RECONSTRUCTION AND EXTRAPOLATION OF THE POTENTIAL BY SLEPIAN FUNCTIONS#
>Rpot_monopolar:= proc(theta,phi)
 i:=1: a4:=0.0:
```

```
 for n from 1 to L+1 do
   a4:=a4+(0.5)*C1[i,1]*slepian(n,0,theta,phi):i:=i+1:
 od:
 i:=i-1:
for m from 1 to L do
for n from 1 to 2*(L-m+1) do
  i:=i+1:a4:=a4+C1[i,1]*slepian(n,m,theta,phi):
od:
od:
end:
#########################################################################
```

We compute the reconstruct potential in the nodes taken over the belt and we associate to it a matrix:

```
######### THE RECONSTRUCT POTENTIAL MATRIX ASSOCIATED ###################
>S1_slepian:=Matrix(N0*NN0,3):jjj:=0:
for k from  1 to N0 do
for j from 1 to NN0 do
  jjj:=jjj+1:
  S1_slepian[jjj,1]:=Rpot_monopolar((E2[k]),EE[j]):
  S1_slepian[jjj,2]:=E2[k]:
  S1_slepian[jjj,3]:=EE[j]:
od:
od:
>s1_slepian:=array(1..N0*NN0):
for i from 1 to N0*NN0 do
s1_slepian[i]:= S1_slepian[i,1]:
od:
#########################################################################
```

The coefficients of its spherical harmonic developpement over the sphere are computed. These coefficients are exported in an output file and used after for FindSource3D as input.

```
####### SPHERICAL HARMONIC COEFFS OF THE RECONSTRUCT POTENTIAL ############
>CRpot_monopolar:=Matrix((L+1)^2,3):
x := 'x'; y := 'y'; k := 'k'; j := 'j':iii:=0:
for n from 1 to L do
for m from -n to n do
   iii:=iii+1:
   CRpot_monopolar[iii+1,1]:=evalf(sum(sum(WW[j]*W3[k]*sin(E3[k])
   *Rpot_monopolar(E3[k],EE[j])*subs(x=cos(E3[k]),y=EE[j],
```

```
     Y(n, m, x, y)),k=1..N0),j=1..NN0)):
   CRpot_monopolar[iii+1,2]:=n:
   CRpot_monopolar[iii+1,3]:=m:
   CRpot_monopolar[1,1]:=evalf(sum(sum(WW[j]*W3[k]*sin(E3[k])
   *Rpot_monopolar(E3[k], EE[j])
    *(1/sqrt(4*Pi)),k = 1..N0),j=1..NN0)):
   CRpot_monopolar[1,2]:=0:
   CRpot_monopolar[1,3]:=0:
end do
end do;
>crpot_monopolar:=array(1..(L+1)^2):
for i from 1 to (L+1)^2 do crpot_monopolar[i]:=CRpot_monopolar[i,1]:
od:
>CRpot_dipolar:=Matrix((L+1)^2,3):
x := 'x'; y := 'y'; k := 'k'; j := 'j':iii:=0:
for n from 1 to L do
for m from -n to n do
   iii:=iii+1:
   CRpot_dipolar[iii+1,1]:=evalf(sum(sum(WW[j]*W3[k]*sin(E3[k])
    *Rpot_dipolar(E3[k],EE[j])
    *subs(x=cos(E3[k]),y=EE[j],Y(n, m, x, y)),k=1..N0),j=1..NN0)):
   CRpot_dipolar[iii+1,2]:=n:
   CRpot_dipolar[iii+1,3]:=m:
   CRpot_dipolar[1,1]:=evalf(sum(sum(WW[j]*W3[k]*sin(E3[k])
  *Rpot_dipolar(E3[k], EE[j])*(1/sqrt(4*Pi)),k = 1..N0),j=1..NN0)):
   CRpot_dipolar[1,2]:=0:
   CRpot_dipolar[1,3]:=0:
end do
end do;
>crpot_dipolar_dipolar:=array(1..(L+1)^2):
for i from 1 to (L+1)^2 do
  crpot_dipolar[i]:=CRpot_dipolar[i,1]:
od:
#########################################################################
```

The exported file will be named in function of the bandwith L, θ_0 and θ_1, the number of sources and their positions. For example, the exported file for the coefficients associated to a potential troncated for $L = 10$ and generated by 1 monopolar source, when the data is taken over the belt $[0, 90]$ will be named $1source\_L10\_B\_0\_90.txt$.

```
##### OUTPUT FILE ########################################################
>#we build the name of the output file
```

```
>name_file_export:=cat(nbSources,sources,_,"L",L,_,B,theta_0,"-",theta_1);
>convert(name_file_export,string);
>#we open the file for writing inside
>ff:=fopen("../datafiles/"||name_file_export||"."||txt,WRITE,TEXT);
>#we write the informations as: bandwidth, monopoles positions, the belt,
the coefficients and the potential on spherical harmonic basis.
>writedata(ff,{"# BANDWITH"},string);
>fprintf(ff,"%d\n",L);
>fprintf(ff,"\n");
>writedata(ff,{"# MONOPOLES"},string);
>for jj from 1 to nbSources do
for ii from 1 to 4 do
  fprintf(ff, "%f ",source[jj,ii] )
od:
fprintf(ff,"\n"):
od:
fprintf(ff,"\n");
>writedata(ff,{"# BELT"},string);
>fprintf(ff,"%d %d\n",theta_0,theta_1);
>fprintf(ff,"\n");
>writedata(ff,{"# COEFFICIENTS HS"},string);
>writedata(ff,crpot);
>fprintf(ff,"\n");
>writedata(ff,{"# POTENTIAL HS"},string);
>writedata(ff,s1);
>fprintf(ff,"\n");
>writedata(ff,{"# NODES"},string);
>writedata(ff,Nodes);
>fclose(ff);
#########################################################################
```

In the next table we give an example of the taken nodes over the sphere and the corresponded weights for $N = 30$.

Figure 1: *Nodes and weights for $N = 30$-points Gauss-Legendre quadrature*

Nodes EE_i	Weights WW_i	Nodes E_j	Weights W_j
0.97594076093434623	0.02503281500824385	0.48797038046717311	0.01251640750412192
0.51308103923682235	0.05801412118384111	0.25654051961841117	0.02900706059192055
0.12559501531978600	0.09042982682197554	0.62797507659893003	0.04521491341098777
0.23184938883146788	0.12189125834194921	0.11592469441573394	0.06094562917097460
0.36894695799720711	0.15206148137871379	0.18447347899860355	0.07603074068935689
0.53543494881847886	0.18062007720493192	0.26771747440923943	0.09031003860246596
0.72954871329723447	0.20726415592410433	0.36477435664861723	0.10363207796205216
0.94923066584311044	0.23171122839432797	0.47461533292155522	0.11585561419716398
1.19215215575067468	0.25370212718680757	0.59607607787533734	0.12685106359340378
1.45573817204794098	0.27300373306944176	0.72786908602397049	0.13650186653472087
1.73719464730237738	0.28941143909239454	0.86859732365118869	0.14470571954619727
2.03353807897558081	0.30275131674358954	1.01676903948779040	0.15137565837179477
2.34162715700806423	0.31288195846135423	1.17081357850403211	0.15644097923067712
2.65819606338856840	0.31969597604533323	1.32909803169428420	0.15984798802266661
2.97988909115127632	0.32312113873262549	1.48994454557563816	0.16156056936631274
3.30329621602830947	0.32312113873262539	1.65164810801415474	0.16156056936631269
3.62498924379101384	0.31969597604533126	1.81249462189550692	0.15984798802266563
3.94155815017152289	0.31288195846135474	1.97077907508576145	0.15644097923067737
4.24964722820400276	0.30275131674358627	2.12482361410200138	0.15137565837179313
4.54599065987720508	0.28941143909238855	2.27299532993860254	0.14470571954619427
4.82744713513164481	0.27300373306944045	2.41372356756582240	0.13650186653472021
5.09103315142891776	0.25370212718682167	2.54551657571445888	0.12685106359341083
5.33395464133647490	0.23171122839432468	2.66697732066823744	0.11585561419716231
5.55363659388234687	0.20726415592408597	2.77681829694117344	0.10363207796204300
5.74775035836111670	0.18062007720497221	2.87387517918055835	0.09031003860248610
5.91423834918237912	0.15206148137871243	2.95711917459118956	0.07603074068935621
6.05133591834811924	0.12189125834195395	3.02566795917405962	0.06094562917097697
6.15759029185980111	0.09042982682198210	3.07879514592990056	0.04521491341099110
6.23187720325590622	0.05801412118387329	3.11593860162795311	0.02900706059193664
6.27342589957023833	0.02503281500806989	3.13671294978511917	0.01251640750403513